Evolution of the remnants of stellar collisions

Evert Glebbeek

This book was typeset by the author using LaTeX2e and printed by Multi-Copy

ISBN-10: 90-393-4832-1
ISBN-13: 978-90-393-4832-1

Evolution of the remnants of stellar collisions

Evolutie van de overblijfselen van sterbotsingen
(met een samenvatting in het Nederlands)

Proefschrift

ter verkrijging van de graad van doctor aan de Universiteit Utrecht op gezag van de rector magnificus, prof.dr. J.C. Stoof, ingevolge het besluit van het college voor promoties in het openbaar te verdedigen op woensdag 25 juni 2008 des middags te 12.45 uur

door

Evert Glebbeek
geboren op 6 december 1979 te Amsterdam

Promotor:	Prof. dr. F. W. M. Verbunt
Co-promotoren:	Dr. O. R. Pols
	Dr. S. F. Portegies Zwart

Dit proefschrift werd mede mogelijk gemaakt door financiële steun van NWO.

Contents

1

Introduction

1.1 Stellar evolution in a dense stellar environment

The notion that star clusters are "stellar evolution laboratories" and "stellar dynamics laboratories" has become something of a cliché, but not without good reason. Most of the stars in a cluster are expected to be formed at roughly the same time and with the same abundance and thus constitute a simple stellar population. It is this property that makes star clusters suitable laboratories, because it allows tests of stellar evolution that are much harder or impossible to make with field star populations. Recently this picture has become somewhat blurred as evidence has been found for the presence of a second population of stars in at least some globular clusters (ω Centauri, NGC 2808, NGC 6441 and NGC 6388, *e.g.* Pumo et al. 2008). This second population appears to be helium rich ($Y \approx 0.35$) compared to the first population. It is currently not clear how this helium enhancement can be explained.

Historically, galactic clusters have been divided into *open clusters* and *globular clusters*. Open clusters show a large spread in ages, from several million up to a few billion years old (*e.g.* M67 is about 4 Gyr old and NGC 188 is at least 5 Gyr old). They are generally metal rich (Population I, $Z \sim Z_\odot \approx 0.02$) and contain relatively few stars ($\sim 10^3$–10^4). Galactic open clusters are located in the galactic disk. Globular clusters on the other hand are old (comparable to the age of the universe itself) and they tend to be metal poor (Population II, $Z \sim Z_\odot/20$). Globular clusters generally have many more stars than open clusters ($\sim 10^4$–10^6) and are associated with the halo.

It was realised that the distinction between globular clusters and open clusters is somewhat arbitrary when young massive clusters were discovered, first in other galaxies (see Larsen & Richtler 1999, for an overview) and later in our own galaxy (*e.g.* Figer et al. 1999). The current view is that globular clusters are old and massive because massive clusters are the ones that preferentially survive to late times while open clusters are younger and less massive because most low mass clusters do not survive until late times.

Historically, the dynamical evolution of star clusters has been studied independently of stellar evolution within the cluster. There are generally two approaches to this study. One approach is to define an average mean-field gravitational potential for the cluster and describe the stars within the cluster using a distribution function. The evolution of this distribution function is then described by the Boltzmann equation or the Fokker-Planck equation, hence the name Fokker-Planck method (*e.g.* King 1966). The other approach is to directly integrate the equations of motion for all stars within the cluster. Because this follows the motion of N individual particles or bodies within the cluster, it is called the N-body method (Heggie et al. 1998; Aarseth 1999). N-body calculations are computationally expensive, which has led to the development of special-purpose hardware to do the force calculations (*e.g.* Makino et al. 2003).

The first N-body models used equal-mass point particles. Later improvements include a mass distribution for the particles and a treatment of binary systems and stellar evolution. A spectrum of different masses is important to consider because in reality not all stars have the same mass, and the mass of a star determines how it responds to the gravitational attraction of other stars. Since stellar evolution alters the stellar mass as a result of a stellar wind or the formation of a compact remnant at the end of evolution, it is clearly also important to take into account stellar evolution. Furthermore, and contrary to what had been assumed before, binaries were found to be important constituents of clusters, both observationally and theoretically, through their influence on the dynamical evolution of clusters (Hut et al. 1992).

Dynamical models of star cluster evolution using equal mass particles showed that they are subject to an instability whereby the cluster core contracts and becomes denser (densities of 10^4–10^5 stars per cubic parsec are possible), while the outer regions of the cluster expand. This is called *core collapse* and the instability is due to the negative gravothermal specific heat (Heggie & Hut 2003). Physically, this is entirely analogous to the contraction of a self-gravitating cloud of gas. The contraction of a gas cloud is halted when an energy source is activated in the centre of the cloud, such as the ignition of hydrogen fusion in stars. Similarly, the activation of an energy source in the core of a cluster halts core collapse (for a review see Hut et al. 1992). One obvious energy source are binaries. Binaries can act as an energy source for the cluster because they have internal energy

in the form of orbital energy. A binary for which the binding energy is larger than the mean kinetic energy of a cluster star is called a *hard binary*. Dynamical interactions between hard binaries and a third star can be quite complicated, but generally the outcome of such an interaction is a harder binary and a single star (but not necessarily the same star as the original intruder). By energy equipartition the escaping star has extracted energy from the binary, making the binary harder and increasing its own kinetic energy. Due to equipartition of energy the most massive stars in a cluster tend to have smaller velocities and migrate to deeper regions of the potential well, *i.e.* the centre of the cluster. This is called mass segregation and has been observed in various clusters.

Close encounters between stars or binaries also affect the evolution of the stars involved in the encounter because they alter the binary orbit. Some encounters can can lead to physical collisions and mergers between two stars. A full understanding of star cluster evolution requires a good understanding of all these processes (stellar evolution, stellar dynamics and hydrodynamics) and their interaction with eachother. To this end, the international MODEST collaboration was started (Hut et al. 2003; Sills et al. 2003; Davies et al. 2006, see also `http://www.manybody.org/modest/`) which brings together experts on stellar dynamics, stellar evolution and hydrodynamics in an attempt to create a software environment in which all of these components can be treated in detail.

During the first MODEST workshops stellar collisions were identified as the process for which a detailed self-consistent treatment is most needed. This work is a first step in that direction. Our main focus is on the evolution of main sequence stellar collision remnants in star clusters, in particular so-called blue straggler stars and collision runaways.

1.2 Stellar collisions and stellar mergers

We can estimate the probability for a stellar collision to occur as follows. The typical separation between stars (or binary systems) is large compared to their size, even in a dense stellar environment, which means that if stars would collide like billiard balls (hard sphere scattering) the collision cross section σ would be very small. However, gravitational attraction enhances the effective collisional cross section (Heggie & Hut 2003). Taking this so-called gravitational focussing into account the collision cross section becomes

$$\sigma = \pi R^2 \left(1 + \left[\frac{v_{\rm esc}}{v_\infty} \right]^2 \right), \tag{1.1}$$

where R is the typical size of the interacting objects (for instance, the sum of the radii $R_1 + R_2$ of the two stars or the semi-major axis of a binary

orbit) $v_{\rm esc}$ is the escape velocity and v_∞ is the typical relative velocity of the stars in the cluster when they are far apart, which is related to and of the same order as the velocity dispersion in the cluster. For large velocities v_∞ the geometrical cross section dominates the interaction cross section, for smaller velocities the gravitational attraction becomes more important.

For single stars, the escape velocity is typically $v_{\rm esc} \sim 500\,{\rm km\,s^{-1}}$, while the velocity in the cluster is typically $v_\infty \sim 10\,{\rm km\,s^{-1}}$. Gravitational focusing then enhances the collision cross section for single stars by a factor of ~ 2500. Even so, for a stellar density of 10^5 stars per cubic parsec a particular single star is expected to undergo a collision once every 250 Gyr – much longer than the age of the universe.

A binary with an orbital separation of 200 $R_\odot$ on the other hand has a much higher probability to interact. If the total mass of the binary is about 1 $M_\odot$, the escape velocity is only about $30\,{\rm km\,s^{-1}}$, so gravitational focussing only enhances the cross section by a factor of 10. However, because the geometrical cross section is about 40 000 times larger, the total cross section is larger than for the single star, bringing the time between close interactions down to about 1.5 Gyr. For more massive binaries gravitational focussing is more important and the time between encounters decreases proportionally. A more careful estimate by Davies et al. (2004) gives 420 Myr for the time between collisions for a typical binary of $2.5\,M_\odot$ in a massive cluster with a density of $3 \cdot 10^4$ stars ${\rm pc^{-3}}$. The outcome of such a close interaction between binaries is not necessarily a collision, but it is still clear that most collisions between individual stars therefore occur in binaries.

Apart from collisions, stellar mergers can occur in binaries for other reasons. If one of the components in the binary transfers mass to the companion (through Roche-lobe overflow) but the companion cannot accrete the material fast enough the material can accumulate in a common envelope around the two binary components. Dissipation of orbital energy of the secondary star causes a spiral in, bringing the two stellar cores close together (see Eggleton 2006 for a discussion of the mechanisms involved). In some cases the energy released by the spiral in will be sufficient to unbind ("expel") the common envelope. If this does not occur either the secondary or the primary core will eventually fill their Roche lobe within the common envelope and cause a merger of the two cores, leaving a single star in place of the binary (Ivanova & Podsiadlowski 2002). If both components of a binary fill their Roche lobe, the system is called a contact binary. In this case the envelopes of the two stars are also closely linked, but stay in thermal equilibrium. The two components of a contact system will also eventually merge.

Stellar mergers, whether resulting from a collision due to a dynamical interaction or from binary evolution, are a possible formation channel for some peculiar stars that seem to have evolved or formed in a non-standard way:

1. Mergers between white dwarfs can produce extreme helium stars (or sub-dwarf O/B stars) if both components are helium white dwarfs. If one of the two is replaced by a carbon-oxygen white dwarf the result is an R Coronae Borealis star, a class of variable hydrogen deficient F/G supergiants (Webbink 1984; Lambert & Rao 1994).

2. The merger of a red giant and a white dwarf has been proposed as the progenitor of the early R-stars, a class of carbon rich K-giants (Izzard et al. 2007).

3. The 2002 eruption of the variable star V838 Monocerotis has been attributed to a merger of an $8\,M_\odot$ and a $0.3\,M_\odot$ star (Tylenda & Soker 2006; Afşar & Bond 2007).

4. While stars with a mass below $10\,M_\odot$ can be formed by accretion in a molecular cloud, it is not clear if this works for more massive stars where the radiation force can be high enough to prevent accretion. Mergers between stars of lower mass in the central regions of young star clusters have been proposed as the normal method of star formation for stars more massive than $10\,M_\odot$ by Bonnell et al. (1998), but it remains unclear whether this is the correct scenario or not.

5. Perhaps the most common type of stars that are associated with mergers are the blue stragglers, stars that appear on the extension of the main sequence in the colour-magnitude diagram of star clusters.

Among field stars binary coalescence is the only merger channel that operates. In clusters the contribution from direct stellar collisions cannot be ignored. Numerical N-body models of star clusters show that the two channels are equally important (Hurley et al. 2005) and analytical estimates support this conclusion (Davies et al. 2004).

1.3 Collisions between low mass stars – blue stragglers

Blue stragglers are stars that are brighter and bluer than the main sequence turnoff in the colour-magnitude diagram of star clusters. They were first identified by Sandage (1953) in the globular cluster M3 and soon afterwards in the open cluster M67 (Johnson & Sandage 1955). Since then they have been found in many other clusters (Ahumada & Lapasset 1995; Piotto et al. 2004; Ahumada & Lapasset 2007).

Their position in the colour magnitude diagram indicates that blue stragglers have a higher mass than other main sequence stars. This is consistent

with direct mass measurements by De Marco et al. (2005) and with kinematic arguments based on the location of the blue stragglers within their host cluster (See the review by Bailyn 1995).

If blue stragglers had formed at the same time as the rest of the stellar population in the star cluster normal stellar evolution theory predicts that they would have evolved away from the main sequence long ago, as other main sequence stars of the same mass have done.

In the past various solutions to this problem have been proposed (for an overview, see Leonard 1989), but the scenarios that are currently thought to be most important are mass transfer by Roche-lobe overflow in binary systems and stellar mergers.

A collisional origin for blue stragglers was first proposed by Hills & Day (1976). Simulations of stellar collisions by Benz & Hills (1987) suggested that the merged remnant of such a collision would be thoroughly mixed. Based on this assumption, Leonard & Livio (1995) constructed homogeneously mixed models of stellar mergers. They estimated the helium abundance of the merger remnant using time averaged luminosities of the progenitor stars. Based on their models they conclude that the blue straggler population of the globular cluster 47 Tucanae is consistent with a collisional origin while the blue stragglers in M3 require both stellar collisions and binary mergers.

Hydrodynamical calculations of stellar collisions at higher resolution performed by Lombardi et al. (1995, 1996) indicated that contrary to the earlier calculations, the merger remnants are not completely mixed during the collision. Instead they found that very little mixing occurs, but it was not clear whether convection during the subsequent evolution would result in mixing.

Evolution calculations using the composition profile of hydrodynamical simulations were performed by Sills et al. (1995), who concluded that complete mixing during the subsequent evolution was required to explain the observed blue straggler population of NGC 6397. This was challenged by Sandquist et al. (1997) who constructed similar models and concluded that neither complete mixing nor the total absence of mixing could explain the observations. Ouellette & Pritchet (1998) constructed models of collision products including the effect of heating during the collision and find that the blue stragglers of NGC 6397 and 47 Tucanae are best explained by unmixed collision products.

Evolution models using both the composition profile and heating predicted by hydrodynamic calculations were calculated by Sills et al. (1997, 2001). Their evolution models likewise did not develop significant convection zones, resulting in little mixing of the merger remnant. Models of off-centre collisions resulted in rapidly rotating collision products that underwent significant mixing due to rotation-induced instabilities.

Based on the agreement between their non-rotating models and observa-

tions, Ouellette & Pritchet (1998) concluded that rotational mixing is not important for blue straggler evolution. There is a problem, however, in that stellar merger remnants are expected to have high angular momentum and rotate very rapidly. It is still not clear how angular momentum can be lost from the collision product. We will return to this point in section 1.5.

1.4 Collisions between massive stars – intermediate-mass black holes

Star clusters commonly host X-ray sources, such as high- and low-mass X-ray binaries (Hut et al. 1992; Bailyn 1995). Of the 100 brightest X-ray sources within the galaxy, 12 are within globular clusters although only 0.01% of the mass is in globular clusters. High-mass X-ray binaries are binary systems in which a massive main-sequence star (with a mass above above $20 M_{\odot}$) transfers material to a companion black hole or neutron star. In a low-mass X-ray binary the mass donating star has a mass below $1.4\,M_{\odot}$. In both of these cases the accreted material radiates X-rays, with luminosities up to about $10^{38}\,\mathrm{erg\,s^{-1}}$. The Eddington luminosity for an accreting stellar mass black hole ($M \sim 10\ M_{\odot}$) is about $2 \cdot 10^{39}\,\mathrm{erg\,s^{-1}}$. Some clusters contain ultra-luminous X-ray sources, with X-ray luminosities at or above this luminosity ($10^{39-41}\,\mathrm{erg\,s^{-1}}$). Such sources can be interpreted as radiation from material that is accreted onto an intermediate-mass black hole.

Intermediate-mass black holes are black holes with a mass between that of stellar-mass black holes ($M \sim 10\,M_{\odot}$) and the supermassive black holes ($M \sim 10^5 M_{\odot}$ and above) that are thought to exist in the centre of galaxies. The typical mass for an intermediate-mass black hole is thought to be 10^2 – $10^3 M_{\odot}$. The interpretation of ultra-luminous X-ray sources as accreting intermediate-mass black holes is not undisputed. Vierdayanti et al. (2006) studied ultra luminous X-ray sources that had been interpreted as accreting intermediate-mass black holes and found that they could explain the observations with models of super-critical accretion onto stellar-mass black holes.

Other arguments for the occurrence of intermediate-mass black holes in clusters are based on the cluster kinematics. Evidence for the existence of an intermediate-mass black hole in the globular cluster M15 was claimed by Gerssen et al. (2002) and van der Marel et al. (2002), but refuted by Dull et al. (2003). Likewise evidence for an intermediate-mass black hole in the globular cluster G1 of M31 was found by Gebhardt et al. (2002), although this has been disputed by Baumgardt et al. (2003). An X-ray source in G1 was reported by Pooley & Rappaport (2006), but it is unclear whether this is associated with an intermediate mass black hole or not. Although observational the evidence for the existence of intermediate-mass

black holes remains uncertain, possible formation mechanisms have been studied by several authors.

It has been argued that the first generation of stars (Population III) may have been quite massive, (about $10^3 M_\odot$, Bromm et al. 1999) and could have collapsed to an intermediate-mass black hole at the end of their evolution. Although such stars are not expected to form at higher metallicity (Weidner & Kroupa 2004), circumstances in the core of a dense cluster can be such that multiple stars collide and merge on a short timescale ($\sim$ 3Myr, Portegies Zwart et al. 1999). It is not clear whether stars formed by such a runaway merger really form an intermediate-mass black hole because the evolution of very massive stars at high metallicity is uncertain. Belkus et al. (2007) have studied the evolution of merger runaways in an approximate way and find that an intermediate-mass black hole does not form. Yungelson et al. (2008) came to a similar conclusion based on a study of the evolution of very massive stars. If the remnant of a merger runaway is not an intermediate-mass black hole, the conditions in the core at the end of the evolution of very massive stars (above $150\,M_\odot$ for $Z = 0.001$, depending on the mass loss rates) are such that they are unstable to an instability triggered by the conversion of photons to electron-positron pairs (Langer et al. 2007). Such pair-creation supernovae are expected to be very luminous, similar to the supernova 2006gy. Merger runaways could be the progenitors of such supernovae (Portegies Zwart & van den Heuvel 2007).

1.5 The physics of stellar mergers

The structure of stellar collision products can be generally understood from a few simple arguments, which will be given here. Some of these will be discussed in more detail in later chapters.

All hydrodynamic calculations find that the two progenitor stars merge very quickly after the initial collision, within a few periastron passages (Benz & Hills 1987; Lombardi et al. 1995). The kinetic energy of the two colliding stars is dissipated into the envelope of the merger remnant. As a result the collision product is out of thermal equilibrium and inflated (Lombardi et al. 1996). The excess thermal energy is radiated away on a thermal timescale, causing the envelope of the collision product to contract.

Because the merger occurs on a short timescale fluid elements do not have time to exchange heat, which means that once the merger remnant settles into hydrostatic equilibrium its structure is determined by the properties of the parent stars, in particular their entropy profiles (Lombardi et al. 2002). As a rule of thumb, low entropy material sinks to the centre of the collision product and high entropy material ends up near the surface. This reflects the tendency of low entropy material to have a higher density than high entropy material for the same temperature. The stability condi-

tion that follows from this principle is equivalent to the standard Ledoux stability condition for convection.

The stability condition in its most general form follows from considering the adiabatic displacement of a fluid element in pressure equilibrium,

$$\frac{\mathrm{d}\rho}{\mathrm{d}r} - \left.\frac{\mathrm{d}\rho}{\mathrm{d}r}\right|_{\mathrm{ad}} < 0. \tag{1.2}$$

For low mass stars consisting of a multi-component ideal gas this can be rewritten in the form

$$\frac{\mathrm{d}A}{\mathrm{d}r} > 0, \tag{1.3}$$

with $A = P/\rho^{\gamma}$ a function of entropy and composition. This allows for an efficient algorithm (referred to as entropy sorting) to compute the structure of the merger remnant from detailed models of the progenitor stars: for each mass shell, one can estimate the local entropy production due to shocks, then sort all mass shells in order of increasing A. Finally, the equation of hydrostatic equilibrium is integrated to obtain a stellar model. This algorithm was used by Lombardi et al. (2002) to develop a simple (and fast) computer program that can be used to calculate the outcome of the collision between low mass main sequence stars.

For massive stars this procedure does not work and needs to be replaced by the more general stability condition (Gaburov et al. 2008c)

$$\frac{\mathrm{d}\log A}{\mathrm{d}r} > \frac{4}{3}\frac{\frac{5}{3}-\Gamma_1}{\Gamma_1-\frac{4}{3}}\frac{\mathrm{d}\log\mu}{\mathrm{d}r}, \tag{1.4}$$

with μ the mean molecular weight, $\Gamma_1 = (\partial \log P/\partial \log \rho)_{\mathrm{ad}}$ the adiabatic index and $A = P/\rho^{5/3}\exp[8(1-\beta)/3\beta]$, with β the ratio of gas pressure to total pressure. This stability condition cannot be written as the gradient of a single monotonic function because Γ_1 is not constant between mass shells. The principle can still be used locally, however, and the structure of the merger remnant can be obtained by iteration. This algorithm was designed by Gaburov et al. (2008c).

The entropy profile in a main sequence star is closely linked to the composition profile. The low entropy material in the core is also helium rich. It is the close link between the entropy profile and the composition profile in combination with entropy sorting that makes the merger remnants weakly mixed. Shock heating can increase the entropy of low entropy material so that this can mix with originally high entropy material, but in practice shock heating is most efficient at heating material from the envelopes of the progenitor stars (Lombardi et al. 2002), resulting in little mixing between the core and the envelope. One uncertainty regarding the amount of mixing is how well the hydrodynamic calculations resolve it. Most stellar collision calculations use the Lagrangian smooth particle hydrodynamics approach,

where fluid elements are followed individually. An alternative approach is an Eulerian finite difference scheme, which suffers from numerical diffusion and is therefore likely to overestimate the amount of mixing. A comparison between the two methods was carried out by Trac et al. (2007). They found that although the Eulerian scheme produced more mixing in the interior, the collision products are still not fully mixed. A by-product of entropy sorting is that the merger remnant does not contain large convection zones after the collision (because it satisfies the Ledoux stability condition everywhere). In principle the collision product could develop a large surface convection zone during its relaxation to the main sequence but in practice this does not happen: the envelope remains radiative throughout the contraction phase (Sills et al. 1997).

Because the total angular momentum is conserved, the orbital angular momentum of the two progenitor stars is equal to the spin angular momentum of the collision product. It is easy to show that for off-centre collisions the orbital angular momentum can exceed the maximum angular momentum that can be accommodated by a star in hydrostatic equilibrium. The orbital angular momentum of the two colliding stars is

$$L = \frac{q}{(1+q)^2}\sqrt{2}\sqrt{\frac{r_\mathrm{p}}{R_1+R_2}}M\sqrt{GM(R_1+R_2)}, \tag{1.5}$$

where $M = M_1 + M_2$ is the total mass in the two progenitor stars, $q = M_2/M_1$, R_1 and R_2 are the radii of the progenitor stars and $r_\mathrm{p} \leq R_1 + R_2$ is the periastron separation at the moment of collision. For a rigidly rotating star, the maximum spin angular momentum is

$$S_\mathrm{max} = I\omega_\mathrm{crit} = k^2 M_* \sqrt{GM_* R_*}, \tag{1.6}$$

where k is the axis of gyration in units of the stellar radius R_*. For main sequence stars the radius of the star scales with the mass (Kippenhahn & Weigert 1990). Setting $R \propto M^\xi$ we have $R_1 + R_2 = R_1(1 + q^\xi)$ and $R_* = R_1(1+q)^\xi$. If we ignore mass loss from the collision for simplicity the orbital angular momentum exceeds the maximum spin angular momentum if

$$\frac{r_\mathrm{p}}{R_1+R_2} > k^4 \frac{(1+q)^{\xi+4}}{2q^2}. \tag{1.7}$$

For main sequence stars, $\xi \approx 0.6$ (Kippenhahn & Weigert 1990) and $k^2 \approx 0.05$, so that for collisions where $1 > q > 0.5$ the orbital angular momentum exceeds the maximum spin angular momentum of the remnant if $r_\mathrm{p}/(R_1 + R_2) > 0.015$ ($q = 1$) or $r_\mathrm{p}/(R_1 + R_2) > 0.032$ ($q = 0.5$). Even for mildly off-centre collisions the merger remnant needs to lose angular momentum (and therefore mass) before it can relax to the main sequence.

The above simplified analysis ignores differential rotation in the merger remnant, which will increase the maximum angular momentum that can be

accommodated by the star because more angular momentum can be stored in the interior. In practice this does not remove the problem. In a simple spherically symmetric model of a star in which each mass shell rotates at its critical rate only increases the maximum allowed angular momentum by 40% over a rigidly rotating star.

Various mechanisms for angular momentum loss have been proposed. Ouellette & Pritchet (1998) suggested two possibilities: angular momentum transfer to a circumstellar disk and transfer of angular momentum to the orbit in a close binary. Sills et al. (2005) studied angular momentum loss by locking the rotation of the star to a circumstellar disk or to an outflowing wind through the action of a magnetic field. They found that either mechanism can allow angular momentum to be lost from the collision product efficiently. Since nothing is known with certainty about the magnetic fields of merger remnants and since there are no self-consistent models it is hard to say how well this scenario works in practice.

What we can say is that any mechanism that removes angular momentum from the merger remnant has to do so efficiently for the collision remnant to survive. Observations of the rotation rate of blue stragglers in M67 (Mathys 1991) suggest that such a mechanism does operate in reality.

As already mentioned in section 1.3 rotation can also significantly affect stellar evolution by rotation induced mixing (See Talon 2007, for a recent description of the various instabilities). This offers a plausible mechanism by which collision products can experience more mixing than is predicted by current non-rotating models, but as indicated many observed blue stragglers do not appear to rotate rapidly. Rotation will be ignored in the remainder of this thesis and we will consider only head-on collisions.

1.6 This thesis

In this work we study the evolution of merger remnants that form due to collisions between main sequence stars. This thesis is divided into two parts. In the first part we present the method we use to study stellar mergers and apply this to mergers of low-mass ($M < 2.4\,\mathrm{M}_\odot$) main-sequence stars. In the second part we apply this method to the evolution of collision products of massive stars ($M > 5\,\mathrm{M}_\odot$).

In the first chapter (Glebbeek, Pols & Hurley 2008, A&A submitted), we study the evolution of the collisional blue stragglers that were formed in the N-body simulation of M67 by Hurley et al. (2005) in detail. We use the time of collision and the masses of the progenitor stars that were found in the N-body simulation as input to construct models of the parent stars at the time of collision. These stars are then merged using the entropy sorting algorithm of Lombardi et al. (2002), the collision remnant is imported back into the stellar evolution code and we follow the subsequent

evolution until the tip of the giant branch. We describe the method used to import the stellar models in some detail and we compare the results of our detailed models with detailed models that have been homogeneously mixed and with the predictions of the parametric binary stellar evolution model (BSE) described by Hurley et al. (2000, 2002), which assumes homogeneous mixing and no mass loss. Our detailed models are not as bright as fully mixed models and do not live as long. Our models also have shorter lifetimes than the BSE prescription predicts, which has implications for the number of blue stragglers predicted from N-body simulations. The number of blue stragglers and their distribution in the colour magnitude diagram are important quantities to compare to observations and provide insights in the dynamics of the cluster.

In Chapter 3 (Glebbeek & Pols, A&A submitted) we extend this work by studying a grid of merger models covering a total mass range of $1.4 < M/\mathrm{M}_\odot < 2.4$ with mass ratios $0.4 < q < 1$ and various times of collision for a metallicity of $Z = 0.02$. This covers the parameter space that is relevant for old open clusters. Our grid allows us to link features in the evolution of the collision product to properties of the progenitor stars and we use these insights to provide a recipe that allows us to approximate the evolution of the collision product using only standard stellar evolution tracks. This recipe can be used to extend the stellar evolution prescription used by N-body calculations to make more accurate predictions of blue straggler evolution. We also calculate a grid at lower metallicity ($Z = 0.001$) that we use to calibrate our recipe for the evolution of collision products in globular clusters. We compare our models with the observed blue straggler populations of the old open clusters M67 and NGC 188 and find that our models are in principle able to explain the observed blue straggler populations. To make a detailed statistical comparison with the observed population requires a dynamical model of the cluster so that each collision can be weighted with the probability for that collision to occur.

In Chapter 4 (Gaburov, Glebbeek, Portegies Zwart & Pols, in preparation)[1] we study massive stellar mergers ($M \gtrsim 5M_\odot$). We present a grid of merger models similar to that presented for low mass star in Chapter 3, but we use smooth particle hydrodynamics (SPH) (*e.g.* Monaghan 2005) calculations to compute the structure of the merger remnant. Although collisions between high-mass stars can also form blue stragglers, the focus here is not on blue stragglers but on understanding the evolution of massive merger remnants. The goal of this work is to gain a better insight in the initial stages of a runaway collision sequence. In particular, we study two scenarios in some detail: one whereby a hydrogen rich main sequence star sinks to the centre of the collision product and one where the collision

[1] My own contribution to this work consists of the stellar evolution calculations of both the progenitor stars and the collision product; the first two authors contributed equally to the paper.

product forms with a hydrogen depleted core.

We continue the investigation of merger runaways in chapter 5 (Glebbeek, Gaburov, de Mink, Pols & Portegies Zwart 2008, A&A to be submitted) where we take three merger sequences from the literature (Portegies Zwart et al. 2004) and recompute the stellar evolution using our detailed stellar evolution code and an approximate model for the merger process itself. We study both detailed mixing models, using the code developed by Gaburov et al. (2008c), and models where the progenitor stars mix homogeneously. Contrary to the earlier chapters, homogeneous mixing is a reasonable approximation of the structure of these very massive merger remnants due to the large extent of the central convection zone. In none of our evolution models does the merger sequence lead to the formation of an intermediate-mass black hole. Instead, the merger products form massive Wolf-Rayet stars. The high Wolf-Rayet mass loss rate reduces the mass of the merger remnant to such a degree that the expected outcome of the evolution is the formation of a stellar mass black hole. The collision product enriches the interstellar medium in helium more efficiently than a population of single stars would have done, although the amount of ejected material is probably not enough to account for the formation of a second generation of helium-rich stars. We also investigate the effect of metallicity on the evolution of the merger remnant by recalculating one of our sequences for $Z = 0.001$. We find that the reduced mass loss rate allows the remnant to remain more massive at the end of its evolution, but the expected end result in this case is a pair creation supernova rather than the formation of an intermediate-mass black hole. The unusually bright supernova 2006gy may have been such a pair creation supernova (Langer et al. 2007; Portegies Zwart & van den Heuvel 2007).

1.7 Beyond this work

We plan to extend the work described here in a number of ways. Rotation and rotational mixing have so far been ignored in our work, partly due to inherent uncertainties in these processes in the context of stellar mergers and partly because neither differential rotation nor rotational mixing were implemented in our evolution code. We have now implemented differential rotation and rotational mixing processes; this is currently being tested. Once completed this will allow a more detailed exploration of the problem of angular momentum loss, continuing and extending the work by Sills et al. (2005).

The evolution of collision products has so far been studied in the context of single star evolution, but as pointed out in the beginning, most collisions occur in binaries. A study of collision products in binary systems is feasible with our evolution code, which is essentially a binary evolution code.

Another logical continuation of this work that fits very well within the MODEST initiative that motivated this research is to link our evolution code to a dynamics code as a stellar evolution module, alongside a hydrodynamics code for the collisions. This work is also underway in the context of the MUSE (`http://muse.li`) project, and a version of the code for single star evolution is currently being tested.

2

Blue stragglers in N-body models of M67

Stellar collisions are an important formation channel for blue straggler stars in globular and old open clusters. Hydrodynamical simulations have shown that the remnants of such collisions are out of thermal equilibrium, are not strongly mixed and can rotate very rapidly. Detailed evolution models of collision products are needed to interpret observed blue straggler populations and to use them to probe the dynamical history of a star cluster. We expand on previous studies by presenting an efficient procedure to import the results of detailed collision simulations into a fully implicit stellar evolution code. Our code is able to evolve stellar collision products in a fairly robust manner and allows for a systematic study of their evolution.

Using our code we have constructed detailed models of the collisional blue stragglers produced in the N-body simulation of M67 performed by Hurley *et al.* in 2005. We assume the collisions are head-on and thus ignore the effects of rotation in this paper. Our detailed models are more luminous than normal stars of the same mass and in the same stage of evolution, but cooler than homogeneously mixed versions of the collision products. The increased luminosity and inefficient mixing decrease the remaining main-sequence lifetimes of the collision products, which are much shorter than predicted by the simple prescription commonly used in N-body simulations.

2.1 Introduction

Blue stragglers are stars that appear above and blueward of the main sequence turnoff in the colour-magnitude diagrams (CMDs) of star clusters,

with masses larger than that of a turnoff star. They were first identified by Sandage (1953) in the globular cluster M3 and soon afterwards in the old open cluster M67 (Johnson & Sandage 1955). Blue stragglers have since been found in other globular clusters and in open clusters of all ages (Ahumada & Lapasset 1995). Various mechanisms have been proposed for their formation (Stryker 1993). Currently, there are three accepted formation channels: mass transfer due to Roche-lobe overflow in binary systems, and stellar mergers, either due to dynamical collisions or through coalescence of close binaries.

Hills & Day (1976) first showed that physical collisions between main-sequence stars are likely to occur in the dense cores of some globular clusters. In most environments collisions between single stars are very rare, but binary systems can significantly enhance the rate of stellar collisions because of their much larger collisional cross sections. Stellar collisions are thus an important formation channel for blue stragglers even in old open clusters such as M67, as is demonstrated by direct N-body calculations (Hurley et al. 2001, 2005). These simulations indicate that, while all the above-mentioned formation mechanisms operate in different regions of the cluster and all are needed to reproduce the observed blue straggler population, all formation paths – including binary mass transfer and binary coalescence – are strongly affected by the dynamical evolution of the cluster. The blue straggler population therefore contains important information on the dynamical history of a cluster. Extracting this information requires understanding not only how blue stragglers are formed but also how they subsequently evolve.

In N-body models collisions between two main-sequence stars are usually approximated by assuming that the stars merge without mass loss and replacing the end product by a normal (evolved) main-sequence star with its age reset in accordance with the assumption of complete mixing (Tout et al. 1997; Hurley et al. 2002). Smoothed particle hydrodynamics (SPH) simulations of stellar mergers (Lombardi et al. 1995, 1996) show that some mass is lost during the collision and that the collision products are generally far from being fully mixed. To understand how this affects their further evolution and the predicted blue straggler population, detailed stellar evolution models of the collision products are needed.

In early attempts to model the evolution of stellar merger remnants simplifying assumptions were made: the two stars were assumed to mix completely (Bailyn & Pinsonneault 1995), a specified chemical profile was imposed on the remnant (Sills et al. 1995) or a simplified prescription for heating during the collision was applied to mimic the presumed pre-main sequence contraction phase of evolution (Sandquist et al. 1997). The first realistic evolution calculations of collision products were performed by Sills et al. (1997) who took SPH simulations of head-on collisions between detailed stellar models and imported the SPH results into a stellar evolution code. Their models demonstrated that none of the previously made simpli-

fications are valid: although the collision products are inflated due to shock heating, they do not develop substantial convection zones during thermal relaxation and do not undergo significant mixing during their evolution.

This situation changes when the angular momentum of the collisions is considered. For collisions that are even slightly off-axis, the remnants retain too much angular momentum to relax into thermal equilibrium without reaching break-up velocity (Lombardi et al. 1996). The evolution of such collisions was studied by Sills et al. (2001). In the absence of a clear mechanism by which the stars can lose their excess angular momentum, they artificially removed a large fraction of the angular momentum to allow thermal relaxation. Nevertheless, the remnants continue to rotate rapidly throughout their main-sequence evolution and rotational mixing makes the remnants bluer and brighter and significantly extends their lifetimes. These conclusions were confirmed by higher-resolution calculations (Sills et al. 2002).

The above studies have focussed on blue stragglers in globular clusters, and investigated only a few interesting cases. This limitation was imposed by the computation time required and numerical difficulties in the evolution calculations. However, the importance of stellar collisions for the evolution of star clusters calls for a more systematic approach, covering a larger parameter space and extending to higher masses and younger clusters. This is the aim of our current work. We have developed a flexible evolution code that is able to evolve stellar collision products under a wide range of circumstances in a fairly robust manner. As our code cannot yet treat rotation and rotational mixing properly, for the moment we consider only head-on collisions and ignore the effects of rotation.

As a first step in a systematic study of stellar merger remnants we have constructed detailed models of the blue stragglers formed by stellar collisions in the N-body model of M67 of Hurley et al. (2005). They evolved a cluster of 36 000 stars from zero age to the age of M67 (4 Gyr) taking into account both cluster dynamics and stellar and binary evolution. In their simulation the cluster evolution resulted in 20 blue stragglers at 4 Gyr, eight of which had a collisional origin. They formed either as a result of dynamical perturbation of a primordial binary, or as a result of three-body (binary-single star) or four-body (binary-binary) interactions. In two of the latter cases, three stars merged in subsequent collisions with the fourth star ending up as a binary companion to the blue straggler. Hence in total ten collisions were involved in the formation of these eight blue stragglers.

We evolve these collision products with our detailed stellar evolution code and compare these models with the evolution tracks of normal detailed stellar models and fully mixed detailed models, as well as with the parametric models used by Hurley et al. (2005). In particular we investigate the effect on the main-sequence lifetime of the merger product (*i.e.*, the time during which it will be visible as a blue straggler), its position in

the Hertzsprung-Russell diagram and the effect on the chemical abundances of the remnant. In a companion paper (Glebbeek & Pols 2008) (paper II) we study the influence of varying the collision parameters, in particular the masses of the two stars and their evolutionary stage.

2.2 Tools

2.2.1 Modelling the merging process

To calculate the structure of the collision remnants immediately after the collision we have used the Make Me A Star (MMAS) code developed by Lombardi et al. (2002), which produces a one-dimensional model that approximates the results of detailed smooth particle hydrodynamics (SPH) calculations. The essence of the approximation is the observation that in a stellar model in hydrostatic equilibrium the quantity A defined by

$$A^{3/2} = \frac{(2\pi\hbar^2)^{3/2}}{m_{\mathrm{u}}^4}\frac{1}{\mu^4}\prod_i \left[\left(\frac{B_i}{\mu}\right)^{5/2}\frac{\omega_i}{X_i}\right]^{-Y_i} \mathrm{e}^{S-\frac{5}{2}} \tag{2.1}$$

increases monotonically from the centre to the surface, at least as long as radiation pressure is negligible (see Appendix 2.A for details). Here, S denotes the entropy per particle in units of Boltzmann's constant, μ is the mean molecular weight of the constituent particles, B_i is the mass of particle species i in units of the atomic mass m_{u}, X_i and Y_i are their abundance fraction by mass and number, respectively. Note that A is a function of entropy and composition only. The factor ω_i denotes the degeneracy of the ground state and is taken as 1 for nuclei and 2 for electrons. For a classical ideal gas, (2.1) reduces to

$$A = \frac{P}{\rho^{5/3}}. \tag{2.2}$$

MMAS modifies the initial A profiles of the parent stars to correct for shock heating during the collision and estimates the amount of mass lost. The amounts of shock heating and mass loss are calibrated to detailed SPH results. The remnant profile is then constructed by collecting all mass-bins from the parent stars, sorting them in order of increasing A and integrating the equations of hydrostatic equilibrium and mass conservation.

The composition profile of the remnant is also determined from the A profile. Shock heating leads to partial mixing of adjacent layers in each of the parent stars. After both A and the individual composition profiles have been corrected for shock heating, the composition in the remnant is set to the average composition of material from the parent stars with that value of A. So if for a particular value of A a fraction f_1 comes from the primary with composition X_1 and a fraction f_2 comes from the secondary

with composition X_2, then the composition $X_{\rm r}$ of the corresponding layer in the remnant is

$$X_{\rm r} = X_1 f_1 + X_2 f_2. \tag{2.3}$$

For more details see Lombardi et al. (2002).

2.2.2 The stellar evolution code

To calculate the evolution of the parent stars as well as the further evolution of the collision product we use the stellar evolution code (hereafter STARS) originally developed by Eggleton (Eggleton 1971) and updated by others (Pols et al. 1995). The code uses an adaptive non-Lagrangian mesh that allocates meshpoints according to a mesh-spacing function that places more meshpoints in regions where a higher resolution is required. This means that stars can be evolved with reasonable accuracy with as few as 200 meshpoints.

Our version of STARS uses nuclear reaction rates from Caughlan & Fowler (1988) and Caughlan et al. (1985) and opacities from Rogers & Iglesias (1992) and Alexander & Ferguson (1994). The assumed heavy-element composition is scaled to solar abundances (Anders & Grevesse 1989).

STARS is fully implicit and solves the equations for the structure and composition of the star simultaneously. Convection is treated using the mixing-length prescription (Böhm-Vitense 1958) and convective mixing is modelled as a diffusion process (Eggleton 1972). We use a ratio of mixing length to local pressure scale height $l/H_P = 2.0$.

Usually the mean molecular weight in stars will be either constant in a region or decrease radially outward. In merger remnants there can be layers in which the molecular weight gradient is inverted and a layer of higher mean molecular weight lies on top of a layer of lower mean molecular weight. Such a situation is unstable and leads to a process known as thermohaline mixing (Ulrich 1972; Kippenhahn et al. 1980). The instability arises because material with high molecular weight is supported by thermal buoyancy. When a fluid element exchanges heat with its environment it loses buoyancy and begins to sink on the timescale for heat exchange, *i.e.* the local thermal timescale. We model this as a diffusion process as described in Stancliffe et al. (2007). The diffusion coefficient is given by the product of the typical velocity and size of the fluid elements and the efficiency of mixing thus depends on their assumed geometry. The efficiency we have adopted in this work corresponds to spherical geometry, as in Kippenhahn et al. (1980). If the fluid blobs are elongated the mixing is more efficient. However, since for our adopted choice the mixing occurs on the local thermal timescale and is fast compared to the nuclear timescale, our results are not sensitive to an increase in the efficiency of thermohaline mixing.

STARS uses a simple model for convective overshooting (Schröder et al. 1997) that allows extra mixing in regions where $\nabla_{\rm rad} - \nabla_{\rm ad} > -\delta$. We have

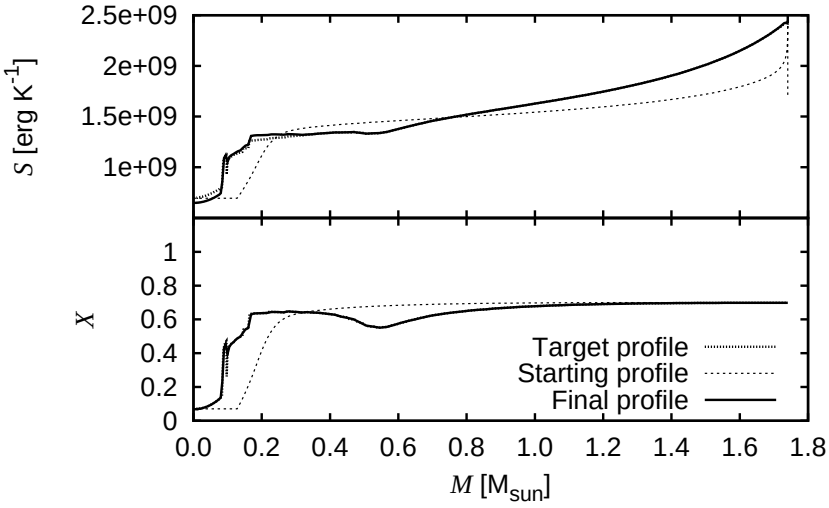

Figure 2.1: *Entropy (top panel) and hydrogen abundance (lower panel) profiles in the merger remnant 2321 (see Table 2.1) as a function of mass coordinate during the convergence stage. The profile at the start of the iteration is indicated by a thin dotted line while the target profile is indicated by a thick dotted line. The solid line is the final profile after the import is complete.*

found that this prescription leads to spurious mixing in the cores of some of our collision products (see §2.5.1), so we have chosen to disable convective overshooting for this work.

2.2.3 Constructing starting models for merger remnant evolution

To construct starting models for the collisions we evolved stars of the appropriate masses from the zero-age main sequence (ZAMS) to the time of collision as listed in Table 2.1 (see §2.3). These models were then used as input for MMAS.

The output from MMAS was converted into an input model for STARS using implicit calculations starting from a normal ZAMS model with the same mass as the collision remnant. This model is first evolved until its core hydrogen abundance matches that of the remnant. At this point, the entropy and composition profiles of the model are adjusted to reproduce

Table 2.1: *Initial conditions for the collisions and collision product lifetimes. The first column lists the number by which the star is refered to in Hurley et al. (2005), followed by the time of collision t, the masses M_1 of the primary and M_2 of the secondary, the total mass M of the remnant according to the detailed models and the remaining main sequence lifetime $t_{\rm ms}$. For comparison we also list the main sequence lifetime $\tau_{\rm ms}$ of a normal star of mass M, the lifetime $\tau_{\rm ms,hom}$ of a homogenised star and the remaining lifetime of the merger remnant according to the parametric BSE prescription ($t_{\rm ms,BSE}$). Time is given in millions of years (Myr) and masses are given in solar masses ($\mathrm{M}_\odot$).*

ID	t	M_1	M_2	M	$t_{\rm ms}$	$\tau_{\rm ms}$	$\tau_{\rm ms,hom}$	$t_{\rm ms,BSE}$
2203	3480	1.23	0.85	1.93	539	1000	745	991
2321	3960	1.29	0.59	1.74	599	1345	862	1305
2565	3650	0.95	0.94	1.76	1016	1297	1122	1336
2973	3170	0.89	0.80	1.56	1569	1850	1685	1877
3121	3890	1.09	0.54	1.52	1428	1993	1629	2051
3289-1	3610	0.82	0.51	1.25	3157	3736	3736	3910
3289-2	3610		0.76	1.86	1024	1103	1058	1020
3445	2770	0.77	0.76	1.41	2172	2502	2361	2547
3835-1	3797	0.82	0.60	1.32	2657	3090	3090	3191
3835-2	3798		0.31	1.56	1765	1849	1793	1776

the profiles of the collision product. Figure 2.1 shows the profiles at the beginning and end of the iteration as well as the output profiles from MMAS for a generic case. The entropy profile was adjusted by adding an artificial energy source $\varepsilon_{\rm art}$ to the luminosity equation,

$$\frac{\mathrm{d}L}{\mathrm{d}m} = \varepsilon_{\rm nuc} - T\frac{\mathrm{d}S}{\mathrm{d}t} + \varepsilon_{\rm art}. \tag{2.4}$$

Here, $\varepsilon_{\rm nuc}$ is the net energy generation rate from nuclear reactions, S is entropy per unit mass, T is the temperature and $-T\mathrm{d}S/\mathrm{d}t$ is the energy released by gravitational contraction. This term vanishes for stars in thermal equilibrium. As mentioned collision remnants are out of thermal equilibrium and the effect of $\varepsilon_{\rm art}$ is to specify $T\mathrm{d}S/\mathrm{d}t$. A suitable form is given by

$$-T\frac{\mathrm{d}S}{\mathrm{d}t} + \varepsilon_{\rm art} = T\frac{\Delta S}{\tau}, \tag{2.5}$$

where ΔS is the difference in entropy between the current model and the target model and τ is an artificial timescale on which the adjustment is to be made. With this choice an equilibrium is reached when the entropy profile

in the model matches that of the target model, $\Delta S = 0$. The timescale τ is arbitrary in principle and can be chosen to change the relative weight of the terms in the energy equation, which affects the speed of convergence. Choosing τ to be of the order of the current timestep was found to work well.

At the same time, the composition profile is changed smoothly by setting

$$X \rightarrow (1 - \lambda)X + \lambda X_{\rm target}, \tag{2.6}$$

where λ is increased monotonically from 0 to 1 in the course of the run. Composition changes due to nuclear reactions and mixing processes were ignored. We continue this procedure until the entropy and composition profiles in the model match those of the collision product. The final model is then used as a starting model for the evolution of the merger remnant.

This implicit scheme is very stable and flexible, and deals well with small irregularities in the output. Figure 2.1 shows that the resulting entropy and composition profiles agree very well with the target profiles. Except for the entropy profile in the core the two curves overlap within the thickness of the lines shown. We have tested whether small deviations like these affect the long-term evolution of the collision product and have found that they are unimportant.

Detailed SPH calculations do not have sufficient resolution to resolve the outer parts of the envelope of the collision product and MMAS likewise does not have any real information about this region. This means that the structure of the outer envelope cannot be determined from these models. Sills et al. (1997) extrapolated the entropy profile and used the condition of hydrostatic equilibrium to reconstruct the outer layers. We have found it easier to assume that these layers are in thermal equilibrium and have not tried to impose a particular entropy profile in these layers. This is reasonable considering that the local thermal timescale is short compared to that of the rest of the star. Because we do not enforce a large entropy on the outer layers our models are somewhat less inflated than those of Sills et al. (1997) and consequently start at a lower luminosity. As pointed out by Sills et al. (1997) the long term evolution of the collision product is determined by the interior properties and is not sensitive to the assumptions made for the outer layers. Comparing their evolution tracks of collision products to tracks computed with our code for the same masses and metallicity confirms this. We find that the contraction timescales are similar and that the tracks agree from the main sequence onward.

In this work we ignore rotation in the collision products by assuming that all collisions are head-on. In the more realistic case of off-centre collisions the effect of rotation on the evolution of collision products can be substantial, as outlined in §2.1. We choose to ignore this problem for the moment and we defer a discussion of this limitation until §2.5.2.

2.2.4 The BSE/NBODY4 prescription

We will compare the outcome of our detailed evolution models with the results obtained in the N-body calculations of Hurley et al. (2005). These calculation were performed using the NBODY4 code Aarseth (1999) in which binary evolution is provided by the Binary Star Evolution (BSE) algorithm (Hurley et al. 2002). In this algorithm a simple analytic prescription is used to model the outcome of stellar collisions where no mass is lost during the collision, i.e. the remnant mass is M_1+M_2. The merger remnant is replaced by a normal evolved main-sequence star with a starting age t' given by

$$t' = \frac{1}{10}\frac{\tau_{\rm ms}}{M_1+M_2}\left(M_1\frac{t}{\tau_{\rm ms,1}} + M_2\frac{t}{\tau_{\rm ms,2}}\right), \tag{2.7}$$

so that the remaining lifetime of the collision product is $t_{\rm ms,BSE} = \tau_{\rm ms} - t'$. Eq. (2.7) is based on the implicit assumption that the remnant is fully mixed. Here $\tau_{\rm ms,1}$, $\tau_{\rm ms,1}$ and $\tau_{\rm ms}$ are the main-sequence lifetimes of the two colliding stars and of a normal star with mass $M_1 + M_2$, respectively. These lifetimes are calculated according to the analytic formulae of Hurley et al. (2000) which are based on detailed models that include convective overshooting (Pols et al. 1998).

2.3 Evolution of the merger remnants

The masses M_1 and M_2 of the colliding stars and the time of collision t are taken from the N-body simulation of M67 by Hurley et al. (2005) and are listed in Table 2.1. The collisions listed as 3289-2 and 3835-2 are further collisions between a collision product and another main sequence star. In the case of 3289-2 this results in a collision product that is more than twice as massive as the most massive progenitor star. The most massive collision product in our list, however, is 2203.

We have constructed starting models for the calculation of the evolution of the collision products in Table 2.1 using the method described in §2.2. All models are calculated for an initial hydrogen mass fraction $X = 0.70$ and a mass fraction of heavy elements $Z = 0.02$. For the double collisions 3289 and 3835 we have used the output of the first collision as input for the second collision. All collision products were then allowed to evolve until the tip of the giant branch.

For each evolution model based on the MMAS output we have calculated two evolution tracks for comparison. One is a star with the same mass as the collision product that is evolved from the ZAMS at composition $X = 0.70$ and $Z = 0.02$, the other is a homogenised version of the collision product.

Table 2.1 also lists the total remnant mass M according to MMAS, the remaining main-sequence lifetime $t_{\rm ms}$ according to our detailed evolution

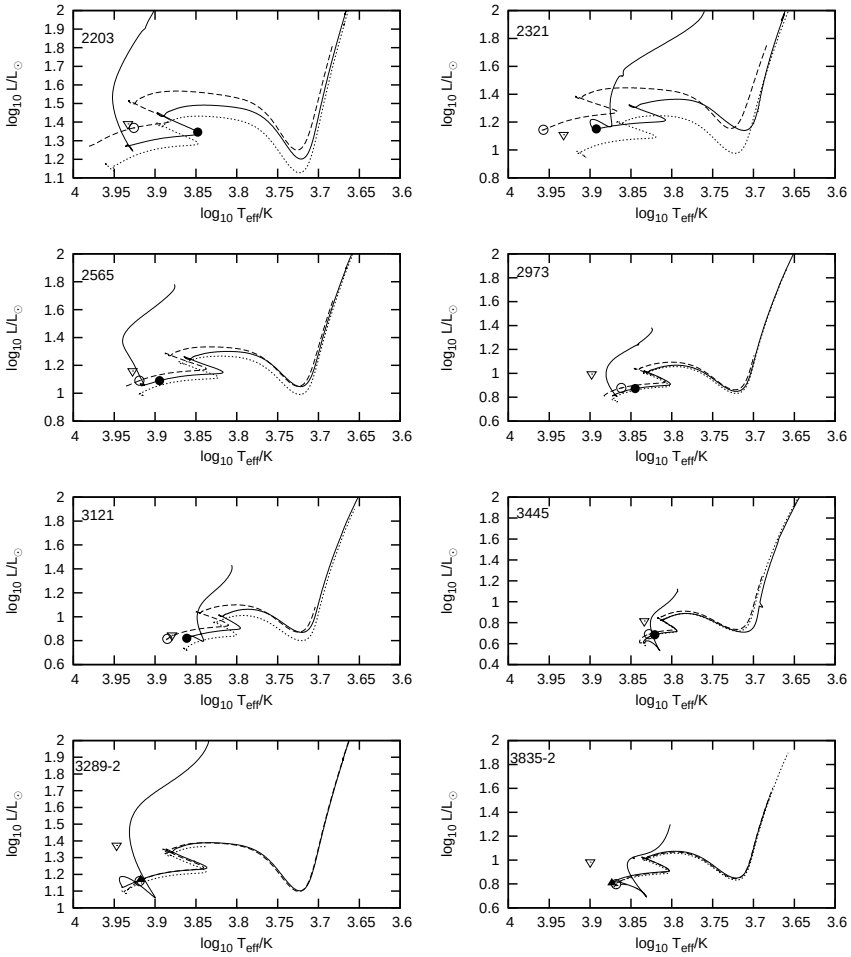

Figure 2.2: *Evolution tracks for the collision products (solid lines) compared to tracks for homogenised models (dashed lines) and a main sequence star of the same ZAMS mass (dotted line). Also marked are the positions at* 4 Gyr *for the detailed models (• for remnants of a single collision and ▲ for the remnants of two collisions), the homogenised models (⊙) and the BSE prescription (▽).*

models, the main-sequence lifetime $\tau_{\rm ms}$ of a star with the same ZAMS mass and the lifetime of a homogenised version of the collision product, $\tau_{\rm ms,hom}$. The lifetimes listed for 3289-1 and 3835-1 are the lifetimes these merger remnants would have had if they had not been involved in a second collision. Also given in Table 2.1 is the remaining lifetime according to the BSE prescription, $t_{\rm ms,BSE}$ (see §2.4 for a comparison and discussion).

In Figure 2.2 we have plotted the evolution tracks of our models in the Hertzsprung-Russell diagram. The solid lines are the evolution tracks of the detailed collision products while the dotted lines are the evolution tracks of the normal stars. The homogenised models are indicated by a dashed line. We see that in general, the homogenised models are hotter and brighter than the normal models, while the collision products tend to be brighter than the normal stars but less luminous than the homogenised models. This is an opacity effect, as will be discussed below.

2.3.1 Initial structure and contraction phase

Initially, all collision products have a large amount of excess thermal energy and the star's main energy source is gravitational contraction. We refer to this initial phase where the collision product is puffed up and out of thermal equilibrium as the contraction phase.

There is no significant mixing during the collision. This can lead to composition inversions in the remnant: the core is rich in helium, on top of which there is a hydrogen-rich layer above which there is again a helium-rich layer of material from the core of the primary. These composition inversions show up in models where the primary star is sufficiently evolved to have burned a significant fraction of its central hydrogen to helium while the secondary is relatively unevolved, *i.e.* where the secondary is much less massive than the primary. Consequently, they are present in models 2203, 2321 and 3121 as well as the two double mergers 3289 and 3835, although the composition inversions are small in this case. As mentioned in section 2.2.2, a composition inversion of this type is secularly unstable and leads to thermohaline mixing. This homogenises part of the central region of the remnant.

As an illustrative example, we will discuss in more detail the various evolutionary stages of the collision product 2321. This exhibits many of the transient features that occur during the evolution of these collision products.

First we consider the composition profile for collision 2321 which is shown in Figure 2.3. During the collision a large portion of the core of the $1.29M_{\odot}$ primary has sunk to the centre, creating a hydrogen poor core below mass coordinate $0.1M_{\odot}$. Above this region material is slightly mixed with material from the $0.59M_{\odot}$ secondary, leading to a hydrogen-rich layer between 0.2 and $0.4M_{\odot}$. On top of this there is a helium-rich layer at mass coordinate $0.6M_{\odot}$. Between this layer and the surface of the star the

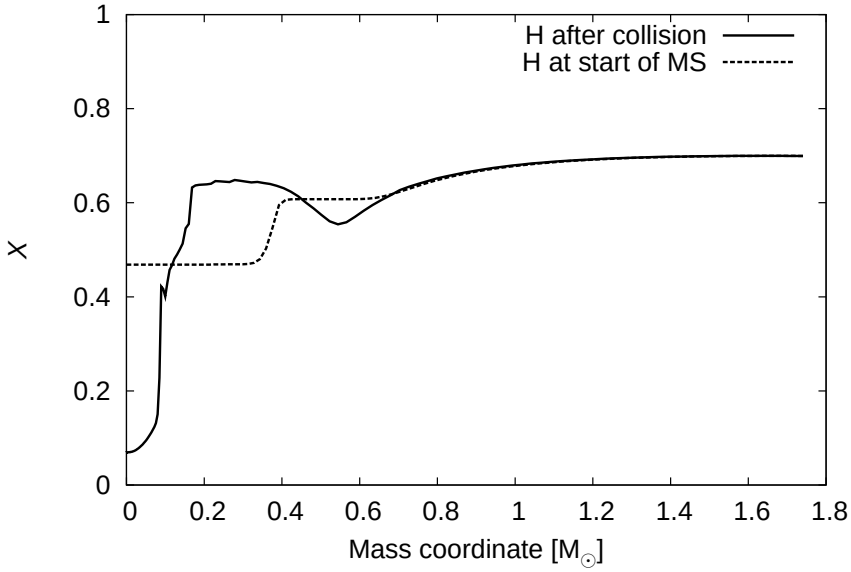

Figure 2.3: *Composition profiles in the merger remnant 2321, immediately after the collision (solid line) and on reaching the main sequence (dashed line).*

composition tends to the primordial composition.

The helium-rich layer at $0.6M_{\odot}$ is unstable to thermohaline mixing, which will mix the helium inward while the star contracts to the main sequence. At the same time, hydrogen will reignite in a shell at $0.1M_{\odot}$. This burning shell forms as a result of a peak in the hydrogen burning rate due to the steep increase of the hydrogen abundance in this region. The shell drives a convection zone that connects to the thermohaline layer and mixes the inner $0.4M_{\odot}$ of the star. This mixes helium-rich material into this burning shell which has the effect of lowering its efficiency. By the time the merger remnant has reached the main sequence the burning shell has extinguished. We define the end-point of the contraction phase as the moment where central hydrogen burning takes over as the main energy source and the star is in thermal equilibrium.

At this point the central hydrogen abundance has increased to a mass fraction of 0.46 and the composition profile has changed to the dashed line in Figure 2.3. The collision product has a convective core on the main sequence that extends to about $0.2M_{\odot}$.

The evolution of the core is shown in Figure 2.4, where the central temperature $T_{\rm c}$ is plotted against the central density $\rho_{\rm c}$. The short-dashed lines

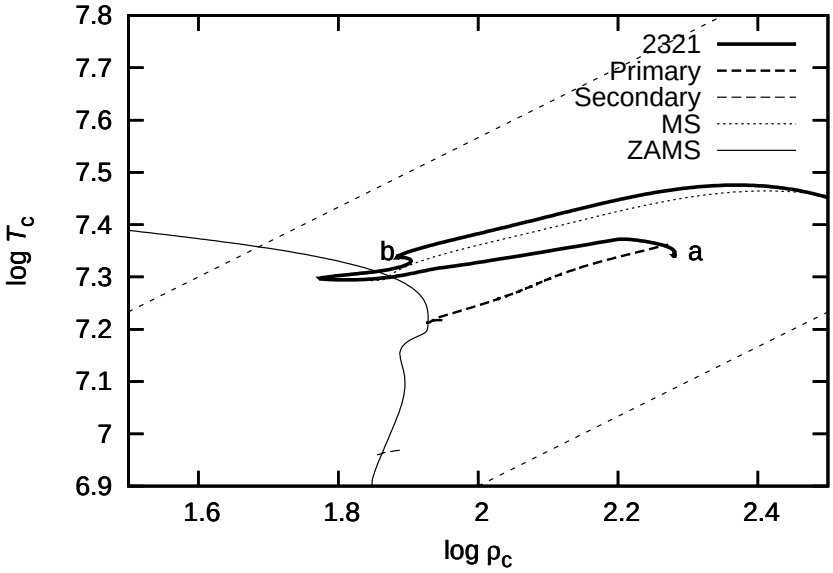

Figure 2.4: *Evolution track for the collision product 2321 in a ρ_c–T_c diagram (thick solid line). Also plotted are the progenitor tracks (dashed lines), the track for a star with the same ZAMS mass as the collision product (dotted line) and the location of the ZAMS (thin solid line). The short-dashed lines represent lines of constant entropy for a given composition. The collision product starts with an overdense core at the point labeled a and reaches the main sequence at point b.*

indicate lines of constant entropy with entropy increasing in the direction of increasing temperature and decreasing density. The core starts at point *a* with an entropy that is close to that of the core of the former primary. This means that the core has an entropy that is too low for a star of its mass and it will need to increase its entropy before the star can come into thermal equilibrium. This increase in entropy is achieved by expansion, which means that the core moves to the left in the diagram until it reaches the correct adiabat. At this point the core starts to contract again until thermal equilibrium is finally reached at point *b*. At this point the core is slightly hotter than the core of a star that was born with the same ZAMS mass.

2.3.2 Main sequence evolution

After the contraction phase the collision products follow more or less normal main-sequence tracks, although their luminosity (Figure 2.2) and central temperature (Figure 2.4) are typically higher than they would have been for a main sequence star of the same ZAMS mass. This is owing to the helium enhancement in their envelopes, which increases the mean molecular weight μ. The luminosity $L_{\rm merger}$ of the collision product scales with the luminosity of a normal star according to the homology relation (Kippenhahn & Weigert 1990)

$$L_{\rm merger} \approx L_{\rm ms} \left(\frac{\mu_{\rm merger}}{\mu_{\rm ms}} \right)^4 , \tag{2.8}$$

with $\mu_{\rm merger}$ and $\mu_{\rm ms}$ the mass-averaged mean molecular weight in the collision product and the main sequence star when these have the same effective temperature. The homology relation (2.8) is strictly valid only for homogeneous stars with constant opacity but it reproduces the luminosity shift of the merger remnants with respect to normal main sequence stars very well.

The higher effective temperature of the homogenised models results from a reduction of the average opacity owing to the increased helium content of their envelopes. The opacity affects the stellar structure by increasing or decreasing the photon mean free path. In the weakly mixed collision products, most of the helium enhancement is in the compact interior while the more extended envelope has the normal ZAMS composition. Thus, throughout most of the volume of the star a photon will 'see' a normal hydrogen rich composition and the opacity is not strongly affected. Conversely, in the homogenised models the helium enhancement is present in the entire envelope and a photon will 'see' a helium-enhanced composition with a lower opacity, leading to a more compact structure.

Because the luminosity is enhanced the collision products do not lie exactly on the extension of the main sequence, but can lie somewhat above it. As a consequence of their higher luminosity, the central temperature of the collision products is slightly increased (see Fig. 2.4) and the main-sequence lifetime (*i.e.* the time until core hydrogen exhaustion) is reduced compared to the lifetime of a normal main sequence star with a similar composition in the core.

2.3.3 Hertzsprung gap and first giant branch

We follow the evolution of the collision products through the Hertzsprung gap up to the tip of the giant branch. We were unable to calculate models beyond the helium flash.

The red giant phase is very similar to that of a normal star. The first dredge-up occurs when the convective envelope penetrates into the helium-rich layer. For our example collision product 2321 this increases the surface

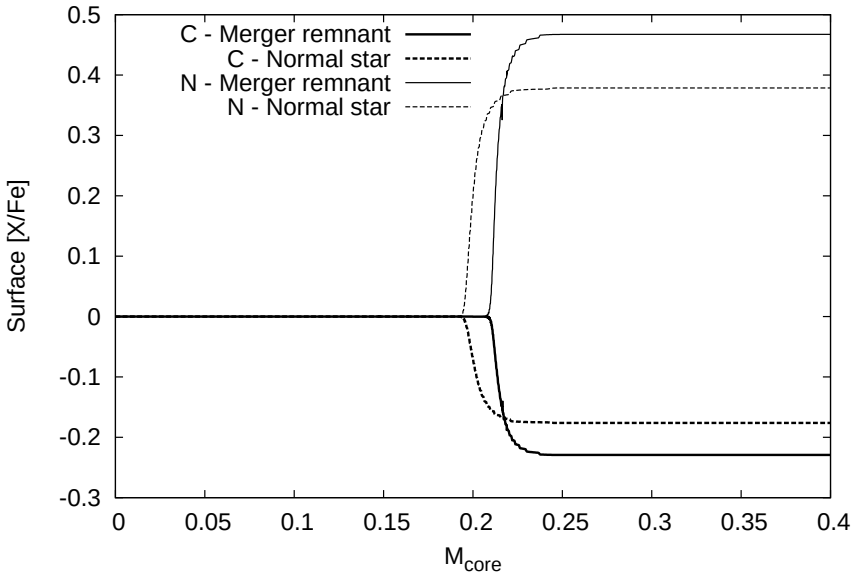

Figure 2.5: *Surface [C/Fe] and [N/Fe] abundances as a function of the helium core mass (as a measure of age) for collision product 2321. The carbon abundance (thick solid line) in the collision product is depleted when compared to a normal red giant (thick dashed line) while the nitrogen abundance (thin lines) is correspondingly enhanced.*

helium abundance to $Y_{\rm s} = 0.334$ compared to $Y_{\rm s} = 0.296$ in a normal red giant of the same mass. More of the dredged-up material has undergone processing than in a normal red giant because part of this material comes from the core of the original primary. As a result, more carbon has been converted to nitrogen by CN cycling, which enhances the nitrogen abundance and depletes the carbon abundance compared to a normal red giant, both by ~ 0.1 dex in the case of collision 2321 as shown in Figure 2.5. Unfortunately this does not exceed the typical observational error bar of 0.15 dex (for instance Gratton et al. 2000).

2.3.4 Double collisions

In the N-body simulation two blue stragglers are present at $t = 4$ Gyr that resulted from consecutive collisions between three stars in a binary-binary interaction. In both cases the second collision happened almost immediately after the first. We have not considered the situation where the time between collisions is long enough for the collision product to have evolved before the

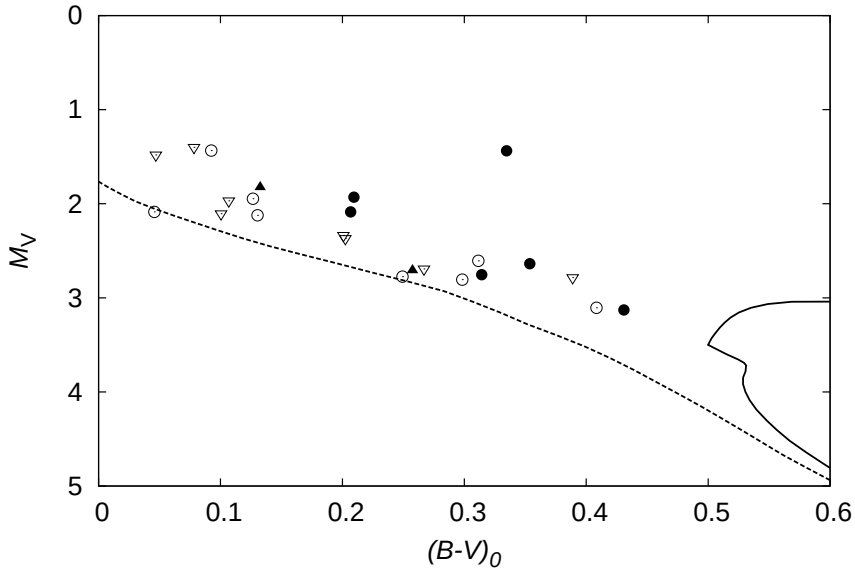

Figure 2.6: *Location in the colour-magnitude diagram of the blue stragglers at* 4Gyr. *Detailed models of the single collision remnants are indicated by* • *and double collision remnants by* ▲. *Homogenised models are indicated by* ⊙ *and the BSE prescription is indicated by* ▽. *The isochrones for* $t = 0$ *and* $t = 4$Gyr *are constructed from the models by Pols et al. (1998).*

second collision. We have calculated the outcome of the first collision and used that as input for the second collision. These double collision remnants evolved in a similar way to single collision products and their main sequence evolution is very similar to that of ordinary stars of their mass. This can be understood from the fact that their progenitors are all fairly low-mass stars that are essentially unevolved at the time of collision. For this reason collision product 3289-2 has the highest effective temperature (Fig. 2.2) and the bluest colour (see Fig 2.6 in §2.4), even though it is not the most massive collision product. It is likely that the structure and evolution of double collisions involving more massive and thus more evolved stars, or with more time passing between the collisions, will produce remnants that stand out more. The bluest blue straggler in M67 (S977; Mathys 1991) is quite possibly the result of a double collision.

2.4 Comparison of different methods

In Fig. 2.2 we show as solid symbols the locations in the Hertzsprung-Russell diagram of each of the merger products listed in Table 2.1 after 4 Gyr (the age of M67 obtained by isochrone fitting in Pols et al. 1998) and compare these to the locations of the homogenised models (open symbols) and the positions according to the BSE prescription (triangles). In Figure 2.6 we show the corresponding locations for all collision products in a colour-magnitude diagram. A comparison between the observed blue stragglers and our models is given in paper II. We converted the theoretical surface parameters (L, $T_{\rm eff}$ and $\log g$) to observable magnitude and colour (M_V, $B-V$) using model atmospheres from Kurucz (1992) with empirical corrections from Lejeune et al. (1997). Also shown is the location of the ZAMS (dashed line) and the $t = 4$ Gyr isochrone from Pols et al. (1998). The detailed models are redder than the homogenised models and the positions predicted by the BSE recipe, with the largest difference occurring for the brightest and most massive blue stragglers.

The homogeneous models are bluer than the detailed models for two reasons. First, the helium abundance in the envelopes of the homogeneous models is enhanced over that of the detailed models, which moves the position of the ZAMS line to the blue. Second, if we compare the lifetimes listed in Table 2.1 we see that the remaining lifetime for the homogenised models is longer than that of the detailed models, so that the homogenised models are closer to their zero-age main sequence. This is particulary striking in remnant 2203 (Fig. 2.2), for which the detailed model has almost reached the terminal-age main sequence point. The longer lifetime of the fully mixed models is due to the larger hydrogen abundance in their cores compared to the detailed models. The largest discrepancy is found for progenitor stars that were substantially evolved at the time of collision, in particular remnant 2321. The best match between detailed and fully mixed models is obtained for the double collision remnants, whose progenitor stars were not very evolved. In general the approximation of homogeneous mixing is worse for collisions involving more evolved stars than for collisions involving less evolved stars.

The BSE recipe gives locations that are brighter and bluer mainly because mass loss from the collision is not considered, leading to higher remnant masses. As can be seen from Figure 2.2 this effect is most noticeable in remnants 2973 and 3445 and the two double collision remnants 3289-2 and 3835-2. Because BSE simply uses a normal main-sequence star model for the collision remnant, the effect of the higher mass on the luminosity is at least partially compensated by neglecting the effect of helium enhancement.

The BSE prescription assumes complete mixing to estimate the remaining lifetime of the merger remnant. The BSE lifetimes are generally longer than those of both our detailed models (by more than a factor 2 in the

case of remnant 2321) and the fully mixed models, despite the fact that the overestimate of the remnant mass by BSE would result in an underestimate of the lifetime by 20–30 per cent. This is, however, counteracted by two effects when compared to our fully mixed models. First, the neglect of helium enhancement leads to an increase of the lifetime by up to 30 per cent for collision remnants of evolved progenitor stars. Second, the inclusion of convective overshooting in the BSE models gives rise to longer main-sequence lifetimes, by 25–30 per cent in the mass range considered (see §2.5.2 for a discussion of this issue). A fairer comparison of the BSE *method* is to compute the remnant lifetime using eq. (2.7) but inserting main-sequence lifetimes of non-overshooting models; we then find BSE lifetimes that are indeed somewhat smaller than those of our fully mixed models.

The homogeneous models and the BSE prescription can both produce blue stragglers that are brighter and bluer than those produced by the detailed models. In the case of the BSE models this is due to the higher mass of the collision products, while in the case of the homogeneous models this is due to the higher helium content of their envelopes. This implies that in order to form the brightest blue stragglers it may be necessary to collide more massive progenitor stars, or that enhanced mixing in the collision products (for instance due to rotation) is necessary.

2.5 Discussion

2.5.1 Convective Overshooting

There is evidence that for ordinary stars in the mass range we consider mixing extends beyond the boundary of the classical convective core, which is usually modelled by convective overshooting as discussed in Schröder et al. (1997). As mentioned in section 2.2.2, we have disabled convective overshooting for the evolution of the merger remnants. During the contraction phase in some of the remnants, regions develop where $\nabla_{\rm rad} - \nabla_{\rm ad}$ is close to zero but remains negative ($\nabla_{\rm rad} - \nabla_{\rm ad} > -\delta$), so that these regions never actually become convective. The overshooting prescription used in our code leads to undesired spurious mixing in such regions.

Convective overshooting affects the lifetime and the shape of the main-sequence track of a star. The progenitor stars will mostly not be overly affected by overshooting (because their masses are too small to develop convective cores), whereas the collision product is massive enough to experience overshooting. The main difference we expect is that for two given parent stars the collision product will have a larger reservoir of hydrogen and live longer. The inclusion of overshooting in our detailed models would likely make the collision remnants of evolved parent stars (such as 2203) somewhat bluer, because the enhanced mixing brings the remnant closer to

its ZAMS position. More importantly, the lifetimes of all our collision products would be increased, perhaps by about 30 per cent (based on comparing overhooting and non-overshooting models from Pols et al. 1998).

2.5.2 Rotation

We have ignored rotation in the present work by treating all collisions as head-on. Rotation will modify our results by extra mixing and possibly by enhanced mass loss. The latter is particularly relevant because off-centre collisions produce remnants that have so much angular momentum that their rotation rate will approach critical rotation during the contraction phase. How the remnant loses angular momentum is still an unsolved problem and it is likely that magnetic fields play a role here, possibly by coupling the star to a circumstellar disk (Sills et al. 2005). At present, nothing is known about the magnetic field in the collision product after the collision.

Rotational mixing provides a larger hydrogen reservoir for nuclear burning and increases the helium content in the envelope, making the remnants bluer and brighter and extending their lifetimes (Sills et al. 2001). By ignoring rotation we implicitly assume that an efficient spin-down mechanism operates in the collision products such that they avoid both the angular momentum problem and significant rotational mixing. It is significant that the blue stragglers in M67 are slow rotators, with projected rotation velocities smaller than typical for their spectral type (Peterson et al. 1984; Mathys 1991). Since all formation mechanisms for blue stragglers are expected to result in rapid rotation, this suggests that they can indeed lose angular momentum efficiently. We will investigate this problem in more detail in future work.

2.6 Conclusions

Hydrodynamical simulations of stellar collisions produce remnants that are out of thermal equilibrium and are not fully mixed. We have developed an efficient procedure for importing the structural and chemical profiles of such collision products into a fully implict stellar evolution code. Our evolution code is fairly robust and can evolve the collision remnants until the tip of the giant branch with a minimum of human intervention. We have applied our code to construct detailed models of collisional blue stragglers formed in the N-body simulation of M67 by Hurley et al. (2005).

The evolution of collision products depends on the amount of mixing during the collision and the thermal relaxation phase. Assuming the collision product has been homogeneously mixed produces evolution tracks that are too blue while replacing the collision product with a normal star of the same mass (as done in the simulations of Hurley et al. 2005) produces an evolu-

tion track that is not bright enough. Both approximations overestimate the lifetime of the collision product. These considerations will affect the predicted colour-magnitude diagram distribution of collisional blue stragglers from a cluster simulation.

Our code is suitable for a systematic exploration of the wide parameter space of collisions in clusters of different ages. This will be the topic of future papers. Eventually we hope to integrate our code into a full N-body code to allow for more realistic and self-consistent star cluster simulations.

2.A Entropy sorting

The entropy s of a multi-component ideal gas can be written as (Landau & Lifshitz 1980; Pols et al. 1995)

$$s = \frac{5}{2} k_{\rm B} N + k_{\rm B} \sum_i N_i \log \left[\frac{(m_i k_{\rm B} T)^{3/2}}{(2\pi\hbar^2)^{3/2}} \frac{\omega_i}{n_i} \right], \tag{2.9}$$

where N is the total number of particles, N_i is the number of particles of species i, n_i is their number density and m_i is their mass. The sum runs over all types of particles present (including electrons). The parameter ω_i is the degeneracy of the ground state and is 1 except for electrons, where it is 2. Introducing the particle number fraction $Y_i = N_i/N$ this can be rewritten as

$$\frac{s}{k_{\rm B} N} - \frac{5}{2} = \log \left\{ \left(\frac{P}{\rho^{5/3}} \right)^{3/2} \frac{\mu^4 m_{\rm u}^4}{(2\pi\hbar^2)^{3/2}} \prod_i \left[\left(\frac{B_i}{\mu} \right)^{5/2} \frac{\omega_i}{X_i} \right]^{Y_i} \right\}. \tag{2.10}$$

Here μ is the mean-molecular weight and B_i is the atomic mass of species i in atomic units. X_i is the mass fraction of species i and the parameter ω_i is the degeneracy of the ground state and is 1 except for electrons, where it is 2. We will simplify the notation by absorbing the composition dependence in a single factor C defined by

$$C \equiv \mu^4 \prod_i \left[\left(\frac{B_i}{\mu} \right)^{5/2} \frac{\omega_i}{X_i} \right]^{Y_i}. \tag{2.11}$$

The stability criterion for a fluid subject to an adiabatic perturbation in pressure equilibrium is

$$\frac{{\rm d}\rho}{{\rm d}r} - \left. \frac{{\rm d}\rho}{{\rm d}r} \right|_{\rm ad} < 0. \tag{2.12}$$

Using (2.10) this gives the condition

$$\left(\frac{\partial \rho}{\partial s} \right)_{P,C} \frac{{\rm d}s}{{\rm d}r} + \left(\frac{\partial \rho}{\partial C} \right)_{P,s} \frac{{\rm d}C}{{\rm d}r} < 0, \tag{2.13}$$

which can be rewritten as

$$\frac{\mathrm{d}s}{\mathrm{d}r} - \left(\frac{\partial s}{\partial C}\right)_{P,\rho} \frac{\mathrm{d}C}{\mathrm{d}r} > 0. \tag{2.14}$$

This is essentially the Ledoux criterion, expressed in s rather than the more familiar T. Evaluating the thermodynamic derivatives this reduces to

$$\frac{\mathrm{d}s}{\mathrm{d}r} - \frac{\mathrm{d}\log C}{\mathrm{d}r} > 0. \tag{2.15}$$

The left hand side can be recognised as the total derivative of a function $\log A^{3/2}$ with A given by (2.1). So the stability condition in this case is

$$\frac{\mathrm{d}A}{\mathrm{d}r} > 0. \tag{2.16}$$

2.B Modifications to the evolution code

It is a feature of the STARS code that it solves the stellar structure equations simultaneously with the reaction-diffusion equations for the different abundances on a moving mesh. The code is normally fast and reliable, but we have found that it sometimes has difficulty evolving our merger remnants and have come up with a scheme that helps it evolve through "difficult" timesteps.

Consider the set of independent variables $\vec{H}$ that represents a solution to the stellar structure equations at time t. The problem is then to find the changes $\Delta\vec{H}$ such that $\vec{H} + \Delta\vec{H}$ represents the solution at time $t + \Delta t$. An initial guess for ΔH can be taken from the previous timestep and then improved by iteration in a Henyey-like solver. If no solution can be found, a smaller timestep can be tried. In some cases, this leads to a runaway situation where repeated convergence failures cause the timestep to drop until it drops below a threshold value and the code aborts.

The cause of the convergence failure is that the initial guess for the corrections $\Delta\vec{H}$ is not close enough to the desired corrections. We have looked for ways to improve the initial guess in case of convergence failure.

Often it is possible to identify the terms in the equations that cause difficulty. A common example are the diffusion terms in the reaction-diffusion equations,

$$\frac{\mathrm{d}X_i}{\mathrm{d}t} = -\frac{1}{\rho r^2}\nabla\rho r^2\sigma\nabla X_i + R_i, \tag{2.17}$$

where X_i represents the abundance of species i, σ is the sum of all diffusion coefficients affecting the composition and R_i is the production (or destruction) rate of species i due to nuclear reactions. In case of convergence problems, it can help te eliminate or reduce ("relax") the diffusion

coefficient σ. The resulting corrections $\Delta\vec{H}'$ are not the final corrections, but they might be a better first guess than the values used previously.

Convective mixing is the most common example where our above relaxation scheme is useful, but it is by no means the only one. Other examples where we have found it useful in our code are the nuclear energy generation rate (which is then relaxed from the value at the previous timestep), the mass loss rate and advection terms in the luminosity equation.

3

A grid of low-mass collisions

In a chapter 2 we studied the detailed evolution of stellar collision products that occurred in an N-body simulation of the old open cluster M67 and compared our detailed models to simple prescriptions. In this paper we extend this work by studying the evolution of the collision products as a function of mass and age of the progenitor stars.

We calculated a grid of head-on collisions covering the section of parameter space relevant for collisions in open clusters. We create detailed models of the merger remnants using an entropy-sorting algorithm and follow their subsequent evolution during the initial contraction phase, through the main sequence and up to the giant branch with our detailed stellar evolution code. We compare the location of our models in a colour-magnitude diagram to the observed blue straggler population of the old open clusters M67 and NGC 188 and find that they cover the observed blue straggler region in the colour-magnitude diagram of both clusters. For M67, collisions need to have taken place recently. Differences between the evolution tracks of the collision products and normal main sequence stars can be understood quantitatively using a simple analytic model. We present an analytic recipe that can be used in an N-body code to transform a precomputed evolution track for a normal star into an evolution track for a collision product.

3.1 Introduction

Star clusters are important laboratories for a wide range of astrophysical processes. It has become clear that the evolution of a star cluster is driven by the complex interplay between stellar dynamics and stellar and binary evolution (Portegies Zwart et al. 1999; Hurley et al. 2001). Physical collisions between stars in the dense cluster core play a pivotal role in this

interaction. The products of stellar collisions between main-sequence stars potentially stand out as blue stragglers in a colour-magnitude diagram. The blue straggler population of a cluster can therefore be used to study its dynamical history. Since stellar collision products generally have a very different thermal and chemical structure than normal main-sequence stars (Lombardi et al. 1996), detailed calculations of their evolution are required (Sills et al. 1997, 2001).

In a previous paper (Glebbeek et al. 2008) we have developed an efficient procedure to import detailed models of stellar collision products into a fully implicit stellar evolution code and to evolve the remnants well beyond the main sequence. Our work is similar to that of Sills et al. (1997) but our code is faster and much more robust, allowing for the first time a systematic study of stellar merger remnants and an exploration of the parameter space. Glebbeek et al. (2008) studied the evolution of collision remnants that occurred in the N-body simulation of M67 by Hurley et al. (2005) and compared these with the evolution tracks predicted by the prescription of Hurley et al. (2002) as well as tracks of fully mixed versions of the remnants. We found that our merger remnants have shorter main-sequence lifetimes than predicted by either the Hurley et al. (2002) prescription or the fully mixed models. Our models are also brighter than normal stars of the same mass, but not as blue as fully mixed models.

In this work we explore the parameter space for collisions between low-mass main sequence stars relevant for blue straggler formation in old open clusters (such as M67) and place the findings of Glebbeek et al. (2008) in context. A large grid of stellar collisions covering this parameter space was calculated by Freitag & Benz (2005). They mainly focussed on collisions with high impact velocity suitable for the galactic centre and their simulations had insufficient resolution to resolve mixing due to the collision. Our work complements theirs by investigating the mixing as well as the long term evolution of the merger remnants. We describe the detailed structure and evolution of the collision products and discuss their dependence on the collision parameters (masses and time of collision) in §3.4. We compare the results of our models with observations of blue stragglers in the open clusters M67 and NGC188 in §3.5. Finally, we show how the global properties of the collision products (luminosity, radius and lifetime) can be described by a simple analytic prescription that can be included in a parametric model of stellar collisions and in N-body simulations (§3.6). We discuss our results in §3.7.

3.2 Initial conditions and parameters of the collisions

The structure of a merger remnant depends on the structure of the two parent stars, the impact parameter of the collision and the relative velocity at infinity. The structure of the parent stars depends on their masses, chemical composition (characterised by their heavy-element content Z) and their evolutionary stage. In this work we have restricted ourselves to a section of this 8-dimensional parameter space.

First of all we assume that the two stars involved in the collision are coeval in the sense that both are at the zero-age main sequence (ZAMS) at $t = 0$ and have the same initial composition, which is a reasonable assumption for stars in clusters. Placing $t = 0$ at an earlier stage, *e.g.* the onset of deuterium burning rather than the ZAMS, will not greatly affect the outcome of our calculations because appreciable composition gradients only build up on the main sequence and we consider a fairly small mass range. We restrict ourselves to collisions between low-mass main sequence stars (by which here we mean that their combined mass does not exceed $2.4M_{\odot}$, see below) and consider only head-on collisions (i.e., with impact parameter $b = 0$), in essence meaning that we ignore the effect of rotation in the collision product. This is despite the fact that rotation can be of considerable importance for the structure and evolution of the collision product: even for collisions with a small impact parameter the remnant has sufficient angular momentum that a main sequence star of the same mass would need to rotate faster than its breakup rate (Lombardi et al. 1996; Sills et al. 1997). The physical mechanism and timescale on which the collision products lose their angular momentum are unclear. Methods to incorporate the effect of rotation in a one dimensional stellar evolution code treat rotation as a perturbation to a non-rotating stellar model (Endal & Sofia 1976; Pinsonneault et al. 1989; Zahn 1992; Heger et al. 2000). These methods are accurate for rotation rates less than about 60% of the critical (Keplerian) value (Yoon et al. 2004) and it is not clear how to model stars that are even closer to critical rotation. We plan to investigate this problem in future research.

This leaves us with four parameters: the composition, the time of collision t and the masses of the two progenitors. Borrowing nomenclature from the field of binary evolution, we refer to the more massive progenitor as the primary and write its mass as M_1. Similarly we refer to the less massive progenitor as the secondary and denote its mass by M_2. With these definitions we can introduce the total initial mass $M = M_1 + M_2$ and the mass ratio $q = M_2/M_1$. To calculate a grid of models we have used the independent parameters Z, t, M and q. We have calculated several grids covering different parts of this parameter space, as listed in Table 3.1. The

Table 3.1: *Values used for the different grid parameters. The grid spacing is listed between parentheses. Note that the grids labelled* M67 *and* NGC188 *overlap in part of their age range. We have calculated models for two extra mass ratios for a limited mass range in the* M67 *grid to more clearly resolve trends at high and low mass ratios.*

Name	Z	t[Myr]	$M[M_\odot]$	q
M67	0.02	2800, 3100, 3400, 3700	1.5–2.4 (0.1)	0.4–1.0 (0.2)
			1.5–2.0 (0.1)	0.5, 0.9
NGC188	0.02	3400, 3700, 4200, 4700, 5200, 5700	1.2, 1.3, 1.4, 1.6, 1.8, 2.0, 2.2	0.4–1.0 (0.2)
GC	0.001	8000–12500 (1500)	0.8–1.3 (0.1)	0.4–1.0 (0.2)

grid labelled *M67* covers the parameter space sampled by the N-body simulation of Hurley et al. (2005) and is relevant for old open clusters like M67. An extension to the *M67* grid is the parameter set labelled *NGC188*, which covers the parameter range of interest for the somewhat older open cluster NGC188. Both these grids use an assumed heavy-element content $Z = 0.02$ and an initial hydrogen abundance $X = 0.70$. The total initial masses for the collision products were chosen such that the lower limit is just above the present-day turnoff mass and the upper limit is roughly twice the turnoff mass ($1.18M_\odot$ for NGC188, $1.29M_\odot$ for M67); see §3.5.

We have also computed a grid (labelled *GC*) with $Z = 0.001$ and $X = 0.757$ that is suitable for comparison with globular clusters. In the presentation of our results we will mostly focus on the *M67* and *NGC188* grids but unless otherwise indicated our results apply to the $Z = 0.001$ grid as well.

3.3 Tools

The method we use in our study has been described in detail in a separate paper (Glebbeek et al. 2008) (hereafter Paper I), so we refer the interested reader to that paper for more details about the procedure of calculating the models and provide just a brief summary here.

For each collision we evolve models of the progenitor stars to the time of collision and then merge the two stars. The structure of the merger remnants is calculated using the Make Me A Star (MMAS) code developed by Lombardi et al. (2002). This code uses the realisation that in low mass stars the quantity

$$A = \frac{P}{\rho^{5/3}} \tag{3.1}$$

increases outward. The quantity A is closely related to the entropy and the tendency of A to increase reflects the tendency of low entropy material to sink to the centre of the collision product. For this reason the procedure by which the remnant profile is constructed is known as *entropy sorting*.

Our evolution code is a version of the STARS code developed by Eggleton (1971) and updated by others (Pols et al. 1995). Nuclear reaction rates are from Caughlan & Fowler (1988) and Caughlan et al. (1985) and we use opacities from Rogers & Iglesias (1992) and Alexander & Ferguson (1994). The assumed heavy-element composition is scaled to solar abundances (Anders & Grevesse 1989). Chemical mixing due to convection (Böhm-Vitense 1958; Eggleton 1972) and thermohaline mixing (Kippenhahn et al. 1980) is taken into account. All models are computed with a mixing-length ratio $l/H_P = 2.0$. As in Paper I, we have neglected convective overshooting in all models in this work.

3.4 Properties and structure of collision products

In this section we present the structure and evolution of the merger remnants. We will discuss how the structure of the parent stars affects the structure of the remnant. Details for all our collision models are listed in Table 3.4 for $Z = 0.02$ models and in Table 3.5 for $Z = 0.001$ models.

3.4.1 Mass loss from the collision

A fraction φ of the total mass $M_1 + M_2$ of the progenitor stars is lost during the collision. The fraction φ is, for central collisions, estimated in MMAS as

$$\varphi = C \frac{q}{(1+q)^2} \frac{R_{1,0.86} + R_{2,0.86}}{R_{1,0.5} + R_{2,0.5}}, \tag{3.2}$$

(Lombardi et al. 2002), where $R_{n,0.86}$ and $R_{n,0.5}$ are the radii containing 86% and 50% of the mass of parent star n (1 or 2). The constant $C = 0.157$ is determined by calibration to SPH calculations. Typical values of φ are in the order of a few percent. A reasonable approximation over the range of our grid is (see Table 3.4)

$$\varphi = 0.3 \frac{q}{(1+q)^2}. \tag{3.3}$$

Material lost from the stars in the ejecta originates from the envelopes of the parent stars and has the composition of the parent star envelope.

3.4.2 Structure of the progenitor stars

We can distinguish four different collision scenarios between main sequence stars based on the structure of the progenitor stars and the collision product. Low mass main sequence stars ($\lesssim 1.2M_{\odot}$) have radiative cores while main sequence stars of higher mass have a convective core. This leads to four possible scenarios for a collision:

1. Convective + Convective → Convective
2. Convective + Radiative → Convective
3. Radiative + Radiative → Convective
4. Radiative + Radiative → Radiative

The composition profile of a collision remnant is determined by the entropy profiles of the progenitor stars, which is in turn determined by their masses and their age. If a star has a convective core the material from the core will have a constant entropy, which directly affects the composition profile in the remnant and its subsequent evolution. In a star with a radiative core the entropy increases outward.

The first case will generate remnants with masses $> 2.4M_{\odot}$ and will be the topic of a future paper. The second case occurs in our grid for the higher mass collision products ($M > 1.7M_{\odot}$) at extreme mass ratios ($q > 0.5$) and is relevant for clusters where the turnoff mass is larger than $1.2M_{\odot}$. The third case makes up the majority of the collision products in our grid and is relevant for old open clusters as well as globular clusters. The main difference with case 2 is that in case 2 the core of the primary has an almost flat entropy profile whereas in case 3 the entropy profile is smoother. The final case is only relevant for clusters where the turnoff mass is below $1.2M_{\odot}$. In younger clusters the collision products of these collisions would be hidden among normal main sequence stars and not stand out as blue stragglers. The progenitor stars are essentially unevolved at the time of collision and the outcome of such a merger is a new unevolved main sequence star.

3.4.3 Composition profile

During a collision material from one parent star is mixed with material of the same entropy from the other star (since it ends up in the same location in the collision product). However, if one of the two stars has a convective core the material from the core can retain its identity because of the nearly flat entropy profile. This can lead to a very steep composition gradient in the remnant.

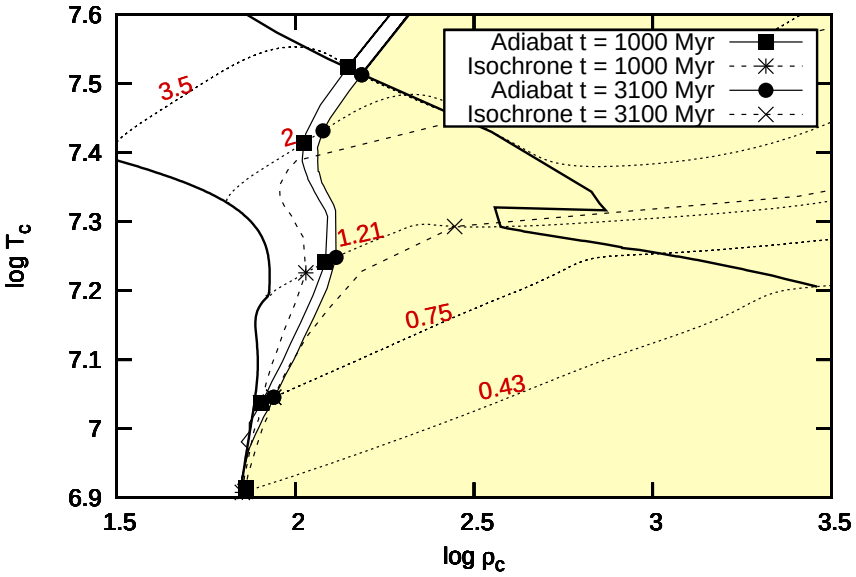

Figure 3.1: *Evolution tracks of low mass stars in the* $\log \rho_c$– $\log T_c$ *plane. Bold lines indicate the locations of the ZAMS (left) and TAMS (right). Dotted lines are evolution tracks, labelled with the ZAMS mass. The solid lines marked with* ■, ● *are lines of constant entropy across different stellar models, the dashed lines marked with* ∗, × *are isochrones. The shaded region indicates the region where the central entropy is lower than that of a* $0.75 M_\odot$ *star at 3100 Myr.*

On the ZAMS lower mass stars have a lower central entropy than higher mass stars (their cores are denser), which means that in a collision between unevolved stars material from the lower mass star will sink to the centre of the collision product. As a result of stellar evolution, the entropy in the core will decrease (the core becomes more compact). Since more massive stars evolve more quickly, the central entropy will decrease more rapidly in massive stars than it will in low mass stars.

Figure 3.1 shows a number of evolution tracks in the $\log \rho_c$–$\log T_c$ plane. The location of the ZAMS is indicated by a thick solid line on the left and the location of the terminal age main sequence (TAMS) by a thick solid line on the right. Evolution tracks are dotted and labelled with the mass of the star and two isochrones are shown, one for 1000 Myr and one for 3100 Myr. Two lines of constant entropy across different stellar models are also drawn for different ages. The shaded region indicates the location where the entropy is lower than in the core of a $0.75 M_\odot$ star at $t = 3100$ Myr. The

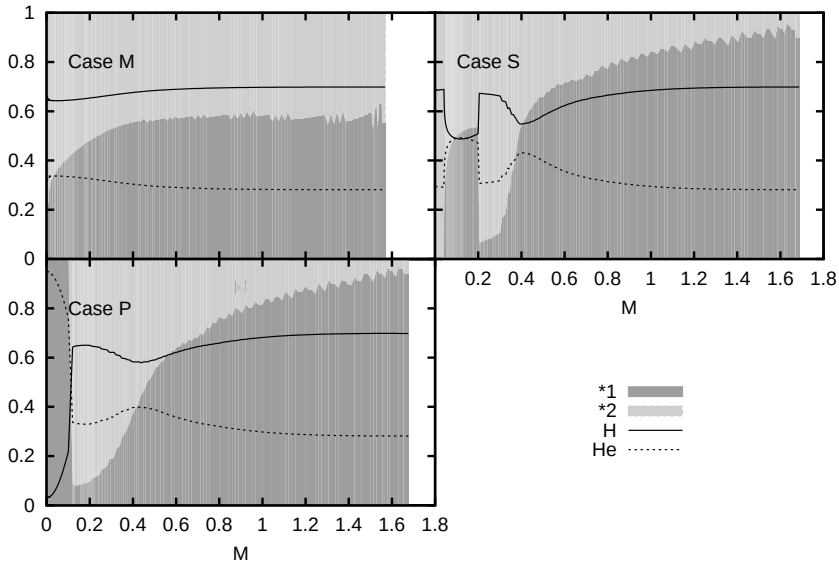

Figure 3.2: *Diagram showing the distribution of material from the parent stars within three of the collision products:* $t = 2800, q = 0.8, M = 1.7$ *(corresponding to case* M*, see text) and* $t = 2800, q = 0.4, M = 1.8$ *(case* S*) and* $t = 3700, q = 0.4, M = 1.8$ *(case* P*) for the bottom row. The dark shading indicates the fraction of material from the primary while the lighter region shows the fraction of material from the secondary. Overplotted are the abundances by mass fraction of hydrogen (solid) and helium (dotted).*

$t = 3100\,\mathrm{Myr}$ isochrone lies almost completely within this region, indicating that in a collision with a more massive star at this age the core of the primary sinks to the centre of the collision product. Conversely, part of the $t = 1000\,\mathrm{Myr}$ isochrone lies to the left of the line of constant entropy at that age, indicating that in a collision with a more massive star, up to $\approx 1.9 M_\odot$, the secondary star will sink to the centre.

For the composition profile in the collision product we can roughly distinguish three cases, which we will denoted by 'M', 'S' and 'P' for 'mixed core', 'secondary core' and 'primary core' respectively. These are illustrated in Figure 3.2. The part of the parameter space in the grid for which each of these cases occurs is illustrated in Figure 3.3 and listed in Table 3.4.

Case M

If the mass difference between the two colliding stars is small (the mass ratio is close to 1), the colliding stars have very similar entropy and composition profiles. The composition profile of the collision product will resemble a stretched version of the composition profile in the progenitor stars. This situation is illustrated by the top left panel in Figure 3.2. There can be a small molecular weight inversion near the centre if most of the material in the core comes from the secondary star. This case is indicated by ⊡ in Figure 3.3. In Figure 3.1 this means that the two models are on or close to the line of constant entropy.

Case P

If the primary is sufficiently evolved that its core entropy is lower than that of the secondary, the core of the primary ends up in the centre of the collision product. In Figure 3.1 this means that the primary is in the shaded region of the diagram. In this case the core of the merger remnant has a reduced hydrogen content with a very steep increase in hydrogen abundance at its edge and possibly a molecular weight inversion further out as well. A hydrogen burning shell can form at the edge of the core (see §3.4.4). This is the situation in the lower left panel of Figure 3.2 and is marked in Figure 3.3 with △. An extreme example of this case occurs when the primary is at the end of the main sequence. The hydrogen depleted core of the primary sinks to the centre of the collision product, producing a new star with a hydrogen depleted core. In other words, collisions involving turnoff stars produce turnoff stars, in agreement with Sills et al. (1997).

Case S

If the entropy in the core of the primary is larger than the entropy in the core of the secondary the secondary will sink to the centre of the collision product. In terms of Figure 3.1 the primary is to the left of the shaded region. The core of the collision product will be hydrogen-rich, with a helium rich layer on top of it, leading to a pronounced molecular weight inversion. This is the upper left situation in Figure 3.2 (a ∗ in Figure 3.3). This case will appear for collisions between main sequence stars when the mass ratio of the colliding stars is small (~ 0.4). If the mass ratio is even smaller ($\lesssim 0.2$), this will happen even after the primary has already evolved off the main sequence.

3.4.4 Reignition of hydrogen and mixing

Initially there is little or no nuclear burning in the core of the collision products and nuclear burning is unimportant as an energy source during

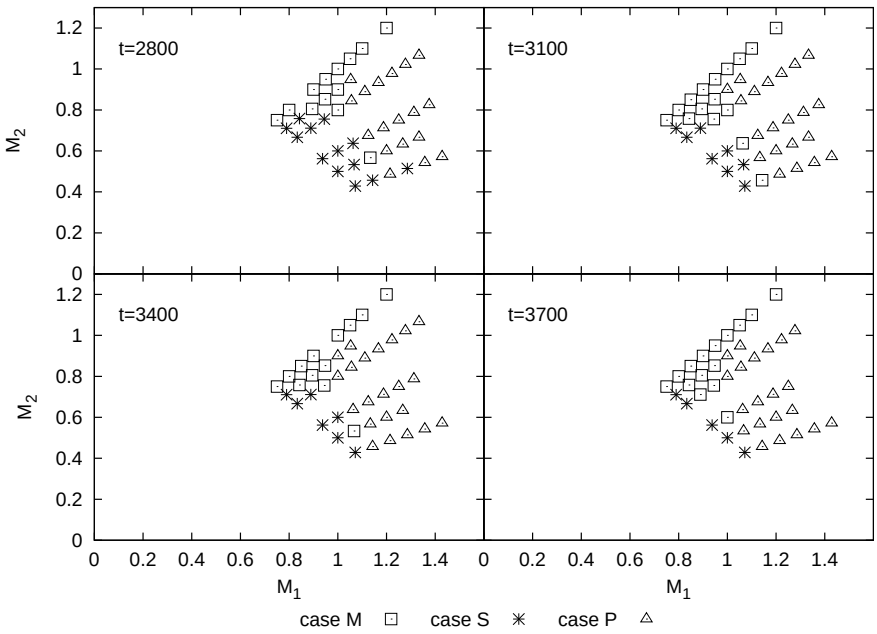

Figure 3.3: *Illustration of the different cases for the composition profiles in the collision products and the grid parameters for which they occur.*

the contraction to the main sequence.

Because the core of the collision product has the entropy of a lower mass star it lies on a lower adiabat than the core of a main sequence star of the same mass and composition. In practice, this means that the collision product is initially to the right of its main sequence position in the $\rho_c - T_c$ plane, at higher central densities. In order for the star to come into thermal equilibrium the entropy in the core needs to increase. The core will first expand and then heat up (see Paper I). Once hydrogen burning takes over as the main energy source the evolution of the collision product proceeds analogously to that of a normal main sequence star but with an abnormal composition profile (again see Paper I).

If there is a steep composition gradient at the edge of the core (when one of the two stars had a convective core), it is possible for the nuclear energy generation rate to peak at this location due to the composition dependence of the reaction rate. In effect, hydrogen will burn in the core as well as in a shell outside the core. This hydrogen burning shell is a transient feature that is destroyed when mixing reduces the steepness of the composition gradient. The hydrogen burning shell is important because it can drive a

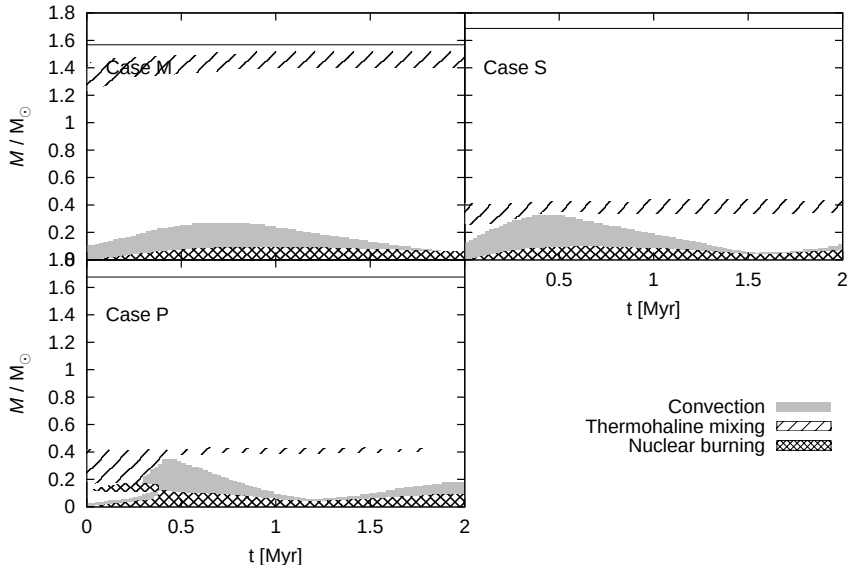

Figure 3.4: *Kippenhahn diagrams showing the mixing regions during the contraction phase for the same collision products as shown in Figure 3.2.*

convection zone that mixes the layers above it. Examples of the mixing regions during the contraction phase in each of the three cases in Figure 3.2 are shown in Figure 3.4.

Because the material outside the core can be hydrogen-rich, convection can bring extra hydrogen to the core, effectively rejuvenating the star. How much hydrogen is mixed into the core depends on mixing processes in the layer outside the core.

Helium-rich material on top of a layer of hydrogen-rich material causes a molecular weight inversion, which gives rise to thermohaline mixing (Kippenhahn et al. 1980). The material with higher molecular weight is supported by thermal buoyancy. Diffusion of heat from the material causes it to lose buoyancy and sink due to its higher mean molecular weight. The mixing continues until the molecular weight inversion is removed. Thermohaline mixing is important in the collision products during the contraction phase in the cases where material from the core of the primary overlies material from the secondary, which happens for cases *P* and *S*, discussed in §3.4.3 and shown in Figure 3.4. By the time the collision products reach the main sequence the molecular weight inversion has been smoothed out. As a result more helium has been mixed into the centre of the collision product than would have been the case if thermohaline mixing had been

ignored. This reduces the amount of hydrogen available for nuclear burning and decreases the lifetime of the collision product.

A hydrogen burning shell at the edge of the core can drive a convection zone that mixes in material from the layers above. This material can be either hydrogen-rich or helium rich, depending on the particular case. The convection zone can connect to the thermohaline layer, which means extra helium is mixed into the inner region of the star.

When the convective core is formed it can in turn connect to the convection zone driven by the burning shell (Figure 3.4, lower left panel). If there is no burning shell, it can connect to the thermohaline layer (Figure 3.4 upper left panel). In either case the end result is that the interior of the collision product is mixed below the molecular weight inversion. This produces a large central region that has been enhanced in helium and is larger than the convective core itself. The net effect is comparable to that of a star in which the convective core was larger initially but has shrunk.

Outside the mixed region, the composition profile is shallower than in a normal star of the same mass. This affects the structure of the star most strongly during the main sequence although it continues to affect the star during later evolutionary stages.

3.4.5 Main sequence evolution

Once the merger remnant has attained thermal equilibrium its further evolution proceeds similarly to that of a normal star of the same mass. In particular, the shape of the evolution track in a Hertzsprung-Russell diagram is the same. The composition profile modifies the evolution mainly in two ways: by affecting the lifetime and by affecting the luminosity. A typical evolution track is shown in Figure 3.5.

The luminosity is affected by the higher helium content of the envelope. This affects the structure of the star through the equation of state (due to the mean molecular weight) and the opacity, as discussed in Paper I, and results in a larger radius and higher luminosity. Because the surface layers do not show helium enhancement the effective temperature is not strongly affected, although there is a systematic trend that the coolest part of the track (just before hydrogen exhaustion at the end of the main sequence) is shifted to slightly lower temperatures. Shifts in the luminosity and effective temperature are listed in Table 3.4 for all our merger remnants.

The remaining lifetime of the star is reduced by the higher luminosity, but also by the central hydrogen abundance which is lower than the abundance in the envelope. Because of this the merger remnants do not resemble zero-age main sequence (ZAMS) stars after they settle down and are both redder and brighter than ZAMS stars of the same mass.

While on the Hertzsprung gap tracks of the merger remnants are still brighter than tracks of normal stars of the same mass. On the giant branch

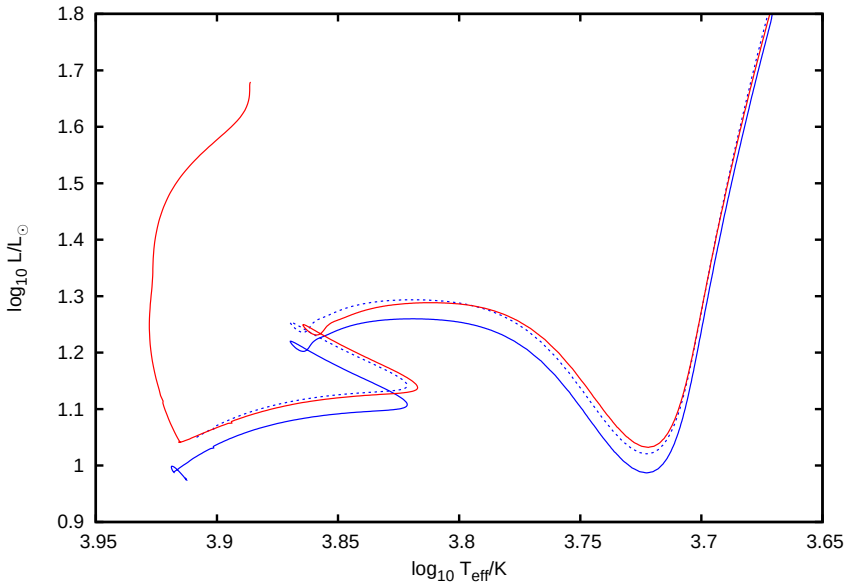

Figure 3.5: *Evolution track of the* $t = 2800, q = 0.8, M = 1.9$ *remnant with a mass of* $1.75 M_{\odot}$ *(top solid line) compared with the evolution track of a normal star of the same mass (bottom solid line). The shape of the evolution tracks after the contraction of the merger remnant is very similar, but the merger track is offset to higher luminosity and is slightly cooler at the end of the main sequence. The dashed line is a shifted version of the main sequence track according to equations (3.13) and (3.19), see §3.6.*

the difference between the two tracks vanishes. When the first dredge-up occurs the convective envelope enters the layer where the composition had been modified by the merger. This enhances the post-dredge-up abundances of helium and nitrogen and reduces the abundance of carbon compared to a normal red giant (see Paper I for more details).

3.4.6 The effect of lower metallicity

The heavy-element abundance Z affects the structure and evolution of stars. In general stars with a lower Z are hotter, more luminous and more compact than stars of the same mass at higher Z. The mass at which a convective core develops is higher and the lifetime is reduced.

This changes the structure of merger remnants in subtle ways. For instance, the relative rate at which the progenitor stars evolve along the main sequence is different for $Z = 0.02$ and $Z = 0.001$. This means that if

Table 3.2: *Ages determined from isochrone fitting for adopted values of distance modulus and reddening. See Pols et al. (1998) for details.*

Name	$\log_{10}$ age/yr	$M_{\rm to}$	[Fe/H]	$m-M$	$E(B-V)$
M67	9.60	1.29	-0.06	9.60	0.032
NGC 188	9.76	1.18	-0.06	11.40	0.12

we consider a $Z = 0.001$ collision at a time when the primary has passed the same fraction of its main sequence lifetime, the secondary will not have spent the same fraction of its main sequence lifetime as in the $Z = 0.02$ collision. Qualitatively the description given in the previous subsections remains valid for smaller Z. The data for the merger remnants calculated for our grid are listed in Table 3.5.

The mass loss from the collisions is slightly lower than for the $Z = 0.02$ grid although $C = 0.3$ is still a reasonable guess. The reason for this can be seen from (3.2): the stars at lower Z are more centrally condensed than at higher Z and the ratio $(R_{1,0.86} + R_{2,0.86})/(R_{1,0.5} + R_{2,0.5})$ is smaller.

3.5 HRD distributions: comparison with M67 and NGC188

In this section we compare the predicted locations of the collision products from our grid with the observed blue stragglers in the open clusters M67 and NGC188. For both of these clusters Pols et al. (1998) determined isochrone fits. For consistency we employ the same cluster parameters they used, as listed in Table 3.2.

In order to make the comparison between our models and the observations it is necessary to convert the theoretical surface parameters $(L, T_{\rm eff}, \log g)$ to the observable magnitude and colour $(M_{\rm V}, B-V)$. This conversion is done using the atmosphere models from Kurucz (1992) with empirical corrections from Lejeune et al. (1997).

Figure 3.6 shows the observed colour-magnitude diagram of M67 (•). The V and $B-V$ data is taken from Sandquist (2004) supplemented with Montgomery et al. (1993) for blue stragglers that were missing from the Sandquist (2004) data. Membership information (based on proper motions) is taken from Sanders (1977). Sandquist (2004) gives a distance modulus $m - M = 9.60$ and reddening $E(B-V) = 0.03$, consistent with the values used by Pols et al. (1998) to construct the 4 Gyr isochrone. The location of the collision remnants at 4 Gyr are plotted with different symbols, corresponding to the different times of collision. It is important to stress that our model is not a population synthesis model, so one should not draw conclusions from the density of the model points.

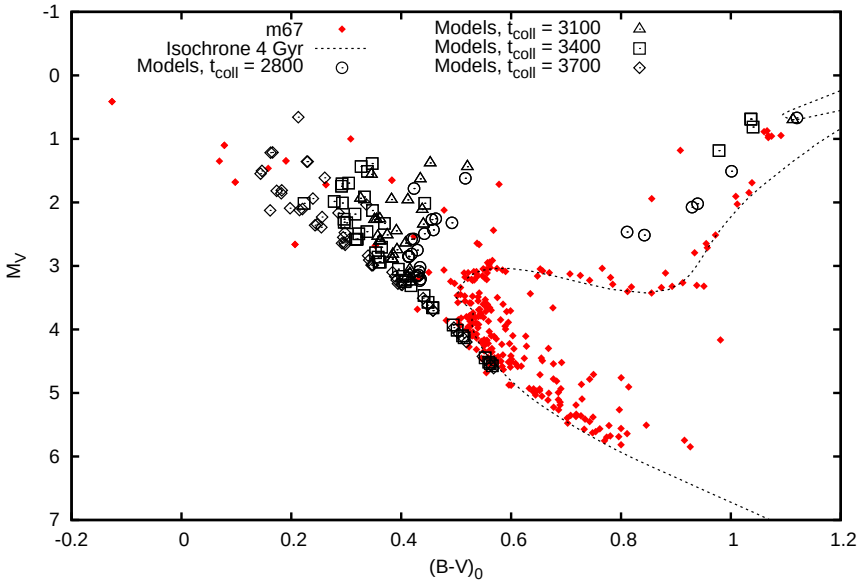

Figure 3.6: *Observed colour-magnitude diagram of the open cluster M67, with blue stragglers highlighted and the positions of the stars in our collision grid at the age of M67 overplotted. Different symbols correspond to different times of collision, as indicated.*

Our models lie in the observed blue straggler region. Some of the lower-mass merger remnants with masses below the turnoff appear among the normal main-sequence stars. The bluest blue straggler (S977 with $M_{\rm V} = 0.413$ and $B - V = -0.126$, Mathys 1991) is clearly outside the region covered by our models, but it is thought to have a mass larger than twice the turnoff mass (Sandquist 2005) and therefore cannot be formed by a single collision event. A few other blue stragglers are somewhat bluer than the region covered by our models. They are apparently single stars and are thus very likely to be the result of a stellar merger. Their blue positions can be explained if they have undergone much stronger internal mixing than our models, or if they have been formed more recently and are in that sense younger than our models. These blue stragglers are all slow rotators ($v \sin i \leq 120\,\mathrm{km/s}$) compared to normal stars of the same spectral type (Mathys 1991), suggesting that rotational mixing has not played a major role in their evolution. We therefore prefer the second explanation, which suggests that M67 is dynamically active, in other words, collisional blue stragglers are still being formed. This conclusion is consistent with the N-body model of Hurley et al. (2005).

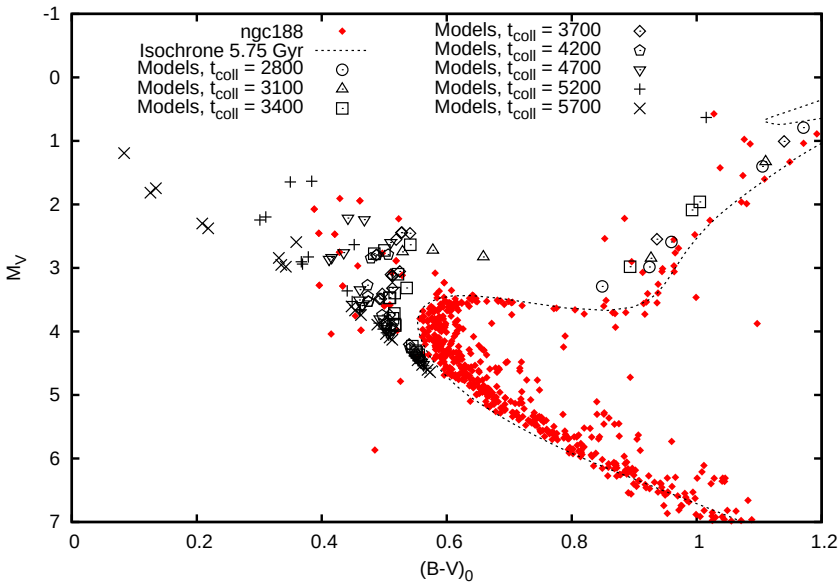

Figure 3.7: *As Figure 3.6 for NGC 188*

A number of our merger remnants have evolved beyond the end of the main sequence and appear on the giant branch but to the blue of the normal cluster giant branch, indicating that merger remnants can still stand out in the CMD even after the main sequence has ended. Two stars in M67 are located in this region (S1040 and S1273); both are spectroscopic binaries as well as unusual X-ray sources (van den Berg et al. 1999). It is not clear whether these stars are merger remnants, their unusual location may also be the result of a superposition of a giant and a turnoff star. In the case of S1040 the companion is probably a white dwarf and the orbit is circular (Mathieu et al. 1990), so the system has likely undergone mass transfer.

Figure 3.7 shows the comparison with NGC188, with V, $B-V$ and membership probabilities taken from Platais et al. (2003). Although NGC188 is known to be older than M67, different authors give different age estimates(von Hippel & Sarajedini 1998; Platais et al. 2003; Carraro et al. 1994). We adopt $m - M = 11.4$ and $E(B-V) = 0.12$ and an age of 5.8 Gyr, as in Pols et al. (1998). By contrast, Bonatto et al. (2005) find $m - M = 11.1$ and $E(B-V) = 0.0$ from fitting a $t = 7$ Gyr Padova isochrone.

Our models fill a larger region than the observed blue straggler region, indicating that NGC188 has not formed massive blue stragglers recently. This suggests that it is less dynamically active than M67. As for M67 we note that a number of merger remnants are beyond the main sequence and

on the giant branch, again parallel to the cluster giant branch.

3.6 Analytical description of results

To quantify the results of our collision calculations and compare the evolution tracks of the collision products with evolution tracks of normal single stars it is necessary to specify which models should be compared. In particular, we need to define an equivalent main sequence star model.

Apart from the mass M of the collision product the remaining lifetime is a good parameter to consider. For this reason it is convenient to introduce the fractional age f, which is the age of a star expressed in units of its main sequence lifetime,

$$f = \frac{t}{\tau_{\rm MS}} \tag{3.4}$$

where t is the absolute age and $\tau_{\rm MS} = \tau_{\rm MS}(M, Z)$ is the main sequence lifetime of a star of mass M and composition specified by Z. As long as the star is on the main sequence, $0 < f < 1$. We define the apparent age $f_{\rm app}$ of the collision product as the fractional age of a normal main sequence star with the same remaining lifetime $t_{\rm MS}$. These two quantities are related by

$$t_{\rm MS} = \tau_{\rm MS}(1 - f_{\rm app}). \tag{3.5}$$

In practice, we know $t_{\rm MS}$ from the detailed models (see Table 3.4) for the collision products and we can thus determine $f_{\rm app}$. If we can predict $f_{\rm app}$ from the global properties of the parent stars we can predict the collision product lifetime. In the following we will describe a formalism that allows us to do this using only standard stellar models and we give a set of transformation rules that can be used to transform a standard stellar evolution track to approximate the track of a merger remnant. By a standard evolution track we mean the evolution track of a single star that is evolved from the zero-age main sequence. For the standard tracks one can use the Hurley et al. (2000) recipe, or interpolate on a grid of single star models. Our recipe can be used to improve the accuracy of evolution tracks for merger remnants in star cluster simulations.

3.6.1 Collision product lifetimes

In normal main sequence stars there is a unique relation between the amount of hydrogen and the age of the star. Collision products show a similar relation. Although it might seem better to relate the age of the star to the amount of hydrogen in the core rather than the total amount of hydrogen, in practice this is not a good measure of the age of the star for collision products because mixing as described in §3.4.4 can increase the central hydrogen abundance compared to its post-collision value.

The relation between the amount of hydrogen and the age of the star is the starting point for a relation between the global properties of the parent stars and the apparent age $f_{\rm app}$ of the collisions product. Let's consider a simple stellar model that divides the star in two parts: a core where hydrogen is burned to helium and an envelope which is not affected by nuclear burning on the main sequence. The core has a mass fraction $q_{\rm c}$ of the total mass M. Such a model is not really applicable to low-mass stars, which do not have a well-defined core. However, we can generalise the model by defining $q_{\rm c}$ to be the fraction of hydrogen that is burned during the main sequence, so that

$$q_{\rm c} = \frac{X_0 - \langle X \rangle_{\rm TAMS}}{X_0}, \tag{3.6}$$

with X_0 the initial (ZAMS) hydrogen fraction. We can think of $q_{\rm c}$ as being the *effective core* mass fraction. If we approximate the nuclear burning rate as steady, the average (total) amount of hydrogen follows from the relative age f as

$$\langle X \rangle (t) = X_0 \left(1 - q_{\rm c} f\right). \tag{3.7}$$

In practice, $q_{\rm c}$ will depend on the stellar mass M and composition Z and needs to be found from detailed stellar models. It is convenient to have an analytic approximation for $q_{\rm c}(M)$. We use the rational function

$$q_{\rm c}(M) = \frac{1 + c_1 M + c_2 M^3 + c_3 M^5 + c_4 M^7}{c_5 + c_6 M^2 + c_7 M^4 + c_8 M^6} \qquad (M \text{ in } M_\odot). \tag{3.8}$$

The coefficients c_i have been found by least-squares fitting to detailed models calculated with the STARS code for masses in the range $M = 0.4 \ldots 75\, M_\odot$. These models were computed without convective overshooting. The fitting coefficients are listed in Table 3.3. In the mass range $0.4 \ldots 4.0\, M_\odot$ a somewhat more accurate fit is possible without the terms involving M^6 and M^7 (second and fourth column in Table 3.3); the quality of this fit for $Z = 0.02$ can be checked against Figure 3.8. It is of course also possible to interpolate on a table of detailed models.

To find an expression for $f_{\rm app}$ we first need to know the amount of hydrogen in the collision product. To do this correctly we should consider the material that is ejected during the collision. This comes from the progenitor star envelopes and therefore has the initial ZAMS hydrogen abundance X_0. If φ is the fraction of mass lost during the collision (see §3.4.1) then the mass M of the collision product is $M = (1 - \varphi)(M_1 + M_2)$. The average hydrogen abundance $\langle X \rangle$ in the collision product immediately after the collision is then given by

$$M \langle X \rangle = M_1 \langle X \rangle_1 (t) + M_2 \langle X \rangle_2 (t) - \varphi(M_1 + M_2) X_0. \tag{3.9}$$

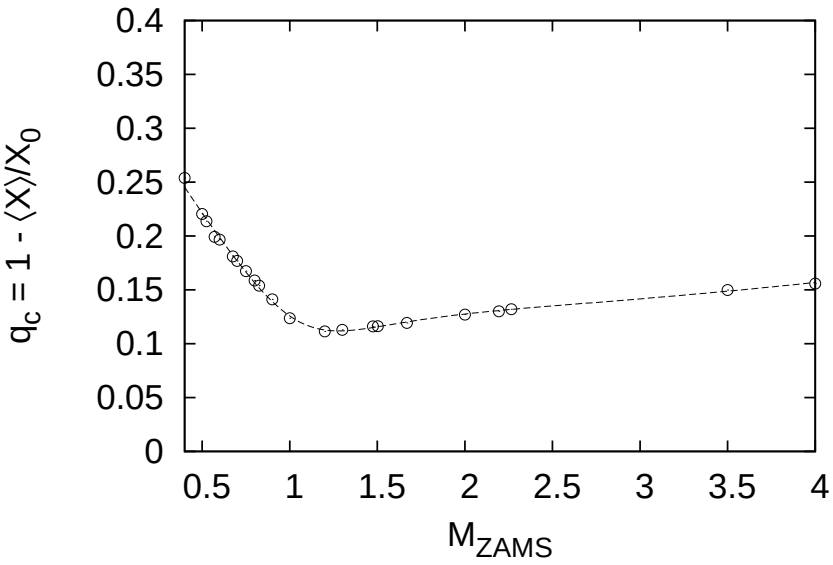

Figure 3.8: *Effective core mass fraction for main sequence stars against ZAMS mass, for $Z = 0.02$ ($\odot$). The fitting formula (3.8) in the mass range* $0.4 - 4.0$ $M_\odot$ *is shown as a dashed line.*

Inserting (3.7) for the hydrogen abundance in the parent stars and solving for $\langle X \rangle$,

$$\langle X \rangle = X_0 \left(1 - \frac{1}{1-\varphi} \frac{q_{\mathrm{c},1} f_1 + q_{\mathrm{c},2} f_2 q}{1+q} \right). \tag{3.10}$$

The equivalent age f_{app} is determined by the amount of hydrogen q_{M} that gets mixed into the burning region through

$$\langle X \rangle = X_0 (1 - q_{\mathrm{M}} f_{\mathrm{app}}). \tag{3.11}$$

As already mentioned in §3.4.4 the larger fraction of processed material within the merger remnant has an effect that is comparable to that of a star with an initially larger core mass. Setting $q_{\mathrm{M}} = \alpha q_{\mathrm{c}}(M)$, we find f_{app} from (3.10) as

$$f_{\mathrm{app}} = \frac{1}{\alpha q_{\mathrm{c}}(M)} \frac{1}{1-\varphi} \frac{q_{\mathrm{c},1} f_1 + q_{\mathrm{c},2} f_1 q}{1+q}. \tag{3.12}$$

The parameter α parametrises the amount of mixing during the collision and settling to the main sequence, with $\alpha = 1$ meaning no mixing at all and $\alpha = 1/q_{\mathrm{c}}(M)$ meaning homogeneous mixing. Our expression (3.12) is

Table 3.3: *Coefficients for the fitting formula (3.8) for q_c. The first column lists values that are valid in the mass range 0.4 – 75 $M_\odot$ for $Z = 0.02$, the second column lists coefficients that give a more accurate fit in the mass range 0.4 – 4.0 $M_\odot$. The third and fourth columns are similar but for $Z = 0.001$. The bottom row (rms) gives the root mean square error of the fits.*

	$Z = 0.02$		$Z = 0.001$	
c	$0.4 - 75\,M_\odot$	$0.4 - 4\,M_\odot$	$0.4 - 75\,M_\odot$	$0.4 - 5\,M_\odot$
c_1	−0.685213	−0.999710	−0.682671	−0.873596
c_2	0.289269	0.276843	0.185036	0.165455
c_3	0.0123223	0.0393513	0.00658021	0.0158297
c_4	3.3357e−6	0	7.5450e−7	0
c_5	2.70964	2.75579	2.71437	2.72675
c_6	1.44963	−1.70434	0.334367	−1.33733
c_7	0.629121	1.46625	0.343889	0.644498
c_8	0.000493117	0	0.000185160	0
rms	1.4%	1.2%	1.7%	1.3%

a generalisation of equation (69) in Tout et al. (1997) and (80) in Hurley et al. (2002), which are recovered in the special case $\varphi = 0$, $q_{c,1} = q_{c,2} = q_c(M) = 1/10$ and $\alpha = 1/q_c(M)$.

The parameter α can be determined from the models in our grid because all other factors in equation (3.12) are known. In principle it should depend on the evolutionary stages of the two stars involved in the collision, but in practice the value $\alpha = 1.67$ works well for all models in our $Z = 0.02$ grid, while $\alpha = 1.43$ works well for our $Z = 0.001$ grid.

Figure 3.9 compares the predicted lifetime according to (3.12) to the lifetime from our detailed models. Overall agreement is very good, although the detailed models show more scatter. The dashed line is the prescription from Hurley et al. (2000), which predicts much longer lifetimes, especially for collisions involving very evolved stars. This increases the predicted number of observable blue stragglers formed through collisions by up to a factor 2 compared to our detailed models.

3.6.2 Collision product luminosities

The luminosity of the collision products follows very well from the homology relation (Kippenhahn & Weigert 1990)

$$L_{\rm merger} = L_{\rm MS} \left(\frac{\mu_{\rm merger}}{\mu_{\rm MS}} \right)^4 . \tag{3.13}$$

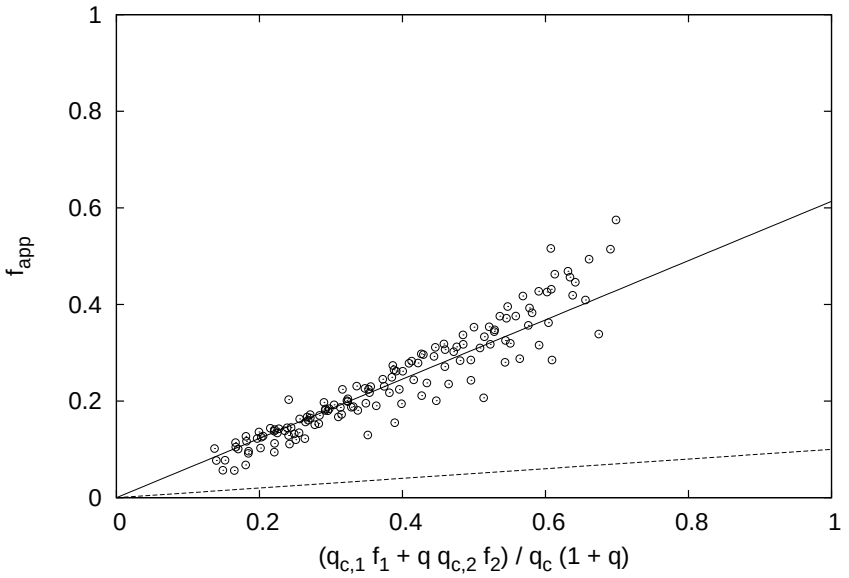

Figure 3.9: *The predicted apparent age according to (3.12), for* $\alpha = 1.67$ *(solid line). The detailed models are indicated by* $\odot$*. The dashed line is the prescription from Hurley et al. (2000).*

Here, $\mu_{\rm merger}$ is the average mean molecular weight in the collision product at the start of the main sequence, which is the same as the average mean molecular weight after the collision because the contraction phase is fast enough that composition changes due to nuclear reactions can be ignored. The average mean molecular weight of the main sequence model $\mu_{\rm MS}$ needs to be chosen at the equivalent stage of evolution. Because the shift in effective temperature is small we can choose the point in the evolution track with the same $T_{\rm eff}$ as the equivalent point. The averages of the mean molecular weight need to be calculated with respect to the mass (as opposed to the radius), which is the same as averaging over all particles.

It is possible to get an estimate for the mean molecular weight using the simple model (3.7). For a fully ionised hydrogen/helium mixture, the mean molecular weight can be approximated by (*e.g.* Weiss et al. (2004))

$$\mu^{-1} = 2X + \frac{3}{4}Y + \frac{1}{2}Z, \tag{3.14}$$

or, by eliminating the helium abundance Y,

$$\mu^{-1} = \frac{1}{4}\left(5X + 3 - Z\right). \tag{3.15}$$

Then

$$\frac{\mu_{\rm merger}}{\mu_{\rm MS}} = \frac{5\left\langle X\right\rangle_{\rm MS} + 3 - Z}{5\left\langle X\right\rangle_{\rm merger} + 3 - Z}. \tag{3.16}$$

For the main sequence star we can use (3.7) directly but to match the hydrogen abundance of the merger remnant we use a modified version of (3.7),

$$\left\langle X\right\rangle_{\rm merger} = X_0\left(1 - \beta - \alpha q_{\rm c} f_{\rm app}\right). \tag{3.17}$$

Physically, this extra parameter is necessary because $f_{\rm app}$ was calibrated to the main sequence timescale $\tau_{\rm MS}$ for a normal star. The collision products behave more like stars with a different initial composition and can have a different main sequence timescale. In other words, $f_{\rm app}$ does not represent the evolutionary stage of the collision product, just its remaining lifetime. Mathematically, the need for an extra parameter arises because we are now fitting two quantities (the lifetime and the hydrogen abundance).

The offset should vanish if the progenitor stars were ZAMS stars (in which case $f_{\rm app} = 0$) or if there was no mixing during the collision ($\alpha = 1$). This is satisfied if $\beta \propto (\alpha - 1) f_{\rm app}$. We find that setting $\beta = (\alpha - 1) q_{\rm c} f_{\rm app}/(1 - q_{\rm c})$ gives a good match for all collisions in our grid. Inserting this expression in (3.17) gives

$$\left\langle X\right\rangle_{\rm merger} = X_0\left(1 - \alpha q_{\rm c}\frac{\alpha(2 - q_{\rm c}) - 1}{\alpha(1 - q_{\rm c})} f_{\rm app}\right). \tag{3.18}$$

Setting $\delta\left\langle X\right\rangle = \left\langle X\right\rangle_{\rm merger} - \left\langle X\right\rangle_{\rm MS}$ and introducing $\mu_0 = 5\left\langle X\right\rangle_{\rm MS} + 3 - Z$,

$$\frac{\mu_{\rm merger}}{\mu_{\rm MS}} = \frac{\mu_0}{\mu_0 + 5\delta\left\langle X\right\rangle} \approx 1 - 5\frac{\delta\left\langle X\right\rangle}{\mu_0}. \tag{3.19}$$

From (3.7) and (3.11),

$$\delta\left\langle X\right\rangle = X_0 q_c f_{app}\frac{(2 - q_{\rm c})(1 - \alpha)}{1 - q_{\rm c}}. \tag{3.20}$$

Physically, $\alpha > 1$ and we see that in that case $\left\langle \mu\right\rangle_{\rm merger} > \left\langle \mu\right\rangle_{\rm MS}$, as we would expect.

The luminosity shift predicted by our analytic prescription is shown in Figure 3.5 (dashed line). The main sequence part of the track is very well represented by our prescription, although the hook at the end is slightly too hot. Even the Hertzsprung gap and the giant branch are very well matched with the same shift.

3.6.3 Collision product effective temperatures and radii

The effective temperature of the merger remnants is not very different from that in a normal star of the same mass (see the listed temperature shifts

in Table 3.4), but the reddest point of the main sequence hook is slightly cooler.

Since the effective temperature of the collision products is very similar to that of normal stars it is possible to use the effective temperature expected for normal stars. Taking the luminosity from (3.13) the radius of the collision product follows from the Stefan-Boltzmann law, so that

$$R_{\rm merger} = R_{\rm MS} \left(\frac{\mu_{\rm merger}}{\mu_{\rm MS}} \right)^2 . \tag{3.21}$$

3.7 Discussion and conclusions

We have calculated a grid of stellar evolution models for the remnants of collisions between main sequence stars. These models improve on the models in the literature by using a better model for the initial structure of the merger remnant (Bailyn & Pinsonneault 1995) or by studying a larger portion of the t, q, M parameter space (Sills et al. 1997).

We have compared the position of our models in the Hertzsprung-Russell diagram with the observed blue straggler regions in the open clusters M67 and NGC 188 and found that our models can populate the blue straggler region, provided that the blue stragglers in M67 are relatively 'young' and those in NGC 188 are relatively 'old'.

We have used our results to formulate a recipe that can be used to transform a normal evolution track, which can be obtained from fitting formulae (Hurley et al. 2000) or by interpolation on a table (*e.g.* Pols et al. 1998; Girardi et al. 2002). This can be used to improve the treatment of collisions in N-body calculations and population modelling.

Our models do not include the effect of rotation. Rotation can modify our results in two ways: collision products need to lose angular momentum and therefore mass to reach hydrostatic equilibrium and rapid rotation can induce mixing. It is clear that for a collision product to survive angular momentum must be lost but the mechanism by which this occurs is unclear. Magnetic fields may be involved, but their role is not well understood. Rotational mixing can enrich the stellar envelope in helium, increasing the luminosity and extending the stellar lifetime. By ignoring rotation we have assumed that an efficient mechanism to remove the angular momentum operates that spins the star down sufficiently that rotational mixing is not important for the long-term evolution. The fact that blue stragglers in M67 are observed to be rotating slowly (Mathys 1991) can be interpreted as an indication that such an efficient mechanism for removing angular momentum does operate in reality.

Although our models can fill the observed blue straggler region in M67 and NGC 188, this does not directly give information about the expected distribution of blue stragglers in the colour magnitude diagram because the

models need to be weighted with the probability for each collision. This requires a dynamical (or statistical, *e.g.* Monte-Carlo) model for the cluster evolution.

There are several directions for future research that could be explored. From the side of cluster modelling it is interesting to study the effect of our predicted corrections to the evolution tracks on the number of expected blue stragglers and on the blue straggler luminosity function. On the topic of detailed modelling of merger remnant evolution, including rotation and rotational mixing (extending the work of Sills et al. 2001, 2005) is a logical next step. However, this needs to be coupled with a mechanism for angular momentum loss from the merger remnant, which requires a better understanding of mass loss from rapidly rotating low mass stars, possibly involving magnetic fields as well. A simple equilibrium dynamo may not be adequate to model the magnetic field of a merger remnant, which might be very different from the magnetic field of a normal star following the collision. Magnetohydrodynamic models of stellar mergers and stellar evolution models including magnetic fields are also relevant in this light and are a logical next step.

Acknowledgements

We thank Frank Verbunt for useful discussion on the comparison with observations of M67. EG is supported by NWO under grant 614.000.303

Table 3.4: *Results for the $Z = 0.02$ collisions. The first three columns list the time of collision t (in Myr), the mass ratio q and the total initial mass M (in $M_\odot$). Column four gives the case for the collision (M, S or P, see §3.4.3). The total remnant mass $M_{\rm rmn}$ is smaller than the initial mass M because of mass loss in the collision. Column six gives the constant in the expression for the mass loss (3.3) for each of the individual collisions. Columns seven, eight and nine give the main sequence lifetime of the primary ($\tau_{\rm ms,1}$), secondary ($\tau_{\rm ms,2}$) and of a star of mass $M_{\rm rmn}$ ($\tau_{\rm ms,2}$). Column ten gives the actual remaining main sequence lifetime $t_{\rm ms}$ of the collision product. Columns eleven and twelve give the central abundance of hydrogen after the collision ($X_{\rm c,0}$) and at the beginning of the main sequence phase ($X_{\rm c,zms}$). The final two columns give the change in $\log_{10}$ luminosity L (in solar units) and $\log_{10}$ effective temperature $T_{\rm eff}$ (in K) at the reddest point of the main sequence track (shortly before core hydrogen exhaustion).*

t	q	M	Case	$M_{\rm rmn}$	$\frac{(1+q)^2}{q}\varphi$	$\tau_{\rm ms,1}$	$\tau_{\rm ms,2}$	$\tau_{\rm ms}$	$t_{\rm ms}$	$X_{\rm c,0}$	$X_{\rm c,zms}$	$\Delta \log L$	$\Delta \log T_{\rm eff}$
2800	0.4	1.5	S	1.41	0.28	6247	181307	2413	2100	0.691	0.676	0.053	-0.004
2800	0.4	1.7	P	1.60	0.29	3337	134060	1726	1234	0.379	0.379	0.074	-0.008
2800	0.4	1.8	S	1.69	0.31	3444	114628	1478	951	0.547	0.574	0.095	-0.009
2800	0.4	1.9	P	1.77	0.32	2751	97623	1273	647	0.063	0.505	0.104	-0.014
2800	0.5	1.5	S	1.41	0.27	8644	124021	2519	2180	0.689	0.672	0.028	-0.002
2800	0.5	1.6	S	1.50	0.29	6382	102516	2103	1709	0.686	0.666	0.039	-0.001
2800	0.5	1.7	M	1.59	0.29	4458	85148	1746	1395	0.490	0.490	0.050	-0.006
2800	0.5	1.8	P	1.69	0.28	4206	70071	1474	1074	0.415	0.415	0.058	-0.006
2800	0.5	1.9	S	1.78	0.28	3438	57523	1261	1126	0.677	0.671	0.028	-0.002
2800	0.5	2.0	P	1.86	0.31	3001	47262	1104	534	0.124	0.128	0.065	-0.003
2800	0.6	1.5	S	1.40	0.28	11552	87227	2608	2253	0.685	0.674	0.016	-0.001
2800	0.6	1.6	S	1.49	0.31	8644	70071	2101	1848	0.683	0.662	0.032	-0.001
2800	0.6	1.7	S	1.58	0.30	6504	56129	1782	1475	0.679	0.645	0.034	-0.005
2800	0.6	1.8	P	1.68	0.28	4907	45016	1485	1152	0.513	0.513	0.041	-0.005
2800	0.6	1.9	P	1.78	0.27	3734	36312	1266	906	0.422	0.422	0.049	-0.005

Table 3.4: *cont.*

t	q	M	Case	$M_{\rm rmn}$	$\frac{(1+q)^2}{q}\varphi$	$\tau_{\rm ms,1}$	$\tau_{\rm ms,2}$	$\tau_{\rm ms}$	$t_{\rm ms}$	$X_{\rm c,0}$	$X_{\rm c,zms}$	$\Delta \log L$	$\Delta \log T_{\rm eff}$
2800	0.6	2.0	P	1.87	0.29	3461	29518	1099	711	0.349	0.348	0.060	-0.005
2800	0.6	2.1	P	1.94	0.32	3159	24457	984	3	0.328	0.328	0.075	-0.004
2800	0.6	2.2	P	2.04	0.30	2722	19931	859	431	0.048	0.048	0.084	-0.008
2800	0.8	1.5	S	1.40	0.26	19036	47262	2493	2352	0.676	0.669	0.016	-0.002
2800	0.8	1.6	S	1.49	0.29	14553	36598	2162	1910	0.672	0.664	0.014	-0.001
2800	0.8	1.7	S	1.57	0.31	11182	28644	1836	1577	0.662	0.649	0.016	-0.003
2800	0.8	1.8	M	1.67	0.29	8644	22659	1511	1259	0.586	0.586	0.021	-0.004
2800	0.8	1.9	P	1.75	0.31	6712	18089	1315	1051	0.550	0.550	0.029	-0.005
2800	0.8	2.0	P	1.86	0.29	5225	14553	1113	819	0.509	0.518	0.030	-0.003
2800	0.8	2.1	P	1.94	0.31	4861	11784	986	707	0.456	0.532	0.051	-0.007
2800	0.8	2.2	P	2.04	0.29	3956	9581	859	570	0.391	0.515	0.057	-0.007
2800	0.8	2.3	P	2.11	0.33	3445	7811	777	470	0.322	0.477	0.071	-0.008
2800	0.8	2.4	P	2.23	0.29	3001	6384	671	361	0.223	0.450	0.080	-0.009
2800	0.9	1.5	S	1.39	0.30	23930	36719	2643	2439	0.668	0.669	0.009	-0.001
2800	0.9	1.6	S	1.49	0.28	18301	28286	2135	1920	0.657	0.661	0.010	-0.002
2800	0.9	1.7	M	1.57	0.31	14150	22050	1818	1586	0.649	0.649	0.013	-0.002
2800	0.9	1.8	M	1.75	0.11	11029	17369	1324	1055	0.612	0.611	0.015	-0.002
2800	0.9	1.9	M	1.76	0.31	8644	13797	1312	1071	0.585	0.620	0.024	-0.005
2800	0.9	2.0	P	1.86	0.28	6801	11029	1111	859	0.554	0.539	0.026	-0.005
2800	1.0	1.5	M	1.39	0.30	29518	29518	2689	2415	0.668	0.668	0.013	-0.002
2800	1.0	1.6	M	1.49	0.28	22659	22659	2149	1924	0.652	0.659	0.008	-0.002
2800	1.0	1.8	M	1.67	0.29	13797	13797	1512	1293	0.623	0.630	0.020	-0.005
2800	1.0	1.9	M	1.75	0.31	10895	10895	1317	1093	0.605	0.613	0.028	-0.005
2800	1.0	2.0	M	1.86	0.28	8644	8646	1110	854	0.580	0.591	0.026	-0.004

Table 3.4: *cont.*

t	q	M	Case	$M_{\rm rmn}$	$\frac{(1+q)^2}{q}\varphi$	$\tau_{\rm ms,1}$	$\tau_{\rm ms,2}$	$\tau_{\rm ms}$	$t_{\rm ms}$	$X_{\rm c,0}$	$X_{\rm c,zms}$	$\Delta \log L$	$\Delta \log T_{\rm eff}$
2800	1.0	2.1	M	1.94	0.30	6885	6885	984	727	0.552	0.559	0.038	-0.006
2800	1.0	2.2	M	2.05	0.27	5493	5493	848	583	0.514	0.518	0.046	-0.006
2800	1.0	2.4	M	2.23	0.29	4206	4261	673	392	0.412	0.414	0.070	-0.009
3100	0.4	1.5	S	1.41	0.29	6247	181307	2443	2064	0.682	0.669	0.058	-0.004
3100	0.4	1.6	M	1.51	0.26	4537	156179	1869	1482	0.457	0.457	0.073	-0.008
3100	0.4	1.7	P	1.60	0.30	3337	134060	1728	1143	0.324	0.324	0.079	-0.008
3100	0.4	1.8	P	1.68	0.31	3444	114628	1487	864	0.204	0.204	0.102	-0.008
3100	0.5	1.5	S	1.41	0.28	8644	124021	2538	2149	0.689	0.666	0.031	-0.003
3100	0.5	1.6	S	1.50	0.27	6382	102516	2067	1674	0.659	0.645	0.041	-0.006
3100	0.5	1.7	P	1.58	0.31	4458	85148	1771	1341	0.465	0.465	0.054	-0.006
3100	0.5	1.8	P	1.69	0.28	4206	70071	1475	1017	0.365	0.365	0.064	-0.005
3100	0.5	1.9	S	1.78	0.28	3438	57523	1261	1126	0.677	0.671	0.028	-0.002
3100	0.5	2.0	P	1.86	0.31	3001	47262	1109	513	0.034	0.471	0.093	-0.012
3100	0.6	1.5	S	1.40	0.29	11552	87227	2534	2295	0.684	0.677	0.033	-0.001
3100	0.6	1.6	S	1.49	0.28	8644	70071	2057	1747	0.681	0.655	0.028	-0.004
3100	0.6	1.7	M	1.58	0.31	6504	56129	1799	1447	0.540	0.540	0.036	-0.006
3100	0.6	1.9	P	1.76	0.31	3734	36312	1301	885	0.387	0.387	0.056	-0.007
3100	0.6	2.0	P	1.86	0.30	3461	29518	1108	673	0.286	0.286	0.068	-0.004
3100	0.6	2.1	P	1.96	0.29	3159	24457	965	534	0.144	0.144	0.088	-0.011
3100	0.8	1.5	S	1.40	0.27	19036	47262	2480	2340	0.673	0.666	0.016	-0.002
3100	0.8	1.6	S	1.48	0.30	14553	36598	2116	1898	0.666	0.655	0.017	-0.001
3100	0.8	1.7	M	1.59	0.27	11182	28644	1768	1511	0.666	0.642	0.019	-0.005
3100	0.8	1.8	M	1.67	0.30	8644	22659	1523	1249	0.573	0.573	0.026	-0.005
3100	0.8	1.9	P	1.77	0.27	6712	18089	1275	982	0.531	0.531	0.030	-0.005

Table 3.4: *cont.*

t	q	M	Case	$M_{\rm rmn}$	$\frac{(1+q)^2}{q}\varphi$	$\tau_{\rm ms,1}$	$\tau_{\rm ms,2}$	$\tau_{\rm ms}$	$t_{\rm ms}$	$X_{\rm c,0}$	$X_{\rm c,zms}$	$\Delta \log L$	$\Delta \log T_{\rm eff}$
3100	0.8	2.0	P	1.86	0.28	5225	14553	1104	777	0.484	0.558	0.032	-0.004
3100	0.8	2.1	P	1.93	0.32	4861	11784	997	680	0.422	0.508	0.057	-0.007
3100	0.8	2.2	P	2.04	0.29	3956	9581	855	534	0.340	0.486	0.066	-0.008
3100	0.8	2.3	P	2.14	0.29	3445	7811	756	434	0.248	0.463	0.079	-0.008
3100	0.8	2.4	P	2.22	0.30	3001	6384	676	1	0.054	0.054	0.579	0.048
3100	0.9	1.7	M	1.57	0.31	14150	22050	1829	1568	0.646	0.643	0.014	-0.002
3100	0.9	1.8	M	1.67	0.29	11029	17369	1515	1265	0.599	0.628	0.022	-0.005
3100	0.9	2.0	P	1.85	0.29	6801	11029	1120	841	0.548	0.585	0.036	-0.006
3100	1.0	1.5	M	1.38	0.31	29518	29518	2588	2388	0.664	0.662	0.015	0.001
3100	1.0	1.6	M	1.49	0.28	22659	22659	2095	1893	0.649	0.654	0.011	-0.003
3100	1.0	1.7	M	1.57	0.31	18175	18175	1840	1575	0.633	0.642	0.014	-0.003
3100	1.0	1.8	M	1.67	0.29	13797	13797	1520	1282	0.615	0.624	0.024	-0.005
3100	1.0	1.9	M	1.77	0.27	10895	10895	1276	1038	0.593	0.601	0.031	-0.006
3100	1.0	2.0	M	1.85	0.29	8644	8646	1122	847	0.566	0.586	0.033	-0.006
3100	1.0	2.1	M	1.93	0.31	6885	6885	997	705	0.535	0.541	0.042	-0.007
3100	1.0	2.2	M	2.04	0.29	5493	5493	862	566	0.491	0.488	0.053	-0.007
3100	1.0	2.4	M	2.21	0.31	4206	4261	682	363	0.378	0.379	0.078	-0.011
3400	0.4	1.2	S	1.13	0.29	16991	314052	5263	4416	0.698	0.690	0.023	0.000
3400	0.4	1.3	S	1.23	0.28	12092	243954	3952	3439	0.691	0.683	0.028	-0.000
3400	0.4	1.4	S	1.32	0.27	8644	210585	3089	2568	0.690	0.676	0.042	-0.002
3400	0.4	1.5	S	1.42	0.27	6247	181307	2495	1968	0.689	0.657	0.055	-0.004
3400	0.4	1.6	P	1.50	0.30	4537	156179	2087	1486	0.411	0.411	0.070	-0.006
3400	0.4	1.7	P	1.60	0.28	3337	134060	1710	1038	0.262	0.262	0.080	-0.007
3400	0.4	1.8	P	1.69	0.29	3444	114628	1467	624	0.106	0.110	0.078	0.002

Table 3.4: *cont.*

t	q	M	Case	$M_{\rm rmn}$	$\frac{(1+q)^2}{q}\varphi$	$\tau_{\rm ms,1}$	$\tau_{\rm ms,2}$	$\tau_{\rm ms}$	$t_{\rm ms}$	$X_{\rm c,0}$	$X_{\rm c,zms}$	$\Delta \log L$	$\Delta \log T_{\rm eff}$
3400	0.5	1.5	S	1.40	0.29	8644	124021	2555	2128	0.681	0.661	0.034	-0.003
3400	0.5	1.6	M	1.50	0.28	6382	102516	2088	1682	0.502	0.639	0.048	-0.005
3400	0.5	1.7	P	1.59	0.30	4458	85148	1762	1268	0.430	0.430	0.058	-0.007
3400	0.5	1.8	P	1.68	0.30	4206	70071	1486	927	0.309	0.310	0.069	-0.006
3400	0.5	1.9	S	1.78	0.28	3438	57523	1262	1129	0.676	0.671	0.028	-0.002
3400	0.6	1.2	S	1.12	0.27	29518	162623	5079	4986	0.689	0.688	0.022	-0.001
3400	0.6	1.3	S	1.22	0.27	21253	133093	4005	3692	0.688	0.681	0.018	-0.001
3400	0.6	1.4	S	1.31	0.26	15571	108190	3152	2812	0.686	0.674	0.018	-0.001
3400	0.6	1.5	S	1.40	0.30	11552	87227	2539	2257	0.684	0.664	0.029	-0.002
3400	0.6	1.6	S	1.49	0.29	8644	70071	2131	1721	0.679	0.648	0.030	-0.004
3400	0.6	1.7	P	1.59	0.27	6504	56129	1746	1367	0.509	0.509	0.040	-0.006
3400	0.6	1.8	P	1.68	0.28	4907	45016	1487	1065	0.440	0.440	0.049	-0.006
3400	0.6	1.9	P	1.76	0.31	3734	36312	1301	830	0.335	0.335	0.060	-0.007
3400	0.6	2.0	P	1.86	0.30	3461	29518	1115	606	0.206	0.203	0.071	-0.004
3400	0.6	2.1	P	1.93	0.34	3159	24457	1000	12	0.037	0.037	0.095	-0.009
3400	0.8	1.2	S	1.12	0.26	47280	102516	4972	3149	0.686	0.684	0.008	0.009
3400	0.8	1.3	S	1.21	0.29	34390	79923	4135	16	0.682	0.680	0.000	0.001
3400	0.8	1.4	S	1.30	0.29	25450	61494	3244	2995	0.679	0.673	0.011	-0.001
3400	0.8	1.5	S	1.40	0.27	19036	47262	2492	2323	0.673	0.661	0.017	-0.002
3400	0.8	1.6	S	1.48	0.30	14553	36598	2126	1886	0.667	0.651	0.018	-0.002
3400	0.8	1.7	M	1.58	0.28	11182	28644	1780	1494	0.596	0.596	0.022	-0.005
3400	0.8	1.8	P	1.68	0.28	8644	22659	1499	1192	0.553	0.553	0.028	-0.005
3400	0.8	1.9	P	1.76	0.31	6712	18089	1311	968	0.513	0.510	0.031	-0.005
3400	0.8	2.0	P	1.85	0.29	5225	14553	1120	782	0.455	0.559	0.046	-0.007

Table 3.4: *cont.*

t	q	M	Case	$M_{\rm rmn}$	$\frac{(1+q)^2}{q}\varphi$	$\tau_{\rm ms,1}$	$\tau_{\rm ms,2}$	$\tau_{\rm ms}$	$t_{\rm ms}$	$X_{\rm c,0}$	$X_{\rm c,zms}$	$\Delta \log L$	$\Delta \log T_{\rm eff}$
3400	0.8	2.1	P	1.95	0.29	4861	11784	970	628	0.378	0.493	0.060	-0.009
3400	0.8	2.2	P	2.03	0.32	3956	9581	877	503	0.297	0.452	0.075	-0.009
3400	0.8	2.3	P	2.13	0.29	3445	7811	759	385	0.185	0.391	0.085	-0.010
3400	0.8	2.4	P	2.18	0.37	3001	6384	709	287	0.201	0.201	0.109	-0.015
3400	0.9	1.7	M	1.59	0.27	14150	22050	1764	1531	0.609	0.621	0.022	-0.004
3400	0.9	1.8	M	1.67	0.30	11029	17369	1526	1245	0.586	0.584	0.023	-0.006
3400	0.9	1.9	P	1.77	0.28	8644	13797	1280	1002	0.559	0.597	0.032	-0.006
3400	0.9	2.0	P	1.86	0.28	6801	11029	1110	801	0.510	0.569	0.037	-0.007
3400	1.0	1.2	M	1.12	0.28	70143	70071	5094	4783	0.681	0.682	0.001	-0.000
3400	1.0	1.3	M	1.20	0.31	52156	52156	4217	3971	0.677	0.678	0.006	-0.000
3400	1.0	1.4	M	1.30	0.28	38969	38969	3243	2928	0.668	0.670	0.007	0.001
3400	1.0	1.5	M	1.38	0.31	29518	29518	2691	2384	0.659	0.659	0.013	-0.001
3400	1.0	1.6	M	1.48	0.29	22659	22659	2166	1894	0.646	0.649	0.012	-0.002
3400	1.0	1.7	M	1.59	0.27	18175	18175	1753	1510	0.624	0.635	0.019	-0.005
3400	1.0	1.8	M	1.67	0.30	13797	13797	1528	1227	0.620	0.605	0.013	-0.006
3400	1.0	2.0	M	1.85	0.30	8644	8646	1132	818	0.552	0.574	0.033	-0.006
3400	1.0	2.1	M	1.95	0.28	6885	6885	970	662	0.512	0.519	0.048	-0.007
3400	1.0	2.2	M	2.03	0.32	5493	5493	876	541	0.467	0.470	0.059	-0.008
3400	1.0	2.4	M	2.22	0.30	4206	4261	676	328	0.325	0.326	0.085	-0.013
3700	0.4	1.2	S	1.14	0.25	16991	314052	4881	4436	0.698	0.687	0.039	-0.000
3700	0.4	1.3	S	1.22	0.29	12092	243954	3962	3405	0.691	0.682	0.034	-0.000
3700	0.4	1.4	S	1.32	0.29	8644	210585	3113	2540	0.690	0.674	0.046	-0.002
3700	0.4	1.5	S	1.41	0.28	6247	181307	2526	1932	0.667	0.648	0.061	-0.004
3700	0.4	1.8	P	1.68	0.34	3444	114628	1501	667	0.032	0.467	0.114	-0.017

Table 3.4: *cont.*

t	q	M	Case	$M_{\rm rmn}$	$\frac{(1+q)^2}{q}\varphi$	$\tau_{\rm ms,1}$	$\tau_{\rm ms,2}$	$\tau_{\rm ms}$	$t_{\rm ms}$	$X_{\rm c,0}$	$X_{\rm c,zms}$	$\Delta \log L$	$\Delta \log T_{\rm eff}$
3700	0.5	1.5	S	1.41	0.26	8644	124021	2507	2054	0.678	0.656	0.038	-0.004
3700	0.5	1.6	P	1.49	0.30	6382	102516	2111	1610	0.479	0.479	0.050	-0.006
3700	0.5	1.7	P	1.59	0.29	4458	85148	1747	1196	0.391	0.391	0.063	-0.007
3700	0.5	1.8	P	1.68	0.31	4206	70071	1494	850	0.251	0.251	0.070	-0.006
3700	0.5	1.9	S	1.78	0.28	3438	57523	1263	1120	0.672	0.669	0.029	-0.002
3700	0.6	1.2	S	1.12	0.27	29518	162623	4958	2885	0.689	0.686	0.008	0.001
3700	0.6	1.3	S	1.22	0.27	21253	133093	4010	3642	0.688	0.679	0.018	-0.000
3700	0.6	1.4	S	1.31	0.27	15571	108190	3181	2796	0.686	0.672	0.018	-0.001
3700	0.6	1.5	S	1.41	0.27	11552	87227	2479	2176	0.680	0.660	0.033	-0.002
3700	0.6	1.6	M	1.49	0.30	8644	70071	2094	1699	0.677	0.645	0.035	-0.004
3700	0.6	1.7	P	1.59	0.28	6504	56129	1765	1335	0.501	0.501	0.042	-0.006
3700	0.6	1.8	P	1.68	0.28	4907	45016	1480	1010	0.403	0.403	0.052	-0.007
3700	0.6	1.9	P	1.77	0.29	3734	36312	1275	753	0.283	0.283	0.060	-0.006
3700	0.6	2.0	P	1.85	0.33	3461	29518	1133	556	0.120	0.134	0.094	-0.012
3700	0.8	1.2	S	1.12	0.26	47280	102516	4972	3149	0.686	0.684	0.001	0.000
3700	0.8	1.3	S	1.21	0.29	34390	79923	4160	3844	0.682	0.678	0.003	-0.000
3700	0.8	1.4	S	1.30	0.29	25450	61494	3261	2972	0.676	0.669	0.012	-0.001
3700	0.8	1.5	S	1.40	0.28	19036	47262	2624	2303	0.658	0.657	0.009	-0.002
3700	0.8	1.6	M	1.48	0.31	14553	36598	2137	1862	0.659	0.644	0.018	-0.002
3700	0.8	1.7	M	1.58	0.29	11182	28644	1790	1466	0.589	0.589	0.022	-0.005
3700	0.8	1.8	P	1.67	0.29	8644	22659	1512	1172	0.541	0.541	0.030	-0.006
3700	0.8	1.9	P	1.75	0.32	6712	18089	1325	931	0.492	0.526	0.032	-0.004
3700	0.8	2.0	P	1.84	0.32	5225	14553	1141	761	0.428	0.545	0.050	-0.008
3700	0.8	2.1	P	1.94	0.30	4861	11784	985	619	0.345	0.463	0.071	-0.008

Table 3.4: *cont.*

t	q	M	Case	$M_{\rm rmn}$	$\frac{(1+q)^2}{q}\varphi$	$\tau_{\rm ms,1}$	$\tau_{\rm ms,2}$	$\tau_{\rm ms}$	$t_{\rm ms}$	$X_{\rm c,0}$	$X_{\rm c,zms}$	$\Delta \log L$	$\Delta \log T_{\rm eff}$
3700	0.8	2.2	P	2.03	0.31	3956	9581	869	481	0.233	0.425	0.081	-0.010
3700	0.8	2.3	P	2.12	0.32	3445	7811	772	1	0.050	0.050	0.153	0.060
3700	0.9	1.5	S	1.40	0.26	23930	36719	2528	2296	0.654	0.657	0.013	-0.003
3700	0.9	1.6	M	1.48	0.29	18301	28286	2160	1871	0.650	0.647	0.014	-0.003
3700	0.9	1.7	M	1.57	0.30	14150	22050	1808	1497	0.599	0.599	0.017	-0.004
3700	0.9	1.8	M	1.67	0.28	11029	17369	1503	1204	0.572	0.572	0.026	-0.006
3700	0.9	1.9	P	1.75	0.31	8644	13797	1319	958	0.541	0.582	0.026	-0.004
3700	0.9	2.0	P	1.85	0.29	6801	11029	1121	777	0.492	0.558	0.040	-0.006
3700	1.0	1.2	M	1.12	0.28	70143	70071	5094	4783	0.681	0.682	0.001	-0.000
3700	1.0	1.3	M	1.20	0.31	52156	52156	4228	4030	0.675	0.675	0.001	0.000
3700	1.0	1.4	M	1.30	0.28	38969	38969	3236	2988	0.665	0.667	0.009	-0.001
3700	1.0	1.5	M	1.40	0.26	29518	29518	2598	2268	0.650	0.651	0.010	-0.000
3700	1.0	1.6	M	1.48	0.29	22659	22659	2178	1878	0.636	0.645	0.013	-0.002
3700	1.0	1.7	M	1.58	0.28	18175	18175	1780	1490	0.618	0.625	0.018	-0.005
3700	1.0	1.8	M	1.66	0.31	13797	13797	1542	1196	0.597	0.596	0.013	-0.005
3700	1.0	1.9	M	1.76	0.29	10895	10895	1296	997	0.572	0.582	0.036	-0.007
3700	1.0	2.0	M	1.84	0.32	8644	8646	1136	783	0.537	0.554	0.035	-0.005
3700	1.0	2.1	M	1.94	0.30	6885	6885	983	641	0.493	0.492	0.053	-0.008
3700	1.0	2.2	M	2.04	0.29	5493	5493	861	411	0.436	0.436	0.001	0.000
3700	1.0	2.4	M	2.20	0.34	4206	4261	695	305	0.281	0.281	0.098	-0.015
4200	0.4	1.2	S	1.14	0.26	16991	314052	5119	4442	0.698	0.684	0.031	0.000
4200	0.4	1.3	S	1.23	0.26	12092	243954	3890	3272	0.689	0.676	0.037	-0.001
4200	0.4	1.4	S	1.33	0.26	8644	210585	3052	2379	0.688	0.666	0.058	-0.000
4200	0.6	1.2	S	1.12	0.29	29518	162623	5056	4728	0.688	0.684	0.028	0.000

Table 3.4: *cont.*

t	q	M	Case	$M_{\rm rmn}$	$\frac{(1+q)^2}{q}\varphi$	$\tau_{\rm ms,1}$	$\tau_{\rm ms,2}$	$\tau_{\rm ms}$	$t_{\rm ms}$	$X_{\rm c,0}$	$X_{\rm c,zms}$	$\Delta \log L$	$\Delta \log T_{\rm eff}$
4200	0.6	1.3	S	1.22	0.28	21253	133093	4050	3623	0.685	0.676	0.018	-0.001
4200	0.6	1.4	S	1.31	0.28	15571	108190	3191	2755	0.683	0.666	0.022	-0.002
4200	0.8	1.2	S	1.12	0.27	47280	102516	5003	4701	0.683	0.681	0.014	0.000
4200	0.8	1.3	S	1.20	0.30	34390	79923	4157	3820	0.679	0.675	0.005	-0.000
4200	0.8	1.4	S	1.30	0.30	25450	61494	3273	2948	0.673	0.665	0.013	-0.001
4200	1.0	1.2	M	1.12	0.28	70143	70071	5117	4757	0.678	0.679	0.001	0.000
4200	1.0	1.3	M	1.22	0.26	52156	52156	4049	270	0.670	0.671	0.004	0.000
4200	1.0	1.4	M	1.30	0.29	38969	38969	3256	2953	0.659	0.661	0.010	-0.001
4200	1.0	2.2	M	2.04	0.30	5493	5493	864	454	0.386	0.386	0.083	-0.011
4700	0.4	1.2	S	1.13	0.27	16991	314052	4934	4420	0.698	0.682	0.062	-0.000
4700	0.4	1.3	S	1.23	0.28	12092	243954	3930	3213	0.687	0.671	0.042	-0.001
4700	0.4	1.4	S	1.32	0.28	8644	210585	3103	2310	0.686	0.669	0.058	-0.003
4700	0.6	1.2	S	1.13	0.25	29518	162623	5176	4571	0.684	0.681	0.006	0.001
4700	0.6	1.3	S	1.21	0.28	21253	133093	4072	12	0.685	0.673	0.007	0.000
4700	0.6	1.4	S	1.31	0.29	15571	108190	3215	2720	0.680	0.660	0.025	-0.002
4700	0.8	1.2	S	1.12	0.27	47280	102516	5023	4810	0.680	0.678	0.021	0.000
4700	0.8	1.3	S	1.20	0.30	34390	79923	486	14	0.676	0.671	0.000	0.000
4700	0.8	1.4	S	1.29	0.31	25450	61494	3299	3009	0.670	0.659	0.035	-0.006
4700	1.0	1.2	M	1.11	0.28	70143	70071	5140	4725	0.675	0.676	0.000	-0.000
4700	1.0	1.3	M	1.21	0.27	52156	52156	4059	3848	0.667	0.667	0.006	-0.000
4700	1.0	1.4	M	1.30	0.30	38969	38969	3275	2922	0.652	0.655	0.011	-0.001
4700	1.0	2.2	M	2.03	0.32	5493	5493	877	431	0.329	0.329	0.100	-0.015
5200	0.4	1.2	S	1.13	0.29	16991	314052	5253	4375	0.698	0.680	0.044	0.001
5200	0.4	1.3	S	1.22	0.29	12092	243954	3955	3166	0.687	0.669	0.050	-0.001

Table 3.4: *cont.*

t	q	M	Case	$M_{\rm rmn}$	$\frac{(1+q)^2}{q}\varphi$	$\tau_{\rm ms,1}$	$\tau_{\rm ms,2}$	$\tau_{\rm ms}$	$t_{\rm ms}$	$X_{\rm c,0}$	$X_{\rm c,zms}$	$\Delta \log L$	$\Delta \log T_{\rm eff}$
5200	0.4	1.4	M	1.33	0.26	8644	210585	3061	2251	0.447	0.421	0.067	-0.004
5200	0.6	1.2	S	1.13	0.25	29518	162623	5250	4687	0.684	0.679	0.020	0.000
5200	0.6	1.3	S	1.22	0.26	21253	133093	3970	3471	0.682	0.668	0.020	-0.001
5200	0.6	1.4	S	1.31	0.26	15571	108190	3153	2628	0.679	0.653	0.029	-0.002
5200	0.8	1.2	S	1.12	0.27	47280	102516	5048	2917	0.680	0.676	0.000	0.000
5200	0.8	1.3	S	1.22	0.26	34390	79923	75	3614	0.672	0.666	0.277	-0.006
5200	0.8	1.4	S	1.29	0.31	25450	61494	3311	2888	0.667	0.653	0.016	-0.002
5200	1.0	1.2	M	1.11	0.29	70143	70071	5162	4703	0.672	0.673	0.001	-0.000
5200	1.0	1.3	M	1.21	0.27	52156	52156	4073	3689	0.661	0.662	0.009	-0.001
5200	1.0	1.4	M	1.30	0.30	38969	38969	3286	2910	0.649	0.652	0.012	-0.001
5200	1.0	2.2	M	2.02	0.32	5493	5493	880	379	0.263	0.263	0.125	-0.018
5700	0.4	1.2	S	1.13	0.30	16991	314052	4884	3914	0.698	0.677	0.009	-0.002
5700	0.4	1.3	S	1.23	0.26	12092	243954	3897	3022	0.684	0.661	0.053	-0.001
5700	0.6	1.2	S	1.13	0.26	29518	162623	4626	4641	0.681	0.675	0.081	-0.001
5700	0.6	1.3	S	1.22	0.26	21253	133093	3551	3463	0.679	0.664	0.125	0.005
5700	0.6	1.4	S	1.31	0.27	15571	108190	3174	2592	0.676	0.647	0.032	-0.003
5700	0.8	1.2	S	1.12	0.28	47280	102516	5068	4926	0.677	0.673	0.041	-0.001
5700	0.8	1.3	S	1.22	0.26	34390	79923	4040	13	0.669	0.662	0.004	0.000
5700	0.8	1.4	S	1.31	0.27	25450	61494	3197	2742	0.662	0.648	0.014	-0.002
5700	1.0	1.2	M	1.11	0.29	70143	70071	5183	4664	0.669	0.671	0.000	-0.000
5700	1.0	1.3	M	1.21	0.27	52156	52156	4127	3669	0.658	0.659	0.004	-0.000
5700	1.0	1.4	M	1.29	0.31	38969	38969	3304	2876	0.643	0.646	0.014	-0.001

Table 3.5: *As Table 3.4 for the $Z = 0.001$ models.*

t	q	M	Case	$M_{\rm rmn}$	$\frac{(1+q)^2}{q}\varphi$	$\tau_{\rm ms,1}$	$\tau_{\rm ms,2}$	$\tau_{\rm ms}$	$t_{\rm ms}$	$X_{\rm c,0}$	$X_{\rm c,zms}$	$\Delta \log L$	$\Delta \log T_{\rm eff}$
8000	0.4	0.8	S	0.76	0.25	43810	695587	14678	13000	0.753	0.751	0.018	0.001
8000	0.4	0.9	S	0.85	0.25	27922	544208	9331	7683	0.752	0.719	0.032	0.002
8000	0.4	1.0	S	0.95	0.25	18612	418946	6214	4645	0.752	0.701	0.062	0.006
8000	0.4	1.1	P	1.04	0.27	12867	313659	4353	2459	0.408	0.403	0.066	0.010
8000	0.4	1.2	P	1.13	0.29	9181	221923	3150	3	0.210	0.210	0.000	0.089
8000	0.6	0.8	S	0.76	0.24	72663	364938	14963	13905	0.752	0.752	0.015	0.001
8000	0.6	0.9	S	0.85	0.24	46528	236659	9496	8484	0.751	0.746	0.016	0.001
8000	0.6	1.0	S	0.93	0.28	31103	178559	6579	5470	0.730	0.722	0.019	0.001
8000	0.6	1.1	M	1.03	0.27	21571	138218	4513	2827	0.573	0.541	0.030	0.001
8000	0.6	1.2	P	1.12	0.28	15409	105374	3241	1986	0.485	0.485	0.027	0.004
8000	0.6	1.3	P	1.22	0.28	11298	79734	2354	935	0.348	0.350	0.028	0.006
8000	0.8	0.8	S	0.75	0.25	109778	202645	15353	14290	0.735	0.733	0.004	0.000
8000	0.8	0.9	S	0.85	0.24	72663	150804	9633	8725	0.727	0.727	0.004	0.000
8000	0.8	1.0	S	0.94	0.25	48790	109778	6487	5614	0.720	0.713	0.006	0.000
8000	0.8	1.2	P	1.12	0.26	24284	57012	3215	2305	0.592	0.592	0.011	0.001
8000	0.8	1.3	P	1.21	0.30	17831	41997	2441	1493	0.526	0.527	0.025	0.002
8000	1.0	0.8	M	0.75	0.26	150804	150804	15550	14471	0.729	0.729	0.003	0.000
8000	1.0	0.9	M	0.84	0.27	105374	105374	9911	9016	0.720	0.720	0.003	0.000
8000	1.0	1.0	M	0.93	0.27	72663	72663	6603	5773	0.705	0.705	0.003	0.000
8000	1.0	1.1	M	1.03	0.26	50701	50701	4509	3695	0.682	0.683	0.008	0.001
8000	1.0	1.2	M	1.12	0.26	36358	36358	3218	2388	0.649	0.651	0.007	0.001
8000	1.0	1.3	M	1.21	0.29	26764	26764	2425	1596	0.612	0.612	0.024	0.001
9500	0.4	0.8	S	0.76	0.26	43810	695587	14847	12884	0.752	0.752	0.023	0.002

Table 3.5: *cont.*

t	q	M	Case	$M_{\rm rmn}$	$\frac{(1+q)^2}{q}\varphi$	$\tau_{\rm ms,1}$	$\tau_{\rm ms,2}$	$\tau_{\rm ms}$	$t_{\rm ms}$	$X_{\rm c,0}$	$X_{\rm c,zms}$	$\Delta \log L$	$\Delta \log T_{\rm eff}$
9500	0.4	0.9	S	0.85	0.27	27922	544208	9479	7438	0.751	0.709	0.037	0.002
9500	0.4	1.0	S	0.94	0.28	18612	418946	6367	4278	0.751	0.680	0.052	0.006
9500	0.4	1.1	P	1.04	0.28	12867	313659	4403	2057	0.313	0.313	0.069	0.011
9500	0.4	1.2	P	1.13	0.29	9181	221923	3151	235	0.047	0.069	0.079	0.017
9500	0.6	0.8	S	0.75	0.24	72663	364938	15051	13767	0.751	0.750	0.015	0.001
9500	0.6	0.9	S	0.85	0.25	46528	236659	1009	8353	0.751	0.729	0.500	0.025
9500	0.6	1.0	S	0.94	0.25	31103	178559	6412	5105	0.723	0.705	0.022	0.002
9500	0.6	1.1	P	1.03	0.26	21571	138218	4469	3073	0.528	0.528	0.028	0.003
9500	0.6	1.2	P	1.12	0.28	15409	105374	3247	1695	0.414	0.415	0.031	0.004
9500	0.6	1.3	P	1.21	0.30	11298	79734	2420	621	0.235	0.235	0.032	0.007
9500	0.8	0.8	S	0.75	0.26	109778	202645	15447	14171	0.729	0.728	0.006	0.000
9500	0.8	0.9	S	0.84	0.25	72663	150804	9702	8612	0.722	0.720	0.005	0.000
9500	0.8	1.1	M	1.02	0.28	33896	78905	4632	3545	0.620	0.631	0.010	0.002
9500	0.8	1.2	P	1.12	0.28	24284	57012	3279	2173	0.557	0.557	0.014	0.002
9500	0.8	1.3	P	1.20	0.30	17831	41997	2336	1285	0.470	0.470	0.050	0.003
9500	1.0	0.8	M	0.75	0.27	150804	150804	15638	14353	0.724	0.724	0.002	0.000
9500	1.0	0.9	M	0.84	0.27	105374	105374	9974	8906	0.713	0.713	0.003	0.000
9500	1.0	1.0	M	0.93	0.28	72663	72663	6663	5653	0.695	0.695	0.004	0.000
9500	1.0	1.1	M	1.03	0.27	50701	50701	4584	3588	0.667	0.667	0.007	0.001
9500	1.0	1.2	M	1.12	0.27	36358	36358	3271	2264	0.627	0.631	0.010	0.001
9500	1.0	1.3	M	1.21	0.26	26764	26764	2368	1410	0.574	0.579	0.032	0.001
11000	0.4	0.8	S	0.76	0.28	43810	695587	14999	12605	0.751	0.746	0.028	0.002
11000	0.4	0.9	S	0.85	0.25	27922	544208	9333	7069	0.751	0.710	0.054	0.005
11000	0.4	1.0	P	0.94	0.28	18612	418946	6329	3858	0.420	0.420	0.059	0.006

Table 3.5: *cont.*

t	q	M	Case	$M_{\rm rmn}$	$\frac{(1+q)^2}{q}\varphi$	$\tau_{\rm ms,1}$	$\tau_{\rm ms,2}$	$\tau_{\rm ms}$	$t_{\rm ms}$	$X_{\rm c,0}$	$X_{\rm c,zms}$	$\Delta \log L$	$\Delta \log T_{\rm eff}$
11000	0.4	1.1	P	1.03	0.30	12867	313659	4484	1377	0.211	0.211	0.036	0.011
11000	0.6	0.8	S	0.75	0.25	72663	364938	15139	13640	0.750	0.749	0.015	0.001
11000	0.6	0.9	S	0.85	0.26	46528	236659	9674	8250	0.750	0.737	0.023	0.002
11000	0.6	1.0	M	0.94	0.27	31103	178559	6499	4849	0.696	0.536	0.010	0.002
11000	0.6	1.1	P	1.03	0.25	21571	138218	4434	2770	0.480	0.480	0.030	0.003
11000	0.6	1.2	P	1.12	0.29	15409	105374	3264	1322	0.336	0.336	0.026	0.005
11000	0.6	1.3	P	1.21	0.29	11298	79734	2383	306	0.104	0.134	0.071	0.009
11000	0.8	0.8	S	0.75	0.26	109778	202645	15514	14031	0.724	0.724	0.005	0.000
11000	0.8	0.9	S	0.84	0.27	72663	150804	9928	8636	0.717	0.713	0.005	0.000
11000	0.8	1.1	P	1.02	0.30	33896	78905	4696	3407	0.596	0.596	0.012	0.002
11000	0.8	1.2	P	1.12	0.27	24284	57012	3257	1940	0.516	0.516	0.015	0.002
11000	0.8	1.3	P	1.21	0.28	17831	41997	2401	1026	0.407	0.407	0.019	0.002
11000	1.0	0.8	M	0.75	0.27	150804	150804	15694	14943	0.720	0.720	0.000	0.000
11000	1.0	0.9	M	0.84	0.28	105374	105374	10036	751	0.706	0.706	0.000	0.000
11000	1.0	1.0	M	0.93	0.28	72663	72663	6723	5559	0.685	0.685	0.003	0.000
11000	1.0	1.1	M	1.02	0.28	50701	50701	4639	3473	0.653	0.653	0.007	0.001
11000	1.0	1.2	M	1.11	0.29	36358	36358	3332	2125	0.606	0.606	0.011	0.001
11000	1.0	1.3	M	1.21	0.29	26764	26764	2321	1175	0.541	0.545	0.025	0.001
12500	0.4	0.9	S	0.85	0.27	27922	544208	9492	6505	0.750	0.690	0.014	0.004
12500	0.4	1.0	P	0.94	0.27	18612	418946	6304	3365	0.355	0.355	0.067	0.007
12500	0.4	1.1	P	1.03	0.29	12867	313659	4440	492	0.095	0.096	0.047	0.016
12500	0.6	0.8	S	0.75	0.26	72663	364938	15230	13508	0.750	0.747	0.017	0.001
12500	0.6	0.9	S	0.85	0.24	46528	236659	9475	7857	0.748	0.718	0.025	0.002
12500	0.6	1.0	M	0.94	0.25	31103	178559	6399	4582	0.546	0.546	0.027	0.002

Table 3.5: *cont.*

t	q	M	Case	$M_{\rm rmn}$	$\frac{(1+q)^2}{q}\varphi$	$\tau_{\rm ms,1}$	$\tau_{\rm ms,2}$	$\tau_{\rm ms}$	$t_{\rm ms}$	$X_{\rm c,0}$	$X_{\rm c,zms}$	$\Delta \log L$	$\Delta \log T_{\rm eff}$
12500	0.6	1.1	P	1.03	0.28	21571	138218	4537	2526	0.433	0.433	0.029	0.004
12500	0.6	1.2	P	1.12	0.30	15409	105374	3301	918	0.249	0.249	0.022	0.007
12500	0.8	0.8	S	0.75	0.27	109778	202645	15605	13908	0.720	0.719	0.007	0.000
12500	0.8	0.9	S	0.84	0.28	72663	150804	10004	8516	0.712	0.706	0.007	0.000
12500	0.8	1.0	M	0.94	0.26	48790	109778	6515	5108	0.630	0.633	0.008	0.001
12500	0.8	1.1	P	1.03	0.27	33896	78905	4552	3115	0.567	0.567	0.013	0.002
12500	0.8	1.2	P	1.11	0.29	24284	57012	3326	1796	0.476	0.476	0.016	0.002
12500	0.8	1.3	P	1.21	0.27	17831	41997	2366	817	0.338	0.338	0.027	0.002
12500	1.0	0.8	M	0.75	0.23	150804	150804	15091	13462	0.712	0.711	0.003	0.000
12500	1.0	0.9	M	0.84	0.28	105374	105374	10100	8680	0.699	0.699	0.004	0.000
12500	1.0	1.0	M	0.94	0.25	72663	72663	6464	5187	0.672	0.672	0.003	0.000
12500	1.0	1.1	M	1.02	0.29	50701	50701	4705	3866	0.639	0.639	0.003	0.001
12500	1.0	1.2	M	1.12	0.26	36358	36358	3235	1911	0.576	0.580	0.012	0.001
12500	1.0	1.3	M	1.21	0.27	26764	26764	2376	1126	0.502	0.507	0.049	0.002

4

Structure and evolution of high mass stellar mergers

In young dense clusters repeated collisions between massive stars may lead to the formation of a very massive star (above $10^2\,M_\odot$). In the past the study of the long-term evolution of merger remnants has mostly focussed on collisions between low-mass stars (up to about $2\,M_\odot$) in the context of blue-straggler formation. The evolution of collision products of more massive stars has not been as thoroughly investigated. In this paper we study the long-term evolution of a number of stellar mergers formed by the head-on collision of a primary star with a mass of 5–40 $M_\odot$ with a lower mass star at three points in its evolution in order to better understand their evolution as a first step to a more complete understanding of merger runaways.

We use smooth particle hydrodynamics (SPH) calculations to model the collision between the stars. The outcome of this calculation is reduced to one dimension and imported into a stellar evolution code. We follow the subsequent evolution of the collision product through the main sequence at least until the onset of helium burning.

We find little mixing between the core and the envelope of the collision products, in agreement with previous studies of collisions between low-mass stars. The evolution of most of the collision products proceeds analogously to that of normal stars with the same mass, but with a larger radius and luminosity. However, the evolution of collision products that form with a hydrogen depleted core is markedly different from that of normal stars with the same mass. They undergo a long-lived period of hydrogen shell burning close to the main sequence band in the Hertzsprung-Russell diagram and spend the initial part of core helium burning as compact blue supergiants.

4.1 Introduction

Dense stellar systems, such as the cores of star clusters or galactic nuclei, are crowded places where stars frequently interact with each other. In globular clusters, close two-body encounters may form binaries (Hut & Verbunt 1983); furthermore, two-body encounters can be close enough that two stars can come into physical contact which can lead to a merger (Hills & Day 1976). Galactic nuclei, where stellar densities reach values in excess of millions of stars per cubic parsec, also harbour stellar collisions. It therefore appears that stellar mergers are natural events in dense stellar systems and this has been demonstrated by several N-body simulations (Portegies Zwart et al. 1999; Hurley et al. 2001; Portegies Zwart et al. 2004).

Stellar mergers provide a formation channel for non-canonical stars that cannot be otherwise explained by the standard theory of star formation and evolution, such as blue stragglers that are observed in both open and globular clusters (Ahumada & Lapasset 1995; Piotto et al. 2004; Ahumada & Lapasset 2007). In a young star cluster stellar mergers might be responsible for the formation of massive stars such as the Pistol Star in the Quintuplet Cluster (Figer et al. 1998). Other massive stars, such as Sher 25 in the massive Galactic cluster NGC 3603, may have been formed via binary mergers. Along with the single merger events, some star clusters, such as the Arches close to Galactic centre or R136 in the Large Magellanic Cloud, are dense enough that runaway stellar mergers can occur (Portegies Zwart et al. 2004).

Simulating stellar collisions has attracted considerable attention in the past decade, mostly focussing on globular clusters with the aim of explaining the formation of blue stragglers. Blue stragglers can be formed by stellar collisions or by mass transfer in binary systems. Either of these mechanisms can dominate in one particular cluster, or in different regions of the same cluster (Davies et al. 2004). N-body simulations of clusters show that both formation channels are necessary to reproduce the observed blue straggler population (Hurley et al. 2001, 2005). Nevertheless, there are still many uncertainties regarding blue straggler formation (Leigh et al. 2007).

Dense stellar systems that are abundant in young massive stars, such as the cores of young dense star clusters, are also a natural environment for stellar mergers (Portegies Zwart et al. 1999; Gaburov et al. 2008b). In contrast to globular clusters, the colliding stars have masses that are much larger than the average stellar mass of their environment. If the cluster is dense enough the same star may experience repeated collisions in a so-called 'merger runaway' (Portegies Zwart et al. 1999). Such a merger runaway is triggered by the gravo-thermal collapse of the cluster core (Bettwieser & Sugimoto 1984) and can continue until the target star leaves the main sequence (Portegies Zwart et al. 1999). To understand the outcome of such a merger event it is important to understand the structure and evolution of the collision product. Only recently have researchers begun to focus their

attention on collisions between massive stars (Freitag & Benz 2005; Dale & Davies 2006; Suzuki et al. 2007; Freitag et al. 2007; Gaburov et al. 2008c). These studies were focused either on global properties, such as mass loss, or on the internal structure of collision products; yet very little is known about the evolution of such objects.

In this paper we attempt to fill the gap in our understanding by systematically carrying out collision simulations between massive main-sequence stars and studying their further evolution. The aim of this work is to understand the evolution of collision products formed in a merger of two ordinary massive main-sequence stars as a function of stellar ages and masses in the context of merger runaways. This paper is structured as follows. In Section 4.2 we present the methods we use carry out this research, in Section 4.3 we describe the initial conditions for our simulations and in Section 4.4 we present our results. A discussion of these results and our conclusions are presented in Section 4.5.

4.2 Methods

4.2.1 Hydrodynamic simulations

We use smoothed particle hydrodynamics (SPH) to model stellar collisions (Monaghan 2005). SPH is a fully Lagrangian method, which means that it easily adapts to any geometrical configuration without some of the problems in finite-difference methods, such as artefacts due to the choice of coordinate system or numerical diffusion. In addition, the conserved fluid quantities, such as composition, are trivially advected. The largest drawback of SPH, however, is that low density regions are poorly resolved. However, stellar interiors, which contain nearly all the stellar mass, are dense enough for SPH to provide sufficient resolution to capture fine details, such as the density and mean molecular weight gradients across the boundary of a stellar core; for example, in Figure 4.1 we show the structure of a 20 $M_\odot$ star at the end of the main sequence phase. One may notice that despite the fact that roughly 30% of the stellar radius is not resovled, this region contributes less than 1% of the stellar mass, so that the internal structure is well resolved.

The simulations that are presented in this paper are carried out by means of a modified version of the `GADGET2` code (Springel 2005); the modifications are described in Appendix 4.A. In particular, we included radiation pressure in the equation of state and the functionality to generate relaxed models of the parent stars in quasi-hydrostatic equilibrium described by Turner et al. (1995) and Lombardi et al. (2006).

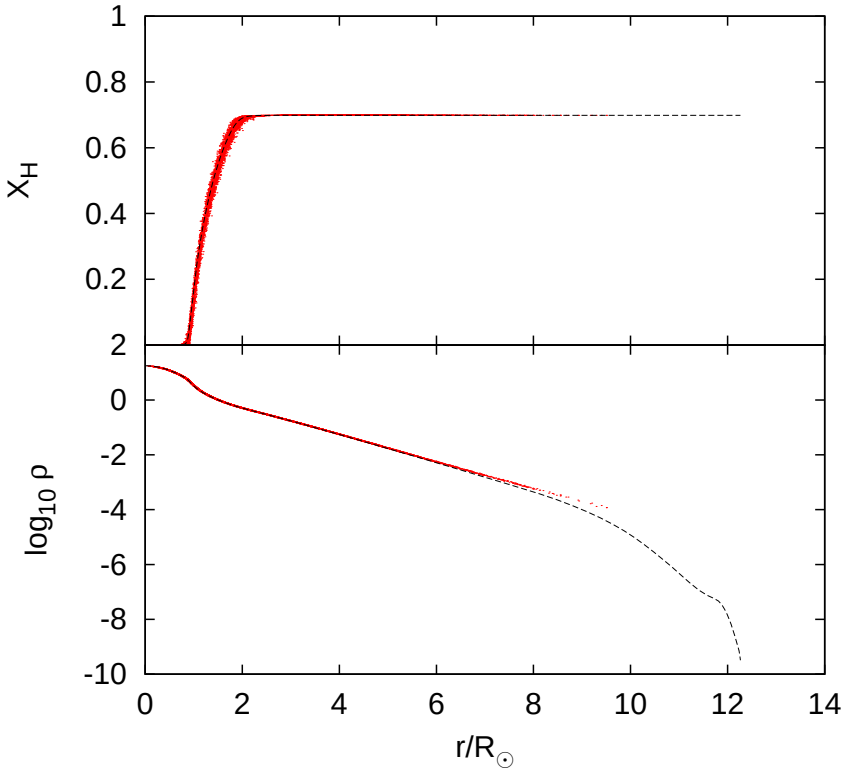

Figure 4.1: *Structure of the 20* $M_\odot$ *primary at the end of the main sequence. The upper panel shows the hydrogen abundance and the lower panel shows the density, both as a function of the enclosed radius. Dots indicate individual SPH particles (only 1 in 10 is plotted), the dashed line shows the one dimensional stellar evolution model.*

4.2.2 The stellar evolution code

We use the stellar evolution code originally developed by Eggleton (1971) and later updated by others (*e.g.* Pols et al. 1995), hereafter `STARS`. `STARS` uses an adaptive non-Lagrangian mesh that allocates meshpoints using a mesh-spacing function that places more meshpoints in regions where a higher resolution is desirable. This means that stars can be evolved with reasonable accuracy with as few as 200 meshpoints. The code is fully im-

plicit and solves for the structure and composition of the star simultaneously. Convective mixing is treated as a diffusion process (Böhm-Vitense 1958; Eggleton 1972), as is thermohaline mixing (Kippenhahn et al. 1980).

The conversion of the collision output to stellar evolution input is also done using implicit calculations. Starting with a normal main sequence model, the composition and entropy profiles are adjusted until they match the merger remnant profiles. The full details of this procedure are described in Glebbeek et al. (2008). Once a suitable input model has been constructed we follow the subsequent evolution of the merger remnant.

For our evolution calculations we have used reaction rates from Caughlan & Fowler (1988) and Caughlan et al. (1985) and we use opacities from Rogers & Iglesias (1992) and Alexander & Ferguson (1994). The assumed heavy-element composition is scaled to solar abundances (Anders & Grevesse 1989). Our assumed mass loss rate is the empirical rate from de Jager et al. (1988).

4.3 Initial conditions

The aim of this work is to understand the structure and the evolution of massive stellar collision products. The structure of the collision product is influenced by the masses and composition of the colliding (parent) stars as well as the parameters of the collision. We therefore need to span a section of the parameter space that encompasses a variety of initial conditions for the geometry of the collisions and the masses and ages of the parent stars. In this study we will focus on head-on parabolic collisions, ignoring the complications associated with rotation in the merger product (*e.g.* Sills et al. 2005) in order to focus on the influence of the parent star masses and ages. The limitation to parabolic collisions can be justified by the fact that the velocity dispersion in young star clusters is much smaller than the escape velocity from the stellar surface and therefore has little influence on the structure of the merger remnant.

4.3.1 Masses and ages of the parent stars

We systematically study collisions between massive stars of different masses and ages, but with the same initial composition. For convenience, the masses of parent stars are described by two quantities: the mass of the primary star, M_1, and the mass ratio of the secondary to the primary star, $q = M_2/M_1 < 1$.

We choose the ages of the parent stars based on the evolution stage of the primary, as illustrated in Figure 4.2: the zero-age main sequence (ZAMS), halfway through the main sequence (HAMS), at the terminal-age main sequence (TAMS) or at core hydrogen exhaustion (CHEX). Here

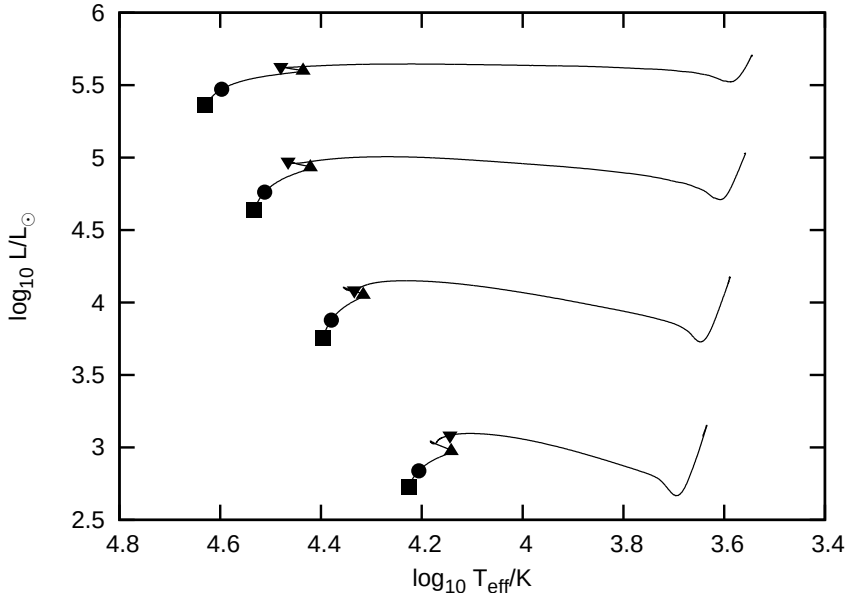

Figure 4.2: *Hertzsprung-Russell diagram of our primary stars, with (from top to bottom) masses of 40, 20, 10 and 5* $M_\odot$*, showing the points chosen for our collisions. The ZAMS is indicated by* ■*, the HAMS by* • *and TAMS and CHEX by* ▲ *and* ▼ *respectively.*

TAMS refers to the reddest point before the hook at core hydrogen exhaustion. This normally corresponds to the moment where the star has 3–4% by mass of hydrogen left in the core, but in some of our TAMS models the central hydrogen abundance is smaller (1–0.1%). The CHEX stage is shortly after this stage, at the bluest point after the TAMS stage but before the Hertzsprung gap. This corresponds to actual core hydrogen exhaustion, or a hydrogen abundance of about 0.01% in the core depending on the mass of the star. The masses of the primaries are chosen to be 5, 10, 20 and 40 $M_\odot$, whereas the masses of the secondary star are chosen according to the mass ratio q, which takes the values 0.1, 0.4, 0.7 and 1.0. This was done to get a reasonable coverage between equal masses and extreme mass ratios. For CHEX stars we choose $q = 0.99$ rather than 1.0, which corresponds to a collision between a CHEX and a TAMS star. To simplify the notation later we will refer to a collision between a 10 $M_\odot$ TAMS star and a 1 $M_\odot$ star (say) as 'TAMS 10+1'.

M_1 [$M_\odot$]	M_2 [$M_\odot$]	q	$N_1/1000$	$N_2/1000$	Age
40	40	1.0	131	131	TAMS, HAMS
40	39.6	0.99	132	130	CHEX
40	28	0.7	155	107	CHEX, TAMS, HAMS
40	16	0.4	400	160	CHEX
40	16	0.4	187	75	CHEX, TAMS
40	4	0.1	239	23	CHEX, TAMS, HAMS
20	20	1.0	131	131	TAMS
20	19.8	0.99	132	130	CHEX
20	14	0.7	155	107	CHEX, TAMS, HAMS
20	8	0.4	187	75	CHEX, TAMS
20	8	0.4	200	80	ZAMS*
20	2	0.1	239	23	CHEX, TAMS, HAMS
10	10	1.0	131	131	TAMS
10	9.9	0.99	132	130	CHEX
10	8	0.8	100	80	ZAMS*
10	7	0.7	155	107	CHEX, TAMS, HAMS
10	4	0.4	187	75	CHEX, TAMS
10	1	0.1	239	23	CHEX, TAMS, HAMS
5	5	1.0	131	131	TAMS
5	4.95	0.99	132	130	CHEX
5	3.5	0.7	155	107	CHEX, TAMS, HAMS
5	2	0.4	187	75	CHEX, TAMS
5	0.5	0.1	239	23	CHEX, TAMS, HAMS

Table 4.1: *This table presents an overview of the simulations used in this work. The first and second columns show the mass of the primary and the secondary star respectively, the third column shows the mass ratio. The fifth and sixth columns display the number of SPH particles used in each of the stars, and the last column indicates the evolutionary stage of the primary. In most of the simulations we use* $2.62 \cdot 10^5$ *particles. One of the CHEX models is also simulated with higher resolution* ($5.6 \cdot 10^5$ *particles) to verify that the lower resolution simulations capture the essential details. All stellar models are of solar metallicity* ($Z = 0.02$).
**These ZAMS models were not simulated, but results of the simulations were taken from Gaburov et a. 2008.*

4.3.2 Stellar models and set up of simulations

The full set of simulations that we carried out is presented in Table 4.1. Most of the simulations use $2.62{\cdot}10^5$ equal mass SPH particles. This number was chosen such that we will be able to accurately resolve the internal structure of the collision product (Sills et al. 2002; Gaburov et al. 2008c).

We prepare our 3D SPH models based on 1D stellar evolution models calculated with `STARS`. Our input models are non-rotating and start with an initial heavy element abundance (metallicity) $Z = 0.02$ and a hydrogen abundance $X = 0.70$. For each collision we calculate the evolution of the primary until the appropriate age (ZAMS, HAMS, TAMS or CHEX) and then evolve the secondary to the same age as the primary. We use the composition, density and temperature profiles of the 1D models to construct a quasi-hydrostatic equilibrium SPH model, as described in Appendix 4.B.

We use the resulting three dimensional SPH models to prepare our collision simulations. The parent stars are initially separated by a distance that is equal to twice the sum of their radii and with the velocity of each star computed in such a way that the total orbital energy, angular momentum and velocity of the centre of mass is zero. The stellar velocities are directed towards each other.

4.3.3 Reduction of three-dimension data

In order to import the results of our collision calculations into the stellar evolution code the three-dimensional data has to be reduced to one dimension and converted into a format that is understandable by the stellar evolution code. A collision between stars is a complex hydrodynamic interaction of self-gravitating fluids, and such interactions do not posses apparent symmetries. Shocks together with turbulent heating result in mixing of the fluid that is intrinsically three-dimensional. However, the structure of a head-on collision product is spherically symmetric once the fluid has settled into hydrostatic equilibrium. This allows us to reduce the three-dimensional data to one dimension by averaging over equipotential surfaces. The details of the reduction are presented in Appendix 4.C.

The collision calculations do not have sufficient resolution to resolve the outer parts of the envelope near the photosphere, which means that we do not know anything about the structure of the envelope at that point. However, for the stellar evolution code the input model needs to satisfy the photospheric boundary condition. Sills et al. (1997) extrapolated the entropy profile and used the condition of hydrostatic equilibrium to reconstruct the outer layers. Because our method to import the stellar evolution models is fully implicit we find it easier to allow the evolution code to simply adjust the unresolved layers in response to the stellar interior (Glebbeek et al. 2008), which is equivalent to assuming that the outer layers are in thermal

equilibrium at the start of our evolution calculations. This is a reasonable approximation because the thermal timescale for these layers is short compared to the thermal timescale of the entire star. As noted by Sills et al. (1997), the long term evolution of the collision product is not sensitive to the treatment of the surface layers.

4.4 Results

4.4.1 Structure of the collision products

It was shown by Lombardi et al. (2002)that there is a simple physical mechanism that determines the structure of a collision product, and this provides a quick method to obtain the approximate structure of the collision product as well as understand the outcome of SPH calculations. The intricate details of shock and turbulent heating cannot be predicted by simple analytical models, but an empirical tabulation of shock heating, which based on a number of simulations, combined with conservation laws provides an accurate estimate of the degree of shock-heating (Lombardi et al. 2002, 2003; Gaburov et al. 2008c).

For a chemically homogeneous star in hydrostatic equilibrium the entropy increases outward. The idea behind the method is to find a function of entropy and composition that increases outward in stars that are not chemically homogeneous. Such a function is $A = P/\rho^{5/3}\exp[8(1-\beta)/3\beta]$ (Gaburov et al. 2008c). We call this function A the buoyancy, since for stable hydrostatic equilibrium the fluid with higher buoyancy should generally be above the fluid with lower buoyancy. The stability condition is (Gaburov et al. 2008c)

$$\frac{\mathrm{d}\log A}{\mathrm{d}m} > \frac{4}{3}\frac{\frac{5}{3}-\Gamma_1}{\Gamma_1-\frac{4}{3}}\frac{\mathrm{d}\log\mu}{\mathrm{d}m}. \tag{4.1}$$

Here m is the enclosed mass, μ is the mean molecular weight of the fluid element and $\Gamma_1 = (\partial\log P/\partial\log\rho)_{\mathrm{ad}}$ is its adiabatic index (Clayton 1983; Kippenhahn & Weigert 1990).

In the case of a monatomic ideal gas ($\Gamma_1 = 5/3$) or a chemically homogeneous fluid ($\mathrm{d}\mu/\mathrm{d}m = 0$) the stability condition simplifies to $\mathrm{d}A/\mathrm{d}m > 0$. Heating is important because it modifies the entropy in each of the parent stars. Therefore, for proper modelling one needs to take into account the conversion of orbital kinetic energy into heat (Lombardi et al. 2002; Gaburov et al. 2008c).

For collisions between unevolved (ZAMS) stars equation (4.1) implies that the core of the lower mass star sinks to the centre of the collision product. For evolved stars the situation is more complicated because stellar evolution decreases A in the core of the primary more quickly than in the core of the secondary, but it is still possible that the core of the secondary

retains its identity and sinks to the centre of the collision product. Following the results of Glebbeek & Pols (2008) for collisions between low-mass stars we identify the cases 'M', 'P' and 'S' depending on whether the core of the collision product is a mixture of material from the progenitor stars, or predominantly comes from the primary or the secondary.

Case M

If the buoyancy in the cores of the two progenitor stars is similar, or if the two stars are very close in mass, the material in the core will be a mixture of the material in the cores of the two parent stars. After the collision the hydrogen abundance in the core will be in between the hydrogen abundances in the progenitor stars. There can be a molecular weight inversion if the material just outside the core predominantly comes from the primary. We schematically present this case in Figure 4.3(a).

Case P

If the primary is sufficiently evolved, the core of the primary becomes the core of the collision product. This does not normally lead to a molecular weight inversion, but it does mean that the collision product has an anomalously small core for a star of its mass. If the core cannot grow, for instance because hydrogen has already been exhausted and there is no nuclear burning, the evolution path of the collision product can be very different from that of a normal star of the same mass, as will be discussed in section 4.4.2. This case is schematically presented in Figure 4.3(b).

Case S

If stellar evolution has not decreased the buoyancy in the primary core sufficiently, the core of the secondary will displace the core of the primary and occupy the centre of the collision product. This can happen at moderate mass ratios if the primary is relatively unevolved, or it can happen at more extreme mass ratios even if the primary is already at the end of the main sequence. In either of these cases the core of the collision product will be hydrogen rich, with a helium rich layer just outside the core. A schematic diagram for this case is shown in Figure 4.3(c)

Zero Age Main Sequence

Collisions between ZAMS stars will be either case M (if the stars have the same mass) or case S. Since the parent stars are chemically homogeneous, the collision product will also be chemically homogeneous, so this will only affect the initial buoyancy profile. Once the collision product has reached thermal equilibrium it will resemble a normal main sequence star.

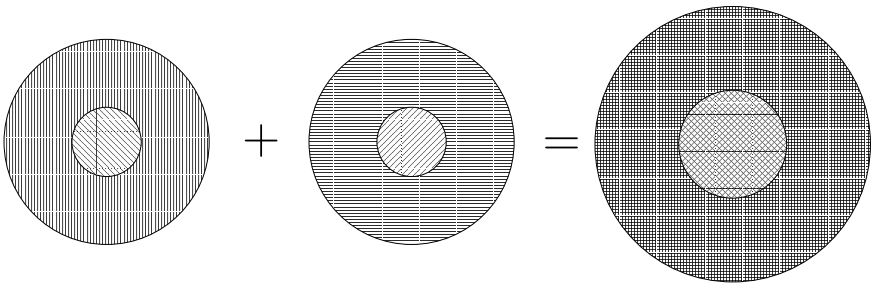

(a) Case M

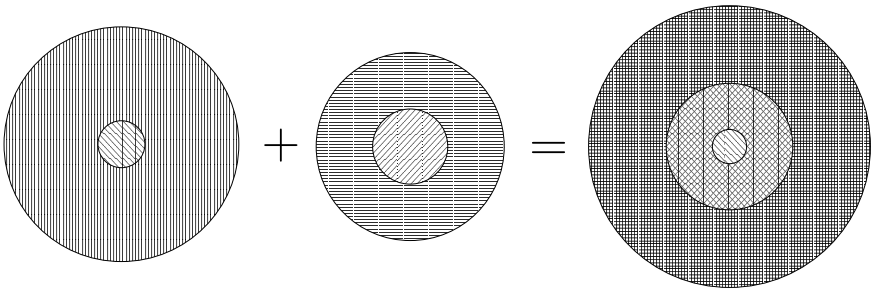

(b) Case P

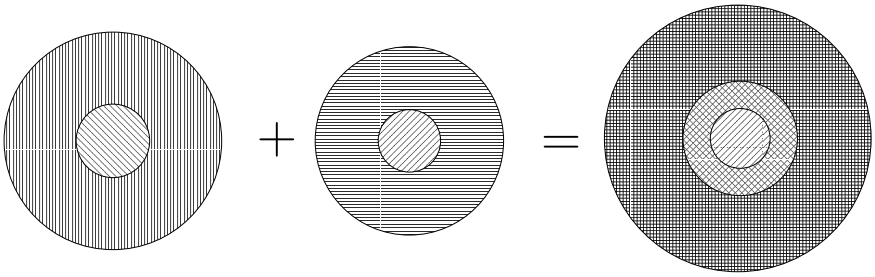

(c) Case S

Figure 4.3: *Schematic structure of the merger products for cases case M, P and S respectively. For each star, we distinguish the core, represented with an inclined lines pattern, and the envelope, represented with vertical (primary) and horizontal (secondary) lines.*

Half Age Main Sequence

Stars at half of their main-sequence age have converted a notable amount of hydrogen into helium. During the collision, the stellar interior is heated via shock waves, turbulent heating and tidal interactions. The result is that

Table 4.2: *Mass lost from HAMS collisions. The first column is the ZAMS mass of the primary star and its mass at the moment of collision in brackets, the second column is the ZAMS mass of the secondary with the mass at the moment of collision given in brackets, the third column is the fractional mass loss as a percentage of the total mass and the last column identifies the collision case (M, P or S, see text).*

M_1 [$M_\odot$]	M_2 [$M_\odot$]	$M_{\rm lost}$ [%]	Case
40 (39.3)	40 (39.3)	6.2	M
40 (39.3)	28 (27.7)	6.2	M
20 (19.8)	14 (14.0)	6.5	M
10 (9.98)	7 (7.00)	6.8	M
5 (5.00)	3.5 (3.50)	6.9	M
40 (39.3)	4 (4.00)	0.70	S
20 (19.8)	2 (2.00)	0.66	S
10 (9.98)	1 (1.00)	0.81	S
5 (5.00)	0.5 (0.50)	1.3	S

some of the helium-enriched material from the interior is mixed into the outer layers; at the same time, part of the weakly bound outer layers are ejected. The amount of mass loss in these collision is relatively small, and shown in Table 4.2.

In Figure 4.4 we show the structure of the HAMS 10+1 collision product, which is an example of case S that illustrates some of the characteristic features. The $1\,M_\odot$ star remains almost completely intact, as can be seen from the hydrogen profile. This results in a molecular weight inversion at the edge of the core at $1\,M_\odot$. Because the secondary retained its identity but now finds itself compressed in the interior of a more massive star, the core of the collision product is overdense and overheated compared to a $1\,M_\odot$ star. However, the entropy in the core is low compared to the entropy in a ZAMS star (which has the same composition) of the same mass as the collision product. This results in a steepening of the density profile below $1\,M_\odot$ and a temperature inversion, with the maximum temperature occurring at 1 $M_\odot$.

Terminal-age main sequence star (TAMS)

For TAMS stars the envelope is less strongly bound compared to HAMS stars and therefore a larger fraction of mass is lost, as shown in Table 4.4. It can be seen that the mass loss fraction is also a decreasing function of the mass ratio q. This is because the orbital kinetic energy, which is dissipated into heat and used to eject the material, is proportional to the product of

Table 4.3: *As Table 4.2 for TAMS collisions.*

M_1 ($M_\odot$)	M_2 ($M_\odot$)	$M_{\rm lost}$ (%)	Case
40 (36.7)	40 (36.7)	8.3	M
20 (19.4)	20 (19.4)	8.0	M
10 (9.98)	10 (9.98)	8.1	M
5 (5.00)	5.0 (5.00)	8.2	M
40 (36.7)	28 (27.2)	8.0	M
20 (19.4)	14 (13.9)	7.6	P
10 (9.98)	7 (7.00)	7.6	P
5 (5.00)	3.5 (3.5)	7.6	P
40 (36.7)	16 (15.9)	8.6	S
20 (19.4)	8 (8.00)	8.2	S
10 (9.98)	4 (4.00)	7.3	S
5 (5.00)	2 (2.00)	7.5	S
40 (36.7)	4 (4.00)	2.1	S
20 (19.4)	2 (2.00)	1.5	S
10 (9.98)	1 (1.00)	1.4	S
5 (5.00)	0.5 (0.50)	2.2	S

Table 4.4: *As Table 4.2 for CHEX collisions.*

M_1 ($M_\odot$)	M_2 ($M_\odot$)	$M_{\rm lost}$ (%)	Case
40 (36.7)	39.6 (36.4)	8.0	P
20 (19.4)	19.8 (19.2)	8.0	P
10 (9.98)	9.9 (9.88)	8.0	M
5 (5.00)	4.95 (4.95)	8.1	M
40 (36.7)	28 (27.2)	7.8	M
20 (19.4)	14 (13.9)	7.7	P
10 (9.98)	7 (7.00)	7.7	P
5 (5.00)	3.5 (3.5)	7.7	P
40 (36.7)	16 (15.9)	8.6 (8.8)	S
20 (19.4)	8 (8.00)	8.2	S
10 (9.98)	4 (4.00)	7.8	S
5 (5.00)	2 (2.00)	7.5	M
40 (36.7)	4 (4.00)	2.1	S
20 (19.4)	2 (2.00)	1.5	S
10 (9.98)	1 (1.00)	1.5	S
5 (5.00)	0.5 (0.50)	2.3	S

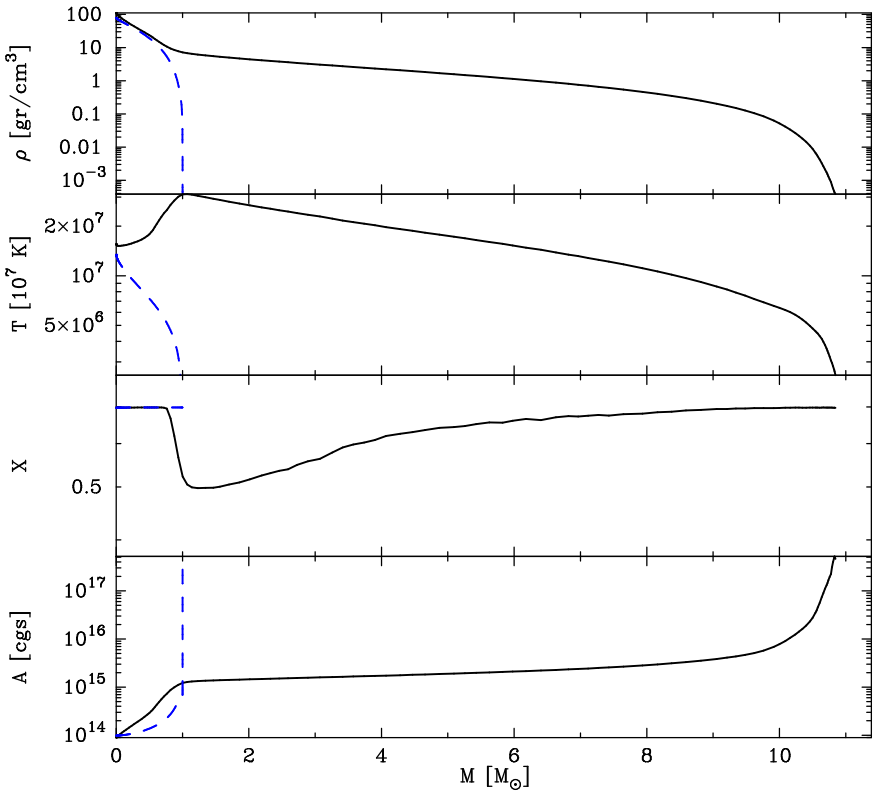

Figure 4.4: *Structure of the HAMS 10+1 merger product. The upper panel shows the density profile as a function of enclosed mass, the second panel from the top presents the temperature profile and the two lowest panels display the hydrogen mass fraction and buoyancy profile as a function of enclosed mass respectively. The blue dashed line is the structure profiles of the secondary star.*

the masses of the parent stars $M_1 M_2 = q M_1^2$. Hence, the smaller q the smaller the amount of mass that is lost.

An example of a case P collision product is the TAMS 10+7 product shown in Figure 4.5. In this case the core of the primary contained 0.1% by mass of hydrogen at the time of collision and the core of the secondary is unable to displace the core of the primary. The inner $0.5\,\mathrm{M}_\odot$ of the remnant consists of hydrogen depleted material from the primary, while the material between $0.5\,\mathrm{M}_\odot$ and $1\,\mathrm{M}_\odot$ is a mixture of material from the primary and the secondary. The central density and temperature are again higher than

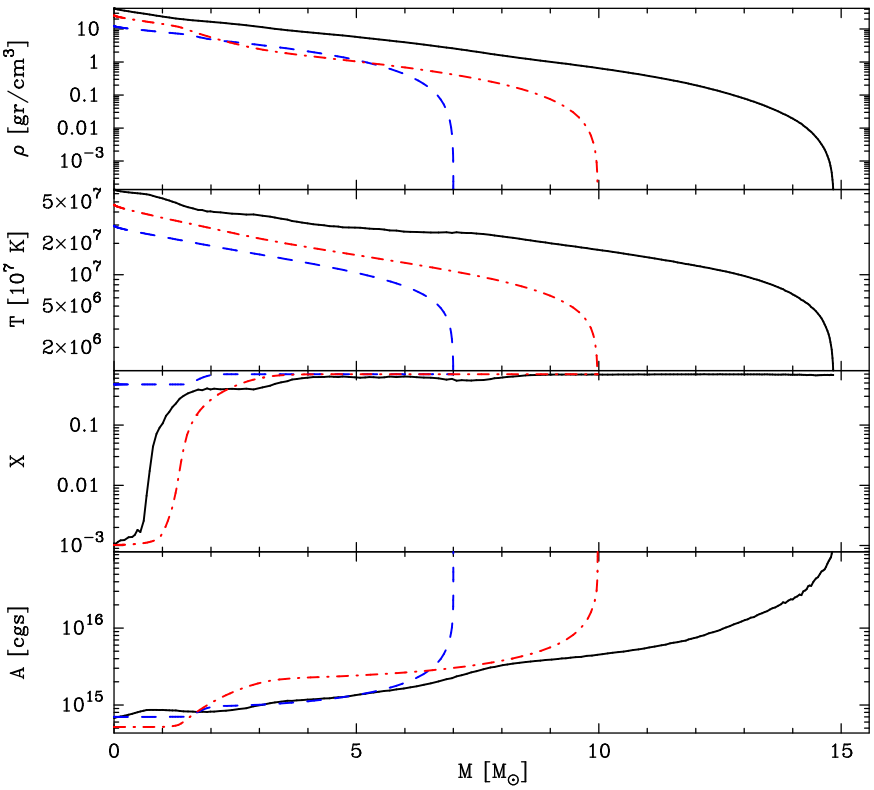

Figure 4.5: *As Figure 4.4 for the TAMS 10+7 collision product. The dashed line (blue) shows the structure of the secondary and the dash-dotted line (red) shows the structure of the primary.*

in the core of the 10 $M_\odot$ primary, but in this case there is no temperature inversion.

Core Hydrogen Exhaustion (CHEX)

Stars that have completely exhausted hydrogen in their cores (CHEX stars) have a similar structure to TAMS stars. Therefore we expect that the structure of the collision products and mass loss are similar to TAMS collisions. Indeed, Table 4.4 shows that the mass lost in collisions between CHEX stars is quantitatively similar to the mass lost in collisions between TAMS stars.

In Figure 4.6 we show the structure of the collision products of which the primary is a 20 $M_\odot$ CHEX star and the secondary covers a mass range such that the mass ratio q is 0.99 (4.6(a)), 0.7 (4.6(b)), 0.4 (4.6(c)) and

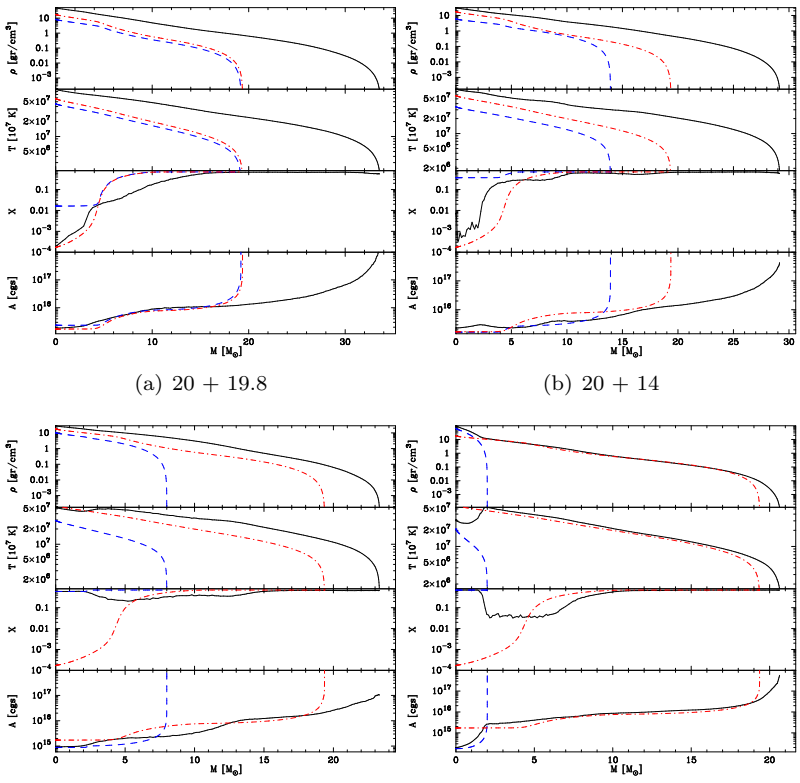

(a) 20 + 19.8 (b) 20 + 14

(c) 20 + 8 (d) 20 + 2

Figure 4.6: *As Figure 4.4 for the CHEX collisions with a 20* $M_\odot$ *primary and 19.8 (upper left panel), 14 (upper right panel), 8 (lower left panel) and 2 (lower right panel)* $M_\odot$ *secondaries. In all cases the dashed line (blue) shows the structure of the secondary and the dash-dotted line (red) shows the structure of the primary.*

0.1 (4.6(d)). Each of the three cases occurs in one of these panels. The CHEX 20+19.8 collision is a clear example of case P, while CHEX 20+14 can be considered case M since a notable amount of hydrogen from the secondary has been mixed into the core. Despite this, the material in the core predominantly comes from the primary and is hydrogen poor. The CHEX 20+8 and CHEX 20+2 are both case S, although the differences are quite interesting. In both cases the inner $\sim 2\,M_\odot$ consists of hydrogen-rich material from the core of the secondary. In the CHEX 20+2 case, this means the entire star occupies the core of the collision product with a strong enhancement in the helium abundance of the envelope. In the CHEX 20+8 case there is an additional $6\,M_\odot$ of hydrogen-rich material that is mixed into the envelope, which dilutes the helium enhancement considerably. As with the HAMS 10+1 collision product, the CHEX 20+2 remnant shows a notable temperature inversion just outside the core and a clear kink in the density profile. No such kink appears in the CHEX 20+8 case, although there is a small temperature inversion. We will return to these features when considering the evolution in section 4.4.2.

4.4.2 Evolution of the merger remnants

We have calculated the evolution of the collision products of the TAMS and CHEX runs and a sub-set ($q = 0.1$ and $q = 0.7$) of the HAMS runs. We did not evolve the result of the ZAMS collisions because these merger remnants are essentially ZAMS stars themselves and are not expected to show any difference in their evolution tracks. The results of our evolution calculations are presented in Table 4.5. A few models are missing from this table: we were unable to follow the evolution of these models for more than a few timesteps before the evolution code broke down. Also missing is the Hertzsprung gap evolution for CHEX 5+0.5, which broke down shortly after the contraction phase.

Table 4.5: *Evolution results for the collision products. The first three columns list the evolutionary stage of the primary (HAMS, ZAMS or CHEX), the mass of the primary M_1 and the mass of the secondary M_2 (both in $M_\odot$). Column four identifies the collision case (M, S or P, see text) and column five gives the total mass of the remnant $M_{\rm rmn}$ at the beginning of the evolution. Columns six through thirteen give the time of collision $t_{\rm coll}$, the total main sequence lifetimes $\tau_{\rm ms,1}$ and $\tau_{\rm ms,2}$ of the progenitor stars, the main sequence lifetime of a star born with the same mass as the collision product $\tau_{\rm ms}$, the actual main sequence (core hydrogen burning) lifetime $t_{\rm ms}$ of the collision product, the time $\tau_{\rm HG}$ spend in the Hertzsprung gap by a star born with the same mass, the time $t_{\rm HG}$ the collision product spends in this part of the Hertzsprung-Russell diagram and the time $t_{\rm HSB}$ between the end of core hydrogen burning and central helium ignition (i.e. the length of hydrogen shell burning). All times are given in Myr. The final two columns give the helium core mass $M_{\rm He}$ at the moment of helium ignition and helium core mass $M_{\rm He,ms}$ in a normal star at helium ignition.*

Stage	M_1	M_2	Case	$M_{\rm rmn}$	t	$\tau_{\rm ms,1}$	$\tau_{\rm ms,2}$	$\tau_{\rm ms}$	$t_{\rm ms}$	$\tau_{\rm HG}$	$t_{\rm HG}$	$t_{\rm Heign}$	$M_{\rm He}$	$M_{\rm He,ms}$
HAMS	5	0.5	S	5.43	41.01	82.03	124027	67.61	45.77	1.73	1.48	1.58	0.77	0.73
HAMS	10	1	S	10.87	9.91	19.82	8646	17.25	11.86	0.13	0.11	0.10	2.13	1.97
HAMS	20	2	S	21.64	3.86	7.72	908	7.12	4.82	0.03	0.03	0.02	6.20	5.54
HAMS	40	4	S	41.23	2.14	4.28	141	4.10	2.63	0.02	0.02	0.01	18.51	16.26
HAMS	5	3.5	M	8.48	41.01	82.03	199	29.80	20.89	0.39	0.27	0.27	1.41	1.22
HAMS	10	7	M	15.85	9.91	19.82	38.89	9.96	7.66	0.05	0.05	0.03	3.87	3.64
HAMS	20	14	M	33.68	3.86	7.72	11.85	5.04	3.50	0.02	0.02	0.01	11.69	10.30
TAMS	10	1	S	10.49	19.82	19.82	8646	17.31	3.09	0.13	0.10	0.10	2.22	1.96
TAMS	20	2	S	20.99	7.72	7.72	908	7.11	1.14	0.03	0.03	0.02	6.43	5.55
TAMS	40	4	S	37.51	4.28	4.28	141	4.06	0.60	0.02	0.02	0.01	17.81	16.56
TAMS	5	2	S	5.73	82.03	82.03	908	45.80	26.94	0.90	0.90	0.95	0.91	0.91
TAMS	20	8	S	24.18	7.72	7.72	29.75	6.03	2.22	0.03	0.02	0.01	9.11	7.24
TAMS	40	16	S	45.57	4.28	4.28	9.96	3.64	1.05	0.01	0.01	0.01	24.25	21.09
TAMS	5	3.5	P	7.58	82.03	82.03	199	30.81	0.00	0.42	8.63	8.60	1.00	1.19
TAMS	10	7	P	15.29	19.82	19.82	38.89	10.18	0.00	0.05	3.19	2.35	1.53	3.55

Table 4.5: *cont.*

Stage	M_1	M_2	Case	$M_{\rm rmn}$	t	$\tau_{\rm ms,1}$	$\tau_{\rm ms,2}$	$\tau_{\rm ms}$	$t_{\rm ms}$	$\tau_{\rm HG}$	$t_{\rm HG}$	$t_{\rm Heign}$	$M_{\rm He}$	$M_{\rm He,ms}$
TAMS	20	14	M	28.73	7.72	7.72	11.85	5.11	1.67	0.00	0.02	0.01	9.72	10.00
TAMS	40	28	M	55.61	4.28	4.28	5.62	3.27	0.88	0.01	0.01	0.01	30.65	26.96
TAMS	5	5	M	8.98	82.03	82.03	82.03	23.00	0.00	0.23	0.61	0.59	1.28	1.50
TAMS	10	10	M	18.39	19.82	19.82	19.82	8.44	0.00	0.04	1.25	0.08	2.34	4.38
TAMS	20	20	M	33.11	7.72	7.72	7.72	4.52	1.01	0.02	0.02	0.01	14.20	13.04
CHEX	5	0.5	S	5.37	82.07	82.03	124027	69.28		1.80				0.72
CHEX	10	1	S	10.73	19.83	19.82	8646	17.37	3.43	0.13	0.10	0.10	2.20	1.96
CHEX	20	2	S	21.25	7.72	7.72	908	7.11	1.14	0.03	0.03	0.02	6.34	5.55
CHEX	40	4	S	39.00	4.28	4.28	141	4.06	0.58	0.02	0.02	0.01	17.84	16.56
CHEX	5	2	M	6.27	82.07	82.03	908	45.83	18.27	0.90	0.65	0.69	1.01	0.91
CHEX	10	4	S	12.49	19.83	19.82	141	13.26	5.85	0.08	0.06	0.05	3.13	2.61
CHEX	20	8	S	24.01	7.72	7.72	29.75	6.04	2.16	0.03	0.02	0.01	8.89	7.23
CHEX	40	16	S	43.68	4.28	4.28	9.96	3.64	1.04	0.01	0.02	0.01	24.29	21.09
CHEX	5	3.5	P	7.72	82.07	82.03	199	30.87	0.00	0.42	8.16	8.10	0.97	1.19
CHEX	10	7	P	15.41	19.83	19.82	38.89	10.20	0.00	0.05	3.20	1.69	1.39	3.54
CHEX	40	28	M	55.76	4.28	4.28	5.62	3.27	0.01	0.01	0.83	0.81	29.01	27.01
CHEX	5	4.95	M	8.58	82.07	82.03	102	25.98	0.00	0.30	1.03	1.02	1.24	1.36
CHEX	10	9.9	M	17.55	19.83	19.82	23.59	8.49	0.00	0.04	1.73	0.35	1.52	4.35
CHEX	20	19.8	P	33.72	7.72	7.72	8.65	4.54	0.00	0.02	1.15	1.06	14.88	12.93

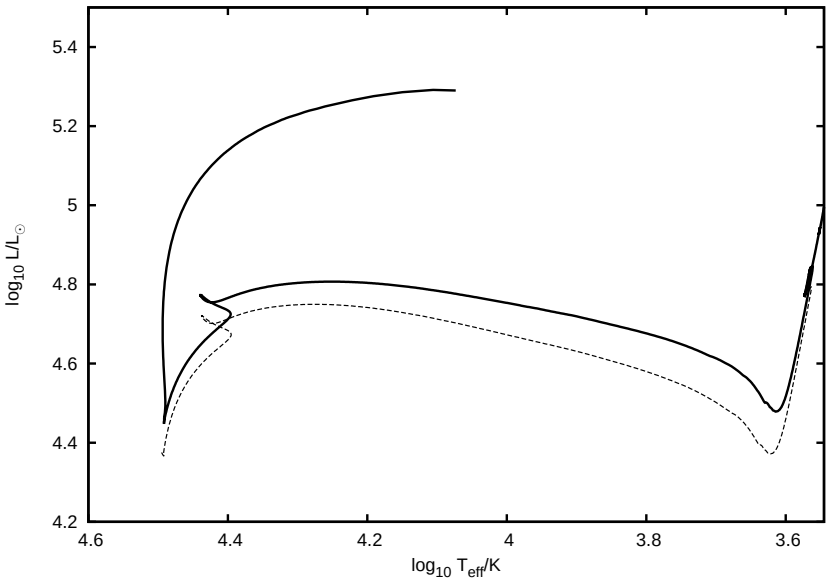

Figure 4.7: *Evolution track of the HAMS 10+7 collision product in the Hertzsprung-Russel diagram (solid line). The dotted line shows the evolution track of a normal star of the same mass as the collision product.*

For completeness Table 4.5 gives the total remnant mass as well as the collision case. The table also lists the time $t_{\rm ms}$ that the collision product spends as a core hydrogen burning star and the time $t_{\rm HG}$ spend in the Hertzsprung gap, between the end of core hydrogen burning (CHEX) and the base of the giant branch. The duration of the hydrogen shell burning phase is given by $t_{\rm HSB}$. This phase ends with the ignition of helium in the core. Note that with these definitions the evolution in the Hertzsprung gap can include part of the core-helium burning phase, in which case $t_{\rm HG} > t_{\rm HSB}$. We will discuss this in more detail in section 4.4.2. The table also gives the core mass $M_{\rm He}$ at helium ignition.

Contraction phase and core hydrogen burning

The first phase of evolution after the collision is the contraction phase, which progresses similarly to that for low-mass collision products, as studied in a previous paper (Glebbeek et al. 2008) and before by other authors (Sills et al. 1997). The evolution track for the HAMS 10+7 collision shown in Figure 4.7 shows the typical features for the collision product evolution tracks. During the contraction phase the collision product is inflated and over-luminous.

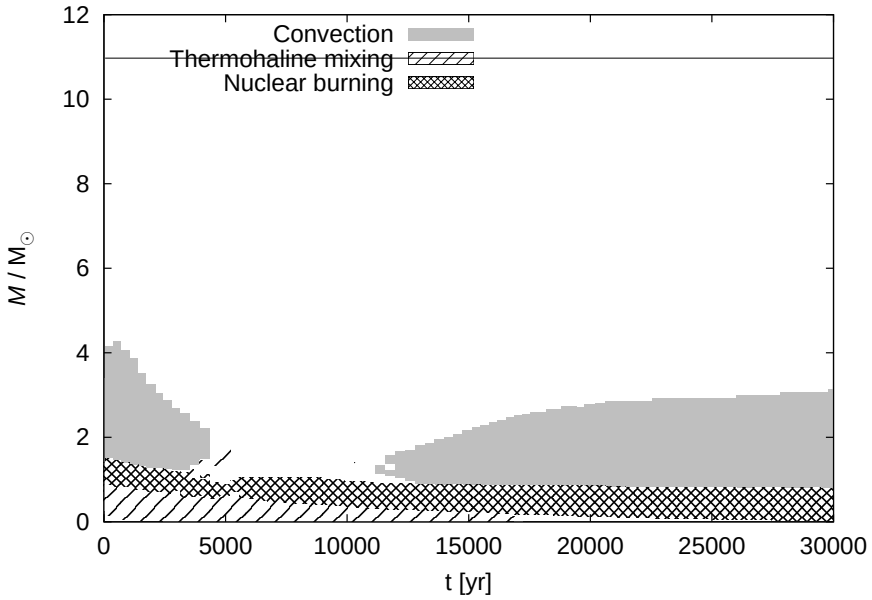

Figure 4.8: *Kippenhahn diagram showing the evolution of the HAMS 10+1 collision product during the contraction phase. Note that initially, hydrogen is burning in a shell outside the core. Thermohaline mixing is responsible for mixing into the central hydrogen rich core while convection mixes the region just above the burning shell.*

Most of the star's luminosity is provided by the release of thermal energy and the envelope contracts on a thermal timescale. In all our collision products the envelope is enhanced in helium, which means it is brighter than a normal star of the same mass, as we found for low-mass mergers (Glebbeek et al. 2008; Glebbeek & Pols 2008). If the core of the collision product is made up of material from the primary (case P) or is a mixture of material from the progenitor stars (case M), the highest temperature occurs in the centre of the collision product. Because the core is hydrogen rich hydrogen ignites in the centre. Temperature inversions like the one found in the HAMS 10+1 collision product can result in the formation of a hydrogen burning shell on top of a hydrogen-rich core if the hydrogen abundance in the region of maximum temperature is high enough. During the contraction phase these temperature inversions are removed and the burning front moves inward to the centre of the remnant. At the same time molecular weight inversions in the interior are removed by thermohaline mixing (Kippenhahn et al. 1980).

The evolution of the stellar interior for the HAMS 10+1 collision product (case S) is shown in Figure 4.8 and Figure 4.9. As discussed in section

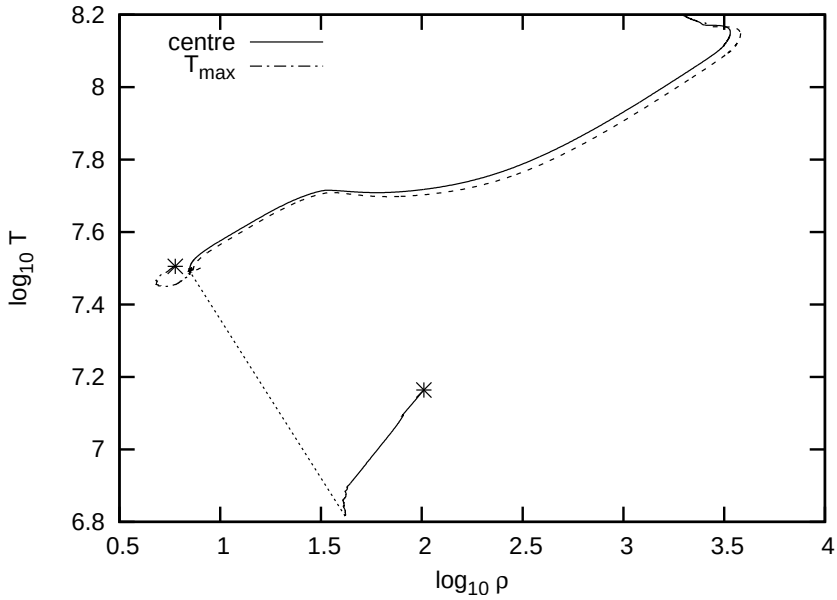

Figure 4.9: *Evolution track of the HAMS 10+1 collision product in the* $\log\rho$–$\log T$ *plane. The solid line shows the evolution of the stellar centre while the dash-dotted line shows the evolution of the locus of highest temperature. The starting point of the evolution is indicated by* $*$*. The dotted line shows the transition of hydrogen shell burning to hydrogen core burning. For reference, the dashed line shows the evolution track of a normal star of the same initial mass as the collision product.*

4.4.1 the core of the collision product consists of material from the $1\,M_\odot$ secondary star and is overdense. This means that it needs to expand in order to reach thermal equilibrium. Because this requires work against the pressure exerted by the envelope and the expansion is nearly adiabatic the temperature in the core decreases. The highest temperature occurs in a helium rich hydrogen burning shell above the core. Local conditions in the burning shell are close to the prevailing conditions in the core of a normal $11\,M_\odot$ star (see the dash-dotted line in Figure 4.9). The burning shell becomes denser. Because the molecular weight in the burning shell is higher than the molecular weight in the core thermohaline mixing operates, which slowly homogenises the inner part of the star. Figure 4.8 shows the evolution in a Kippenhahn diagram. The burning front moves gradually inward on a thermal timescale while convection mixes the layers above the core.

The configuration of an contracting burning shell and an expanding core

(both on a thermal timescale) leads to an instability because it drives the core to a density inversion. We were able to follow the transition from hydrogen shell burning to hydrogen core burning until the bottom of the burning shell was within $0.03\,M_\odot$ of the centre. At this point we expect the transition from shell burning to core burning to happen very shortly. The transition of (stable) hydrogen shell burning to central hydrogen burning that we find for some of our collision products is analogous to the transition of (unstable) off-centre helium shell burning to helium core burning in the helium flash. Although we were not able to follow the transition to core burning self-consistently, we can study the long term evolution of the collision product by constructing a 'post core ignition' model. This procedure is similar to the procedure that is commonly used to model stellar evolution after the helium flash (*e.g.* Serenelli & Weiss 2005). In Figure 4.9 this transition is indicated by a dotted line. After central hydrogen ignition the evolution of the collision product is very similar to that of a normal star of the same mass (dashed line), although the central density and pressure are a bit lower in the collision product for the same central temperature. The collision product has a slightly larger radius and the decrease in central pressure is in agreement with the scaling relation $P_c \sim GM^2/R^4$.

Two other interesting case S collision products are the CHEX 20+8 and 20+2 collision products (and the similar TAMS 20+8 and 20+2), described in section 4.4.1. In contrast to the HAMS 10+1 case, in these cases no hydrogen burning shell is formed because the hydrogen abundance at the location of maximim temperature is too low. Thermohaline mixing very quickly homogenises the core. In neither of these cases do we find significant mixing of the star due to convection outside the region of the stellar core. Although both merger remnants have a hydrogen rich core of about $2\,M_\odot$, the inner $7\,M_\odot$ (corresponding to the extent of the convective core) of the 20+2 remnant contains more helium than the inner $10\,M_\odot$ of the 20+8 remnant. As a result and as can be seen from Table 4.5 the 20+8 has a longer main sequence lifetime than the 20+2. The same effect can be seen for 40+16 and 40+4.

Core hydrogen burning in these collision products proceeds normally and these stars are very similar to normal stars of the same mass. After core hydrogen exhaustion, hydrogen continues to burn in a shell. Because the region of the burning shell can have an enhanced helium abundance compared to a normal star of the same mass, the core mass at which helium ignites in the centre is larger than in a normal star. As a result, the shell burning phase (lifetime in the Hertzsprung gap, $t_{\rm HG}$ in Table 4.5) is slightly shorter than for a normal star.

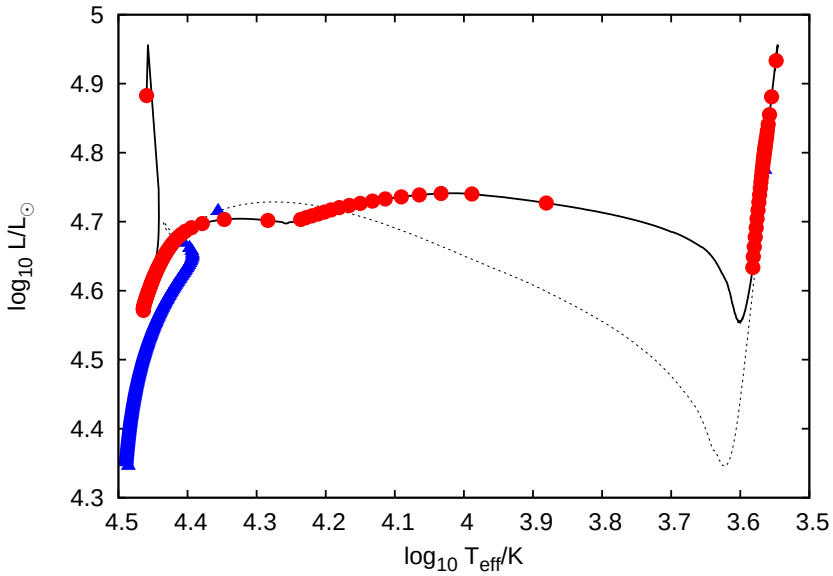

Figure 4.10: *Evolution track of the TAMS 10+7 collision product (solid line) compared to the evolution track of a normal star of the same mass (dotted line). Points are plotted along the curves every* 50 000 *years. Note that the collision product spends a considerably longer time in the blue part of the region corresponding to the Hertzsprung gap than the normal star of the same mass.*

Collision products with hydrogen depleted cores

If the collision product has a hydrogen-depleted core (case P for TAMS or CHEX collisions and some case M for TAMS or CHEX collisions with $q \geq 0.99$) the evolution track can be very different from that of a normal star of the same mass or the collision products discussed in 4.4.2. These collision products do not have a core hydrogen-burning phase and begin their evolution with hydrogen shell burning on top of a helium core. Because the initial mass of the helium core is determined by the mass of the primary it can be significantly smaller than the core of a normal star with the same total mass, and in many cases it is smaller than the Schönberg-Chandrasekhar (SC) limit (Kippenhahn & Weigert 1990; Padmanabhan 2001),

$$M_{\mathrm{SC}} = 0.37 \left(\frac{\mu_{\mathrm{env}}}{\mu_{\mathrm{c}}} \right)^2 M. \tag{4.2}$$

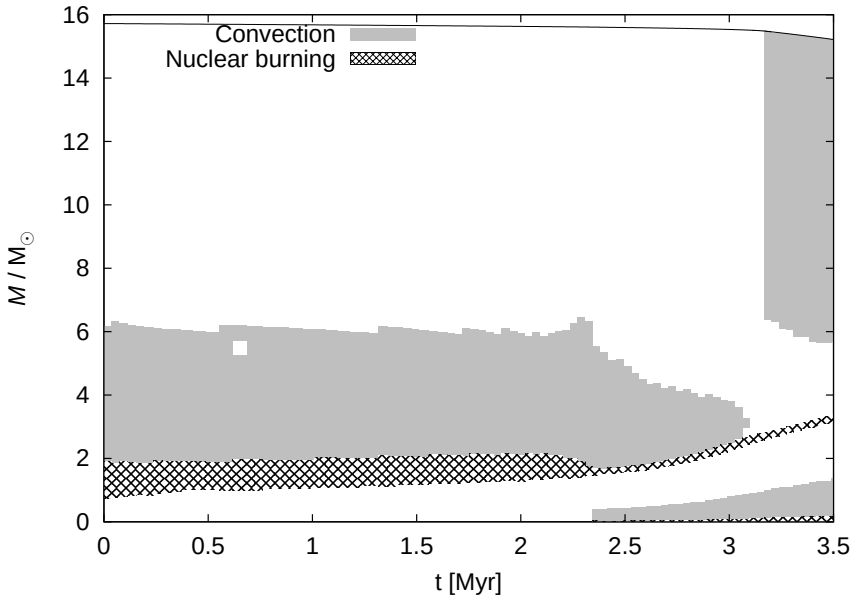

Figure 4.11: *Kippenhahn diagram showing the evolution of the 10+7* $M_\odot$ *TAMS collision product. Hydrogen burns in a shell around the helium core.*

Here M is the total mass of the star, $\mu_{\rm env}$ the average mean molecular weight of the envelope and $\mu_{\rm c}$ the average mean molecular weight in the core. As long as the core mass is below this limit the collision product can be in thermal equilibrium without becoming a red giant.

Figure 4.10 shows the evolution track of the TAMS 10+7 collision product. The location in the Hertzsprung-Russell diagram after the contraction phase is similar to that of a normal star of the same mass late on the main sequence although the evolution track lacks the distinctive hook that appears when the convective core disappears in a normal star. The evolution of the interior is shown in Figure 4.11. The hydrogen burning shell is replenished by the convection zone above it, which mixes in extra hydrogen. The extend of this convection zone is comparable to the extend of the convective core in a normal star of the same mass. As a result, the hydrogen burning shell mimics the hydrogen core of a normal star. Because of the presence of a convection zone above the burning shell the core mass grows slowly, increasing by only $0.5\,M_\odot$ in the first 2.3 Myr. After 2.3 Myr helium ignites in the centre. The convection zone that sustained the burning shell shrinks but does not disappear. This causes the core growth rate to increase after helium ignition.

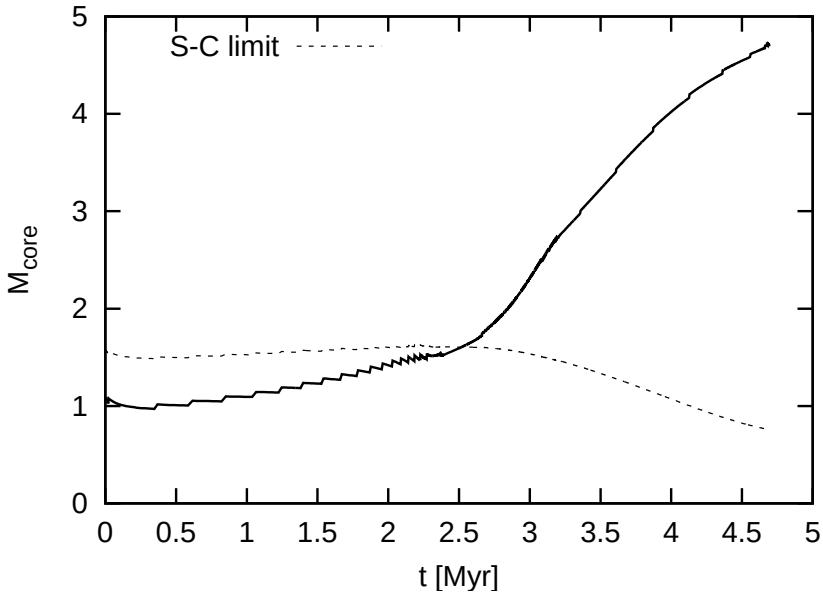

Figure 4.12: *Core mass as functions of time for the TAMS 10+7 collision, in solar units. The dashed line represents the Schönberg-Chandrasekhar limit for the core mass. The collision product ignites helium after 2.3 Myr.*

In Figure 4.12 we show the core mass of the TAMS 10+7 collision product as a function of time. The core mass is below the SC limit (dashed line) until 2.5 Myr. When the core mass approaches the SC limit the core contracts rapidly and heats up, leading to helium ignition. At this point the collision product is still in the blue part of the Hertzsprung-Russell diagram and becomes a blue supergiant, as can be seen from Figure 4.10. In Table 4.5 the collision products that form blue supergiants all have a helium core mass $M_{\rm He}$ smaller than the core mass $M_{\rm He,ms}$ of a normal star and $t_{\rm HSB}$ much smaller than $t_{\rm HG}$.

Not all stars with $M_{\rm He} < M_{\rm He,ms}$ form blue supergiants, however. The remnant of the TAMS 5+3.5 collision, shown in Figure 4.13, also stays in the blue part of the Hertzsprung-Russell diagram during a prolonged hydrogen shell burning phase, but in this case helium ignition does not occur before the star reaches the red part of the Hertzsprung-Russell diagram.

An analytical recipe

An analytic recipe that can be used to predict collision product lifetimes and luminosities was developed by Glebbeek & Pols (2008) In brief, they

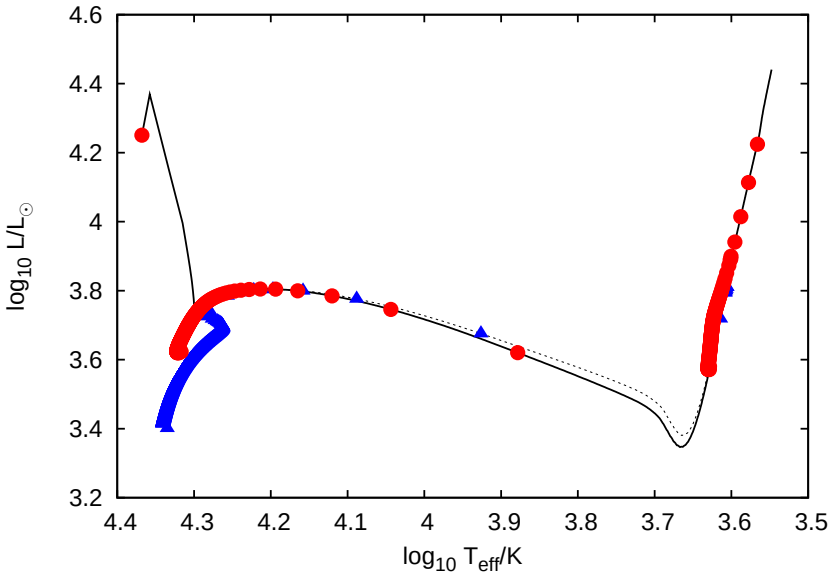

Figure 4.13: *As Figure 4.10 for the TAMS 5+3.5 collision.*

found that the lifetime $t_{\rm MS}$ of the collision product can be found from $t_{\rm MS} = \tau_{\rm MS}(1 - f_{\rm app})$, where

$$f_{\rm app} = \frac{1}{\alpha q_{\rm c}(M)} \frac{1}{1-\varphi} \frac{q_{\rm c,1} f_1 + q_{\rm c,2} f_1 q}{1+q}. \tag{4.3}$$

Here $\tau_{\rm MS}$ is the main sequence lifetime of a star of the same mass as the collision product, f_1 and f_2 are the ages of the primary and secondary star, in units of their main sequence lifetimes, φ is the fraction of material lost in the collision, $q_{\rm c}(M)$ is the fraction of hydrogen that is consumed during the main sequence and α is a free parameter. Glebbeek & Pols (2008) found that a single value of $\alpha = 1.67$ works well for collisions between low-mass stars. We find that $\alpha = 1.14$ works well for the high mass collision products discussed here (see Figure 4.14).

Glebbeek & Pols (2008) also give a prescription for calculating the increase in luminosity due to the helium enhancement in the envelope, based on the homology relation

$$L_{\rm merger} = L_{\rm MS} \left(\frac{\mu_{\rm merger}}{\mu_{\rm MS}} \right)^4. \tag{4.4}$$

We find that this homology relation is no longer valid for the massive merger remnants discussed here and that it underpredicts the luminosity.

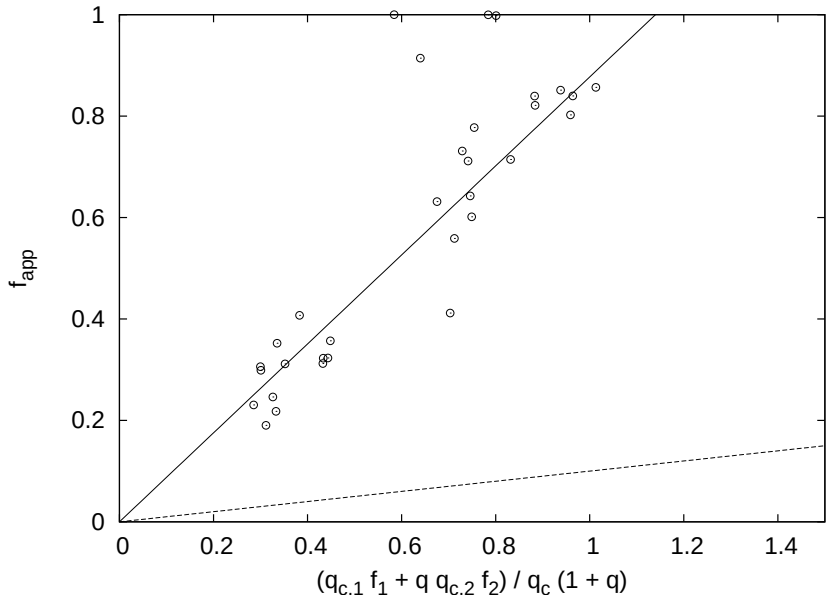

Figure 4.14: *Collision product apparent age according to (4.3). The models are indicated by* $\odot$*, the solid line is the prediction of (4.3) for* $\alpha = 1.14$*. The dotted line is the prediction of equation (80) in Hurley et al. (2000).*

4.5 Summary & Conclusion

We have studied the evolution of stellar mergers formed by a collision involving massive stars. This is a first step in following the evolution of stellar merger runaways using detailed stellar models. Mass loss from the collisions is generally small, up to about 8% of the total mass for collisions involving equal mass stars at the end of the main sequence. The structure of these merger remnants can be well understood using a modification of the entropy sorting principle of Lombardi et al. (2002).

During the collision, the core of one of the parent stars can retain its identity and sink to the centre of the collision product. Whether this occurs for the core of the primary or the secondary depends on the buyancy profile $A(m)$ in the parent stars. In cases with extreme mass ratio the secondary star as a whole can migrate to the centre of the collision product. In general we find little mixing of material from the cores with the envelopes as a result of the merger. However, if the core of the secondary displaces the core of the primary at the centre of the collision product, material from the primary core is mixed with the secondary envelope and this can result in more extended mixing. The shell with the location of highest temperature

can initially be off-centre, resulting in a hydrogen-burning shell in the merger remnant. The burning front moves inward towards the centre on a thermal timescale.

The main sequence evolution of the merger remnant is qualitatively similar to the evolution of low mass collision products (Sills et al. 1997, 2001; Glebbeek et al. 2008; Glebbeek & Pols 2008): in both cases helium enhancement of the lower envelope increases the star's radius and luminosity. This increases the cross section of the merger remnant for a possible subsequent collision, which may be relevant when considering merger runaways. The main-sequence lifetime of massive collision products can be predicted in a similar manner to that of low mass collision products (Glebbeek & Pols 2008), but this is not true of their luminosity.

Merger remnants that result from collisions with main sequence stars at the end of the main sequence and where the core of the primary remains in tact (case P) begin their evolution with an anomalously small hydrogen-depleted core and evolve differently from normal main sequence stars or merger remnants that form with a hydrogen-rich core. The collision products can be in thermal equilibrium during hydrogen shell burning if the mass of the helium core is below the Schönberg-Chandrasekhar limit. In this case the star can ignite helium while still in the blue part of the Hertzsprung-Russell diagram. Observationally, many O and B stars appear to be in the Hertzsprung gap (Evans et al. 2006), between the end of the main sequence and the bluest part of the blue loop during core helium burning, although this conclusion is sensitive to the treatment of convective overshooting in the evolution tracks used for comparison. Stellar mergers involving turnoff stars, either through a collision as discussed in this work or by unstable case-B mass transfer in a binary, offer a mechanism to explain the presence of at least some stars in this part of the Hertzsprung-Russell diagram.

4.A Modification of GADGET2 code

In this paper we focus on collisions between massive stars and it is of crucial importance to include a proper equation of state. While the intricate equation of state used by the stellar evolution code is in principle suitable, for the purpose of numerical hydrodynamics the equation of state can be well approximated by the much simpler equation of state of a mixture of a monatomic ideal gas and radiation in thermal equilibrium. The equation of state for such a mixture is given by the following equations:

$$P = \frac{\rho k T}{\mu m_{\mathrm{u}}} + \frac{a T^4}{3}, \tag{4.5}$$

$$u = \frac{3}{2}\frac{k T}{\mu m_{\mathrm{u}}} + \frac{a T^4}{\rho}. \tag{4.6}$$

Here μ is the mean molecular weight, $m_{\rm u}$ is the atomic mass unit and other symbols have their usual meaning.

The GADGET2 code uses the "entropy formulation" of SPH where an entropy-like variable, A (which we have called buoyancy), is integrated instead of the thermal energy. In the case of an ideal gas the relation between buoyancy and thermal energy is an algebraic expression which can be solved analytically. That is given density, composition and buoyancy one can easily find the pressure. However, if radiation pressure cannot be ignored the equation becomes transcendental and generally does not admit analytical solution. Some SPH codes that include radiation pressure (Lombardi et al. 2006; Freitag & Benz 2005) use the "energy formulation"of SPH. However, bearing in mind the advantages of the "entropy formulation" we modified GADGET2 to be consistent with radiation pressure. The modifications are minimal and require only changes in the equation of state and the equation for shock heating. The shock heating term becomes

$$\frac{dA}{dt} = A\frac{2\rho}{3P\beta}\frac{dQ}{dt}. \tag{4.7}$$

Here dQ/dt is the SPH shock heating term which we keep the same as that of `GADGET2`, A is the buoyancy of a fluid element, and β is the ratio of gas pressure to total pressure. We ignored nuclear energy generation in our simulations since it has been shown that these do not to play an important role in stellar collision between main-sequence stars (Mathis 1967; Rozyczka et al. 1989).

4.B Modelling stars in SPH

In this section we present two different methods which we used to model stars in SPH. We underline the importance of using a relaxed model when material mixing is a question of interest. The failure of producing a properly relaxed model may result in artificial mixing which is not exhibited when properly relaxed models are used.

4.B.1 Random sampling

The easiest method to prepare the initial models is random sampling. For a given radial density profile the particle positions are sampled by the von Neumann acceptance-rejection method (Press et al. (1992)); each particle is assigned appropriate values of conserved quantities, such as composition and buoyancy. The resulting distribution of particles produces in a relatively noisy density distribution. Nevertheless, the location of the particles are close to their "proper" position. To let the particle to find their "proper" location we relax the star by keeping the buoyancy of each particle constant

and only solve the equations of motion for the particle position. Since the stellar structure in quasi-hydrostatic equilibrium is completely defined by the buoyancy and composition profile, the position of the particles will converge to the position that guarantees a smooth density profile that is consistent with the density profile of the one-dimensional stellar model. The resulting profile of conserved quantities remains relatively noisy but the level of noise does not exceed the local resolution, which is controlled by a smoothing length.

4.B.2 Scaling method

The scaling method is the method presented in Turner et al. (1995). The main idea of this method is to prepare the initial configuration by scaling an uniform lattice of a given constant density ρ_0. The scaling preserves the infinitesimal mass element $\mathrm{d}m$. At the old location of a particle, r_{old}, its infinitesimal mass element is $\mathrm{d}m_{\mathrm{old}} = 4\pi\rho_0 r_{\mathrm{old}}^2\,\mathrm{d}r_{\mathrm{old}}$. The new location of the particle, r_{new}, should be such that the new mass element $\mathrm{d}m_{\mathrm{new}} = 4\pi\rho(r_{\mathrm{new}})r_{\mathrm{new}}^2\,\mathrm{d}r_{\mathrm{new}}$ equals $\mathrm{d}m_{\mathrm{old}}$. This results in the differential equation

$$4\pi\rho_0 r_{\mathrm{old}}^2\,\mathrm{d}r_{\mathrm{old}} = 4\pi\rho(r_{\mathrm{new}})r_{\mathrm{new}}^2\,\mathrm{d}r_{\mathrm{new}}. \tag{4.8}$$

This differential equation can be readily integrated to give an implicit algebraic equation for r_{new}

$$m(r_{\mathrm{new}}) = \frac{4}{3}\pi\rho_0 r_{\mathrm{old}}^3. \tag{4.9}$$

The resulting distribution of particle produces the desired density profile with very little noise. However, even in this case the gravitational and pressure forces are not perfectly balanced because the pressure is still affected by noise and the star has to be relaxed as in the case of random sampling. The advantage of the scaling method over random sampling is that in the relaxation process takes less time. The final structures obtained by the two methods are consistent with each other and with the one dimensional stellar profile

4.B.3 Relaxation

Once the particle are distributed according to a given density profile, even though this may closely follow the desired one, the pressure forces are quite unlikely to be fully balanced by gravitational forces. This difference is stored as a tension energy, and if no precautionary steps are taken, this tension will be dissipated into heat. The result is that the thermal profile is affected and particles may migrate from their proper location, affecting the stellar structure.

As we have mentioned above the structure of a star in hydrostatic equilibrium is defined by the buoyancy and composition profile. Therefore one way to relax the star is to make sure that the buoyancy and composition of each particle remain constant during relaxation. However, one needs to take measure that the tension energy is dissipated away and not converted into heat. This can be accomplished by adding an artificial drag force to the equations of motion

$$\mathbf{a}_{\rm fric} = -C_{\rm fric}\mathbf{v}\frac{|\mathbf{v}|}{h}. \tag{4.10}$$

Here, $\mathbf{v}$ is the velocity of the particle, h is its smoothing length and $C_{\rm fric} \gtrsim 1$ is a dimensionless constant determining the strength of the friction force; in our relaxation runs we use $C_{\rm fric} = 4$.

The advantage of this form of the drag force is that the timescale of velocity decay is naturally defined by the local conditions, and is of order of $h/|\mathbf{v}|$. This leads to a consistent relaxation through the star, such that that fastest relaxation occurs in high density regions and the slowest relaxation in low density regions. Typically the relaxation run takes a few dynamical timescales and the resulting stellar structure (density, pressure and temperature profiles) closely resemble the one-dimensional structure profile. The tension energy which was the result of the unbalance between gravitational and pressure force has been dissipated and the stellar model is stable for many dynamical timescales.

4.C Reduction of the data from 3D to 1D

In order to be able to study the evolution of a collision product one needs to reduce three-dimensional hydrodynamical data into a one-dimensional stellar structure profile that can be imported into a stellar evolution code. Such a reduction is possible since configurations in hydrostatic equilibrium posses various symmetries. In particular, the structure of a non-rotating collision product is spherically symmetric and one can therefore average thermodynamical quantities on spherical surfaces, which are also equipotential surfaces. Because the fluid is in hydrostatic equilibrium the isopycnic and isobaric surfaces coincide; this is not necessary true for the chemical composition profile (Gaburov et al. 2008c). We use the enclosed mass as an independent variable. The temperature, density and chemical composition profiles are obtained by conservative averaging over equipotential surfaces.

Initially, we sort SPH particles according to their pressure. Given a number of desired bins along the mass coordinate, we sort particles in each bin such that the particles with the highest pressure are placed in the lowest mass bin and the particles with the lowest pressure are located in the highest mass bin. In the next step we compute the density in each bin using

conservative averaging

$$\rho(m_I) = \frac{\sum_{(j\in I)} m_j}{\sum_{(j\in I)} m_j/\rho_j}. \tag{4.11}$$

Here, the index I refers to the I-th bin, m_I is the mass of the I-th bin, and the sum is carried out of j particles in the bin I.

The thermal energy and chemical composition of each bin are averaged in the following way

$$\zeta(m_i) = \frac{\sum_{(j\in I)} m_j\zeta_j}{\sum_{(j\in I)} m_j}. \tag{4.12}$$

Here ζ represents either the thermal energy u or the chemical composition X_k of an SPH particle.

Having the average value of density, thermal energy and composition for each bin we can derive other thermodynamical quantities of interest, such as pressure, buoyancy and temperature from the equation of state.

5

The evolution of runaway stellar collision products

In the cores of young dense star clusters repeated stellar collisions involving the same object can occur, which has been suggested to lead to the formation of an intermediate-mass black hole. In order to verify this scenario we compute the detailed evolution of the merger remnant of three sequences. We follow the evolution until the onset of carbon burning and estimate the final remnant mass to determine the ultimate fate of a runaway merger sequence.

We use a detailed stellar evolution code to follow the evolution of the collision product. At each collision, we mix the two colliding stars, taking account of mass loss during the collision. During the stellar evolution we apply mass loss rates from the literature, as appropriate for the evolutionary stage of the merger remnant. We compute models for high ($Z = 0.02$) and low ($Z = 0.001$) metallicity to quantify metallicity effects.

We find that the merger remnant becomes a Wolf-Rayet star before the end of core hydrogen burning. Mass loss from stellar winds dominates over the mass increase due to repeated mergers for all three merger sequences that we consider. In none of our high metallicity models an intermediate-mass black hole is formed, instead our models have a mass of 10–14 $M_\odot$ at the onset of carbon burning. For low metallicity we expect the final remnant of the merger sequence to explode as a pair creation supernova. We find that our metal-rich models become inflated as a result of developing an extended low-density envelope. This may increase the probability of further collisions, but self-consistent N-body calculations with detailed evolution of runaway mergers are required to verify this.

5.1 Introduction

The usual mode of star formation leads to a spectrum of masses between the theoretical hydrogen burning limit and some upper limit, which appears to be close to about $100\,M_\odot$ (Elmegreen 1999; Weidner & Kroupa 2004; Figer 2005). In young and dense star clusters more massive stars can form when two or more high-mass stars coalesce. The cluster environment helps in driving these stars together. If this happens in sufficiently young and dense star cluster the same star may experience multiple collisions in what is named a 'collisional runaway' (Portegies Zwart et al. 1999). During such a chain collision several stars collide in short succession. The trigger for a chain collision is the gravothermal collapse (Bettwieser & Sugimoto 1984) of the core of a young and dense star cluster. If cluster core collapse is initiated before the most massive stars leave the main sequence the collision runaway sets in (Portegies Zwart & McMillan 2002) and continues until the target star leaves the main sequence (Portegies Zwart et al. 1999).

If the star explodes as a supernova, this supernova is likely to be unusually bright and rich in hydrogen (Portegies Zwart & van den Heuvel 2007). The star may also collapse completely into a black hole, without a visible supernova. The black hole remnant of such a star may be considerably more massive than hitherto observed (Portegies Zwart et al. 2004), though less massive than the supermassive black holes found in the nuclei of large galaxies (Kormendy & Richstone 1995). Various groups have now confirmed the formation of such collision runaways, and conjecture that the final merger product collapses to a black hole of up to about $10^3\,M_\odot$ (Portegies Zwart et al. 1999, 2004; Freitag et al. 2006; Gürkan et al. 2006).

Two of our aims in understanding merger runaways are understanding the structure of the merger remnant and the influence of stellar evolution of the merger runaway. Stellar evolution of very massive stars (with masses above $150\,M_\odot$) has recently been studied by Belkus et al. (2007), Yungelson et al. (2008) and Langer et al. (2007). These studies all seem to come to the same conclusion: at high metallicity mass loss is copious enough to prevent the formation of a black hole of more than $50\,M_\odot$, which is much lower than the conjected intermediate-mass black hole mass. These studies, however, either used approximate formulae for stellar evolution (Belkus et al. 2007) or studied the evolution of very massive stars from the zero-age main sequence with an initially homogeneous composition (Yungelson et al. 2008; Langer et al. 2007). According to the dynamical simulations the massive star grows in mass by means of repeated collisions with less massive stars. The consequences of the collisions, the evolution between collisions and the differences in stellar age and structure at the moment of collision are not considered by these studies. A first attempt to overcome these problems by calculating collisions between massive stars and computing the evolution of these merged objects did not result in very different conclusions

(Suzuki et al. 2007). Ideally, one would like to perform a fully self-consistent simulation in which the stellar dynamics, the hydrodynamics of the stellar collisions and the further evolution of the collision products are taken into account self consistently. Such multiscale simulations, however, will have to await the development of the appropriate numerical methodology. The MUSE software environment may provide the necessary functionality for such simulations[1].

In this work we investigate the evolution of three collision runaways that occurred in the direct N-body simulations of the dense and young star cluster MGG-11 in the starburst galaxy M82 Portegies Zwart et al. (2004). The simulations were performed using the `kira` integrator of the `starlab` software environment Portegies Zwart et al. (2001) and run with 131072 stars on a special purpose GRAPE-6 computer Makino (2001). For each collision the two stars are evolved to the moment of collision using a stellar evolution code (described in §5.2.2) and each merger is resolved as described in §5.2.1. The evolution is continued using the output of the merger calculation as a starting model. After the last collision we follow the evolution of the merger product until the evolution code fails to converge or until the onset of carbon burning, applying mass loss rates from the literature. We estimate the final mass of the collision product and estimate the mass of the remnant of the collision runaway. We also provide the chemical yields that result from the merger sequence and compare them to the combined yields of a population of normal single stars. Finally we comment on the effect of the initial composition, especially the heavy element content Z (metallicity) on the structure of the merger remnant.

5.2 Methods

5.2.1 Stellar collisions

We use two different methods to model stellar collisions. The first assumes that the collision product is in hydrostatic and thermal equilibrium and mixed homogeneously. The second method uses the prescription of Gaburov et al. (2008c) to model the structure of the remnant. In this case the collision product is not homogeneously mixed and it is not in thermal equilibrium (although it is still in hydrostatic equilibrium).

All collisions are treated as head-on collisions with vanishing velocity at infinity (*i.e.*, parabolic collisions). We ignore rotation in this work despite the fact that rotation can have a significant influence on the evolution of a massive star (Maeder & Meynet 2000b).

[1] see `http://muse.li`.

Homogeneous mixing

In this approach, detailed models of the progenitor stars were merged and homogeneously mixed at each step of the sequence. We assume that the merger remnant is in hydrostatic and thermal equilibrium. The mass loss from the collision is estimated according to Gaburov et al. (2008c).

In general merger remnants are not fully mixed (Lombardi et al. 1996; Gaburov et al. 2008c; Glebbeek & Pols 2008; Gaburov et al. 2008a). However, Suzuki et al. (2007) find that their massive collision products are almost completely mixed during the subsequent evolution. Similarly, we find (§5.3.1) that the central convection zone in our merger remnants encompasses $\gtrsim 90\%$ of the stellar mass. Rotational mixing, which we have ignored, will result in even more extended mixing of the collision product, so to first order homogeneous mixing is a reasonable approximation for our models.

Detailed merger models

Our detailed merger models were calculated using Make Me A Massive Star (MMAMS) (Gaburov et al. 2008c). The code has a prescription for the mass lost from the collision that is based on the results of smooth particle hydrodynamics calculations. Heating due to the dissipation of the kinetic energy of the progenitor stars in shocks and tides is also taken into account. After the ejected mass has been removed and heating has been applied to the material from the parent stars the structure of the collision remnant is determined by searching for a configuration that is dynamically stable (*i.e.* satisfies the Ledoux stability criterion, Kippenhahn & Weigert 1990). An algorithm for doing this was first developed by Lombardi et al. (2002) for low-mass stars, for which it is sufficient to sort the mass shells in order of increasing entropy and then integrate the equation of hydrostatic equilibrium. For massive stars where radiation pressure is important this does not necessarily produce a stable configuration and some mass shells need to be moved again after the equation of hydrostatic equilibrium has been integrated. This procedure is repeated until a stable model is converged upon.

The output model is imported into the stellar evolution code using the method described in Glebbeek & Pols (2008) and evolved until the time of the next collision.

Due to heating during the collision the merger product is not in thermal equilibrium. The excess of internal heat is radiated away during the contraction of the star to the main sequence. Because the stars were not in thermal equilibrium, we encountered more numerical problems when importing the stellar models than we did for the homogeneously mixed models.

5.2.2 Stellar evolution

Our stellar evolution code is a version of the STARS code originally developed by Eggleton (1971) and later updated (*e.g.* Pols et al. 1995). This version of the code uses the opacities from Iglesias & Rogers (1996) that take into account enhancement of C and O, as described in Eldridge & Tout (2004) and Ferguson et al. (2005). The assumed heavy-element composition is scaled to solar abundances (Anders & Grevesse 1989). Chemical mixing due to convection (Böhm-Vitense 1958; Eggleton 1972) is taken into account.

STARS uses an adaptive mesh in which the mesh points automatically redistribute themselves according to a mesh spacing function that places more meshpoints in regions of the star where a higher resolution is required. For the models presented here we used 200 mesh points for the main sequence phase and 500 for the core helium-burning evolution. Because our stars form an extended low-density envelope (see §5.3.1) we have found it necessary to increase the number of mesh points in the outer layers compared to our standard stellar models.

We use a mass fraction of heavy elements $Z = 0.02$ for our standard runs. In order to study the effect of metallicity we have also recalculated one of our sequences with $Z = 0.001$. This affects the mass-loss rate and therefore the mass of the progenitors at each collision. We terminate the evolution at central carbon ignition and estimate the final remnant mass according to Belczynski et al. (2002).

5.2.3 Mass loss

Since our collision products become very massive and luminous, even exceeding the Humphreys-Davidson limit (a luminosity cutoff above which few stars are observed, Humphreys & Davidson 1979), mass loss plays a key role in their evolution. Unfortunately, neither observations nor theoretical models of mass loss exists for the full range of masses and luminosities reached by our models. We have considered three possible mass-loss prescriptions: the empirical rate from de Jager et al. (1988) and theoretical rates from Vink et al. (2000, 2001) and Kudritzki (2002). None of these rates cover the range of parameters of our models. The empirical de Jager rate has too few data points for luminosities above the Humphreys-Davidson limit. Their 20 point Chebyshev fit needs to be extended beyond $\log L/\mathrm{L}_\odot = 6.7$. The theoretical rate from Kudritzki needs to be extrapolated for $T_{\rm eff} < 40\,000\mathrm{K}$ while the models for the Vink rate are calculated for $\log L/\mathrm{L}_\odot < 6.25$ and $10\,000\mathrm{K} \lesssim T_{\rm eff} \lesssim 50\,000\mathrm{K}$.

We have made some trial calculations using these three mass loss prescriptions to decide which rate we should adopt for our calculations. The results of our trial calculations were qualitatively similar and independent

of the mass-loss recipe used. For our quantitative analysis we have adopted the Vink et al. (2001) rate because of the three rates mentioned it best covers the range of effective temperatures for our models and only needs to be extrapolated in luminosity. By contrast, the Kudritzki (2002) rate needs to be extrapolated to lower effective temperatures, which is less reliable than extrapolating to higher luminosities because the presence of spectral lines that drive the wind depends sensitively on the temperature. In the region where the Kudritzki (2002) rate is valid it is very similar to our extrapolated Vink et al. (2001) rate. Note that our adopted mass-loss rate likely underestimates the true mass loss rate since our stars are much closer to their Eddington limit than the model calculations on which the Vink rate is based. We will return to this point in the discussion. The Vink rate is not applicable to red supergiants and predicts a mass loss rate that is too low for cool stars. For this reason we adopt the de Jager rate rather than the Vink rate at effective temperatures below 10 000K. Our models only reach this temperature for luminosities that are within the validity range of the de Jager rate.

All our models become helium-rich and evolve into Wolf-Rayet stars. We follow the criterion used by Eldridge & Vink (2006) to decide when our stars become Wolf-Rayet (WR) stars. Specifically, we start applying the mass-loss rate from Nugis & Lamers (2000) when the surface abundance of hydrogen drops below 40% by mass and $T_{\rm eff} > 10\,000$K. This happens *before* the star finishes core hydrogen burning (compare Langer et al. 2007; Yungelson et al. 2008). For our low metallicity run we used the metallicity scaling found by Vink & de Koter (2005) for the WR mass-loss rate. The Vink et al. (2001) rate already includes metallicity scaling.

5.2.4 Rotation

It has been shown that for off-axis collisions the angular momentum of the collision product can be so large that it cannot reach thermal equilibrium before losing a large fraction of its angular momentum (Lombardi et al. 1996; Sills et al. 1997). We may therefore underestimate mass loss from the collision. The mechanism for this angular momentum loss is unclear but it has been suggested that magnetic fields can play a key role (Leonard & Livio 1995; Sills et al. 2005). Rapid rotation can also enhance the mass-loss rate of a star, especially close to the Eddington limit (Maeder & Meynet 2000a). This increases the uncertainty in the mass-loss rate.

Rotation also influences the star through various instabilities that can induce mixing (Endal & Sofia 1976; Pinsonneault et al. 1989; Heger et al. 2000). This mixing is important because it can bring helium to the surface, affecting the opacity of the envelope and increasing the luminosity and effective temperature of the star. As mentioned above, rotational mixing is not expected to alter the outcome of our calculations very strongly because

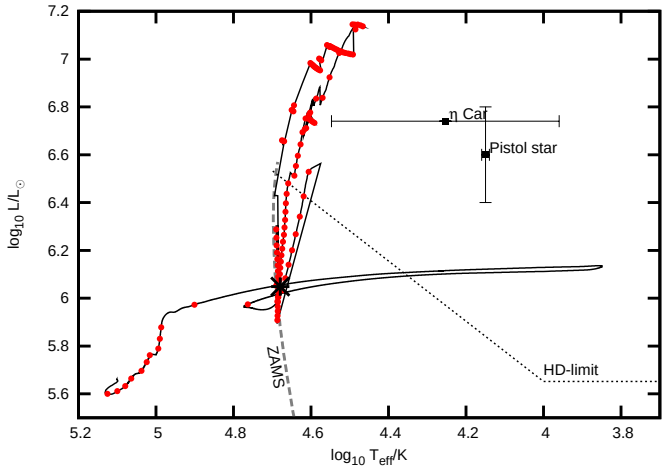

Figure 5.1: *Evolution track of the merger from sequence 1 in the Hertzsprung-Russell diagram. The starting point is indicated by ∗ and points are plotted on the evolution track after each* 30 000 yr. *The dotted line indicates the Humphreys-Davidson limit. For reference, the theoretical ZAMS (running up to 200* $M_\odot$*) and the locations of η Carinae and the Pistol Star are also plotted.*

our collision products are alomst fully convective.

5.3 Results

The initial conditions and outcome of each of our merger sequences are listed in Tables 5.1, 5.2 and 5.3. The tables give the time of collision t, the secondary mass M_2 and the mass of the primary according to the different merger prescriptions. Sequence three was recalculated for $Z = 0.001$ and the results for this run are given in Table 5.4.

The evolution track in the Hertzsprung-Russell diagram (HRD) for the first merger sequence (Table 5.1) is shown in Figure 5.1. The two other sequences are similar. The location of the ZAMS (up to 200 $M_\odot$) is indicated with a dashed line and every 30 000yr is marked with •. The repeated collisions drive the collision product to high luminosities, exceeding the Humphreys-Davidson limit, but the collision product never moves far from the extension of the ZAMS, instead evolving nearly vertically in the HR diagram (similar to the evolution tracks for homogeneously evolving stars, Yoon & Langer 2005). For reference, the locations of the Pistol Star and η Carinae are also shown. The location of η Car is based on Hillier et al.

Table 5.1: *Parameters and results of the first collision sequence studied in this paper. For each subsequent collision N we list the time of collision t (in Myr), the primary mass according to the N-body model $M_{1,N\mathrm{body}}$, the primary mass according to our models, assuming complete mixing during the collision $M_{1,\mathrm{mix}}$, the mass of the secondary M_2 and the mass of the remnant after the collision M_{merger} (all in solar masses). For comparison we also give the masses $M_{1,\mathrm{MMS}}$ for the MMAMS models that we were able to calculate. The final row gives the age at which our evolution calculations stopped and the mass of the collision product at the end of the evolution (assumed black hole mass).*

N	t	$M_{1,N\mathrm{body}}$	$M_{1,\mathrm{mix}}$	$M_{1,\mathrm{MMS}}$	M_2	M_{remnant}
1	0.22577	92.4	90.9	90.9	79.4	154.3
2	0.22782	171.8	154.3	152.8	85.3	217.1
3	0.23702	257.1	216.7	213.6	7.7	223.3
4	0.31217	264.8	219.8	215.3	77.8	274.4
5	0.40122	342.6	268.2	261.6	13.8	279.7
6	0.43480	356.4	277.2	268.0	71.9	327.1
7	0.43480	428.3	327.1	315.1	79.4	382.2
8	0.74123	507.7	348.2		30.1	371.8
9	0.83549	537.7	360.2		66.7	406.7
10	0.90575	604.5	397.3		1.2	398.5
11	1.29919	605.7	353.5		98.2	415.2
12	1.33450	703.9	411.0		24.2	430.8
13	1.42468	728.0	417.6		8.9	425.7
14	1.50261	736.9	409.0		2.2	411.2
15	1.60190	739.1	216.7		60.2	256.5
16	1.63186	799.4	221.0		9.2	228.9
17	1.68112	808.5	186.0		81.1	237.1
18	1.75684	889.6	177.3		40.9	205.5
19	1.90688	930.5	193.6		31.6	216.3
20	2.07245	961.9	129.9		2.6	132.2
21	2.59778	963.1	47.6		55.2	88.6
22	3.10786	1012.7	40.9		75.4[a]	110.1
	3.72835	1118.9	13.9			

[a] See text

Table 5.2: *As Table 5.1 for collision sequence 2*

N	t	$M_{1,N\mathrm{body}}$	$M_{1,\mathrm{mix}}$	M_2	M_{merger}
1	0.72251	91.8	86.5	81.9	150.1
2	0.72252	173.7	150.1	80.2	206.7
3	0.88257	253.8	198.9	68.6	245.6
4	0.88522	322.5	245.4	72.9	294.5
5	0.95998	395.4	287.7	1.8	289.4
6	1.41050	397.1	250.0	95.8	309.6
7	1.50639	492.9	298.4	86.1	352.3
8	1.97200	578.8	282.1	97.6	338.2
9	2.22324	676.2	79.8	75.2	130.4
10	2.22325	751.5	130.2	55.4	166.3
11	2.45320	806.7	83.9	23.5	100.4
12	2.68305	829.8	66.7	28.4	86.8
13	2.74781	858.0	78.8	1.0	79.8
14	3.08766	857.3	53.5	82.6	105.2
15	3.19983	939.2	46.1	56.3	86.3
16	3.27682	995.0	64.8	41.6	93.6
	4.51074	1036.6	10.1		

Table 5.3: *As Table 5.1 for collision sequence 3*

N	t	$M_{1,N\mathrm{body}}$	$M_{1,\mathrm{mix}}$	M_2	M_{merger}
1	0.53120	77.8	75.3	70.7	131.5
2	0.57294	148.5	130.7	82.8	191.3
3	0.65612	231.3	188.1	58.5	228.6
4	0.89154	289.8	215.4	96.6	279.9
5	0.89155	386.4	279.9	78.5	332.5
6	1.02208	464.9	318.1	1.5	319.5
7	1.31086	466.4	289.3	56.3	327.9
8	1.50575	522.6	305.7	48.9	340.1
9	2.05327	571.3	164.0	72.7	209.2
10	2.27966	643.8	73.1	2.0	74.8
11	2.60213	645.0	35.1	3.5	37.7
12	3.12235	642.8	19.8	49.3	60.7
	4.59400	692.1	9.7		

Table 5.4: *As Table 5.3 but for $Z = 0.001$. Note that the merger sequence was terminated earlier than for $Z = 0.02$ and that the merger remnant did not finish its evolution before the evolution code broke down.*

N	t	$M_{1,N\mathrm{body}}$	$M_{1,\mathrm{mix}}$	M_2	M_{merger}
1	0.53120	77.8	77.7	70.7	135.4
2	0.57294	148.5	135.4	82.8	198.3
3	0.65612	231.3	198.1	58.5	239.6
4	0.89154	289.8	239.1	96.6	308.5
5	0.89155	386.4	308.5	78.5	364.2
6	1.02208	464.9	363.5	1.5	364.9
7	1.31086	466.4	363.4	56.3	404.7
8	1.50575	522.6	403.4	48.9	440.2
9	2.05327	571.3	434.9	72.7	487.5
10	2.27966	643.8	390.1	2.0	392.0
11	2.60213	645.0	260.1	3.5	263.3
	2.83153	648.5	171.9[b]		

[b] Mass and time at the moment the evolution code broke down, rather than the onset of carbon burning.

Table 5.5: *Times t and secondary masses m_2 for the sub merger sequence leading to the secondary of collision 22 in the merger sequence in Table 5.1.*

N	t	$M_{1,N\mathrm{body}}$	$M_{1,\mathrm{mix}}$	M_2	M_{merger}
1	0.88048	66.6	63.6	65.2	113.4
2	1.08887	131.8	110.4	16.4	114.1
	3.10786	106.2	75.4		

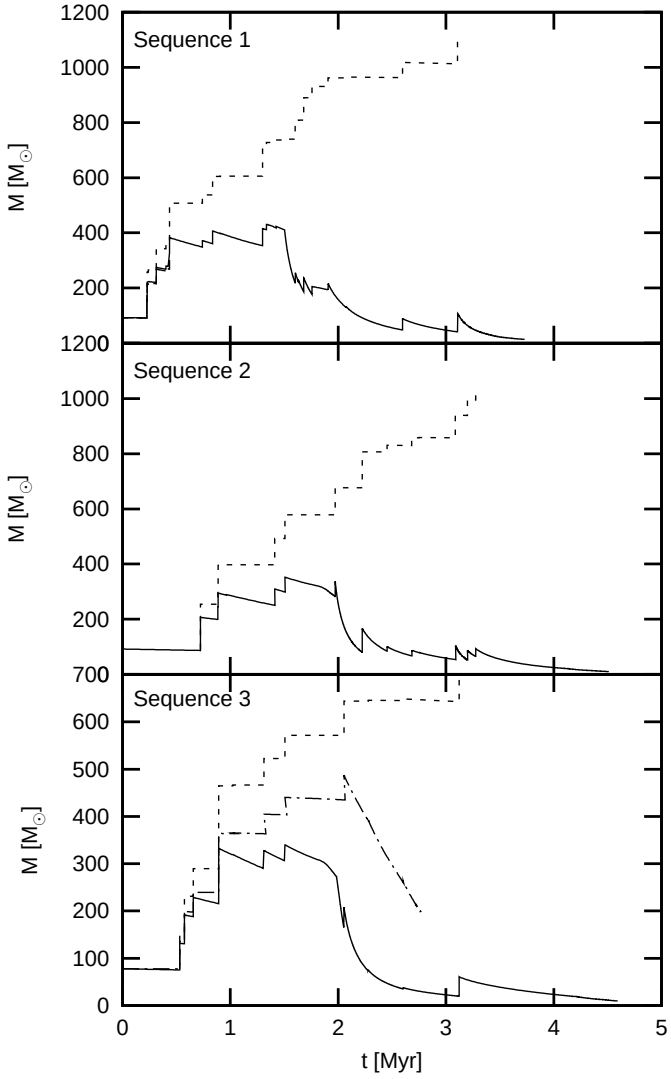

Figure 5.2: *The mass of the merger product as a function of time for the three merger sequences listed in Tables 5.1–5.3. The solid line is the mass found from the detailed models assuming homogeneous mixing, the dashed line is the mass predicted from the N-body calculation. The dash-dotted line in the bottom panel is the mass of the* $Z = 0.001$ *run.*

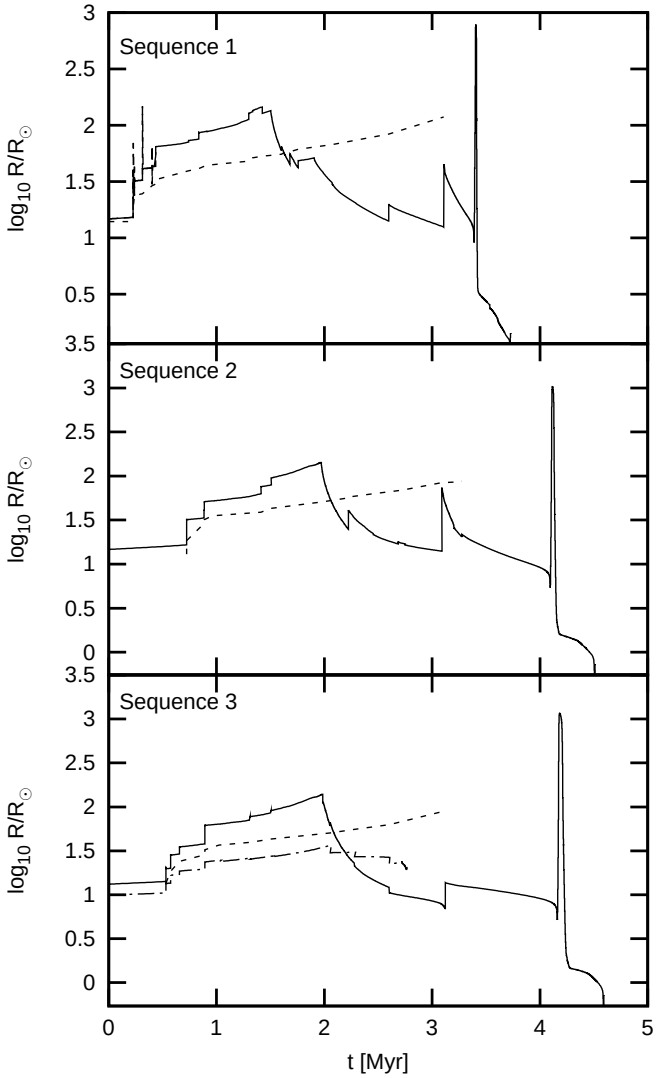

Figure 5.3: *The radius of the merger remnant of the three sequences against time. The solid line is the prediction from our homogeneous models while the dashed line is the radius from the N-body code. The long dashed line in the top panel is the radius from the MMAMS model, which shows spikes at each collision because the merger remnant is out of thermal equilibrium immediately after the merger. The dash-dotted line in the bottom panel is the radius of the* $Z = 0.001$ *run.*

(2001), with the errorbar in effective temperature due to the range in their radius estimates. The luminosity is based on the infrared flux. The location of the Pistol Star is based on the low luminosity solution of Figer et al. (1998). We see that the merger remnant is always hotter than either of these two stars, except when it becomes a red supergiant (the red loop in Figure 5.1), at which time it is less luminous. During the merger sequence the luminosity can exceed the luminosity of these stars. On the other hand, η Carinae and the Pistol Star are both obscured by optically thick outflows, which means that comparing with the effective temperature of our model can be misleading because we do not model such an optically thick wind. The location of the collision product above the Humphreys-Davidson limit suggests that it is a luminous blue variable (LBV) star, so that in reality its position in the HRD is likely to be variable.

The high luminosity increases the mass-loss rate, leading to a competition between mass loss due to stellar winds and mass increase due to collisions (see also Suzuki et al. 2007; Belkus et al. 2007). The time evolution of the mass of the mergers is shown in Figure 5.2. The dashed lines give the mass that was predicted in the N-body simulation while the solid lines show our fully mixed models for $Z = 0.02$. The two agree well for the first few collisions, but mass loss due to stellar wind prevents the mass from exceeding $500\,\mathrm{M}_\odot$. The surface of the merger remnants becomes helium rich and after 1.5–2 Myr turns the star into a Wolf-Rayet star. The strong WR mass-loss rate (up to $3.6 \cdot 10^{-3}\,\mathrm{M}_\odot\,\mathrm{yr}^{-1}$ when the collision product first becomes a WR star) brings the mass down on a timescale of 10^4–$10^5\,\mathrm{yr}$, to $\sim 100\,\mathrm{M}_\odot$ after the final collision and 10–14 $\mathrm{M}_\odot$ at the time of carbon ignition.

In Figure 5.3 we follow the evolution of the radius. Despite the smaller mass our collision products have substantially larger radii (up to a factor three, note the logarithmic scale) than was assumed by the N-body code. This is due to a peculiarity in the structure of the collision product, which will be discussed in detail in §5.3.1. When the collision product becomes a WR star, the radius decreases substantially and the collision product can be up to an order of magnitude smaller than was assumed in the N-body calculation. After core hydrogen exhaustion the collision product still has a thin hydrogen-poor ($X \approx 0.04$) envelope. Expansion of this envelope is responsible for turning the star into a red supergiant and causes the spike in the radius at 3.5 Myr (first sequence) and 4.1 Myr (second and third sequence). During the red supergiant phase the collision product is again above the Humphreys-Davidson limit, but this phase is very short, lasting $17 \cdot 10^3\mathrm{yr}$ ($< 1\%$ of the lifetime of the star).

We have also plotted the mass and radius from the MMAMS models that we were able to calculate. In the upper panel of Figure 5.2 the MMAMS model is indistinguishable from the homogeneous model. After the collision the merger remnant is out of thermal equilibrium and is inflated. The

increase in radius at each collision can be seen in the upper panel of Figure 5.3. Once the collision product reaches thermal equilibrium (after $\sim 10^4$ yr) the radius closely follows the radius of the homogenised model, indicating that the homogenised model is indeed a reasonable approximation of the structure of the merger remnant. Because the radius is larger while the collision product is out of thermal equilibrium it is more likely to interact or collide with other stars at this time, but since we do not take feedback on the dynamics into account this effect is not important for our present considerations.

The collision sequences mostly involve main-sequence stars but a few of the listed collisions are special. Collision 22 of the first sequence involves the remnants of two collision runaways. The star that has undergone the longest sequence of collisions (the "primary") is an early type Wolf-Rayet star at this point with a surface hydrogen abundance of 0.24 and a mass of $41\mathrm{M}_\odot$. However, it is still undergoing core hydrogen burning. The star that has undergone the shortest merger sequence (the "secondary", see Table 5.5) is a core helium burning star of $75\mathrm{M}_\odot$ that has not yet become a Wolf-Rayet star although its surface hydrogen abundance is 0.44, which is close to our criterion. In our homogeneous mixing treatment the result is a collision product that has been enhanced in carbon (see the surface abundance plot in Figure 5.5), which is converted into nitrogen through CNO processing. In a more detailed treatment of the merger process we expect the dense helium core of the secondary to sink to the centre of the collision product so that the merger remnant would have a hydrogen depleted core.

A similar situation occurs for collision 14 from the second sequence, for which the secondary has also become a core helium-burning star at the time of collision.

5.3.1 Structure and size of the merger remnants

Apart from the mass the size of the merger remnant is one of the parameters that determines the probability of subsequent collisions in a cluster. As mentioned, the large radius of the $Z = 0.02$ models during the first 1.5–2 Myr in Figure 5.3 is caused by a peculiarity of the stellar structure.

The merger remnants become very massive and are almost fully convective. The lower panel in Figure 5.4 shows the location of convection zones against the enclosed mass, the upper panel shows the same information as a function of the radius. The central convection zone contains about 90% by mass of the merger remnant. As can be seen from the figure, mass loss between the collisions can reveal material from the central convection zone at the stellar surface (for instance, the mass of the star at 1.3 Myr is lower than the mass of the convective core at 0.8 Myr).

The outer 10% by mass of the merger remnant is radiative, but the upper panel of Figure 5.4 shows two convection zones in this region which

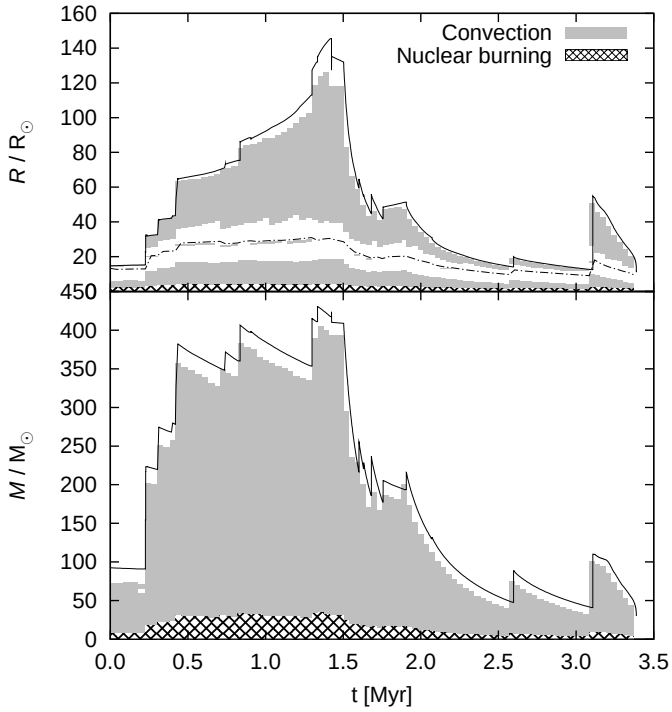

Figure 5.4: *Kippenhahn diagram showing the evolution of the collision product of the first merger sequence. The plot shows convection zones against the radius (upper panel) and against mass coordinate (lower panel) as a function of time. In the upper panel the radius containing a fraction* $1 - 10^{-5}$ *of the stellar mass is indicated with a dash-dotted line. The convective core encompasses 90% of the mass but a much smaller fraction of the radius (at most* $20\,\mathrm{R}_\odot$*). Mass loss between collisions exposes material from the convective core.*

correspond to different peaks in the opacity of the stellar material. An extended convective layer that corresponds to the "Fe bump" is located at large radii. The Fe bump is an increase in opacity around $\log T \approx 5.3$ which was found after introducing the treatment of spin-orbit splitting of iron and nickel into the computation of the opacity tables (Rogers & Iglesias 1992; Seaton et al. 1994). Deeper down a thin convective layer can be seen, caused by the "deep Fe bump", occurring around $\log T \approx 6.3$.

Together, these convection zones are very extended in radius but contain almost no mass. It is especially the convection zone corresponding to the Fe-bump which expands even more while the star evolves. When the star reaches its maximum radius of about 150 $R_\odot$ after 1.4 Myr, this convection zone extends over 90 $R_\odot$, while it contains only about $10^{-4}\,M_\odot$. At this moment the star consists of a core of less than 30 $R_\odot$ in size containing almost all of the mass surrounded by an extended "halo" reaching from 30 to 150 $R_\odot$. This halo has an almost constant temperature and density of $10^{-10}\,\mathrm{g\,cm^{-3}}$. This is indicated in Figure 5.4, which shows the radius outside which a fraction 10^{-5} of the stellar mass is located.

This "core-halo" structure has been found before in models of massive stars, for example by Ishii et al. (1999) for hydrogen-rich stars and by Petrovic et al. (2006) for helium stars. Petrovic et al. (2006) note that to provide the high mass-loss rate from the surface a large outward velocity is needed in the outer layers where the density is low. In their models the necessary velocity is larger than the local sound speed by an order of magnitude. This means that the halo cannot be modelled realistically under the assumption of hydrostatic equilibrium and may not be stable. They find that with a more detailed treatment the halo disappears as a result of the high mass-loss rate. Because our merger remnants have a much larger radius the outflow velocity in the halo is about 2–3 orders of magnitude smaller than the sound speed, which suggests that the halo structure is stable in this case. The halo disappears when the merger remnants become Wolf-Rayet stars and the mass-loss rate increases.

5.3.2 Final remnant masses

For each of the three merger sequences the collision product is close to core hydrogen exhaustion when the merger sequence ends. After the end of the main sequence hydrogen continues to burn in a shell very close to the surface. The hydrogen envelope expands, driving the star into a red loop in the HRD. Mass loss from the surface gradually removes the hydrogen envelope, reducing the efficiency of the hydrogen burning shell. When the hydrogen shell is extinguished the star returns to the blue part of the HRD. The remaining hydrogen envelope is lost and the star becomes a massive ($\sim 20 - 30 M_\odot$) helium star. By the end of core helium-burning the mass has gone down to $10 - 14\,M_\odot$, 80% of which is taken up by the C/O core.

The expected outcome of the evolution for such stars is a complete collapse to a black hole. In each of these sequences 600 – 900 $M_\odot$ is lost to the interstellar medium (see Table 5.6).

5.3.3 Surface abundances and chemical yields

In the course of its evolution the surface of the merger remnant gradually becomes helium rich, as can be seen in the top panel of Figure 5.5. The CNO abundances (shown in the bottom panel of Figure 5.5) change strongly at the first collision and then stay mostly constant up to $t \approx 3$ Myr.

The abundances change most strongly during collisions. This is because the merger remnant is fully mixed at this stage. The abundances also change in between the collisions, as mass loss strips away the surface layers and reveals the deeper layers, but the change is not visible on the scale of the plots until the merger remnant becomes a Wolf-Rayet star. In sequences 1 and 2 the merger remnant undergoes a collision with a core helium-burning star at 3Myr. This results in a strong increase in the carbon abundance (and oxygen, for sequence 2) and a decrease in the nitrogen abundance (through dilution). CNO cycling then converts the carbon into nitrogen, producing a nitrogen-rich WR star. However, our assumption of complete mixing is unlikely to be valid for collisions with core helium-burning stars. More likely, most of the carbon and oxygen would remain in the core of the collision product and such a strong increase in surface C and N probably does not occur.

As the collision product continues to evolve after the end of the merger sequence, the surface helium abundance increases until the hydrogen envelope has been lost and the surface is nearly pure helium. The stellar wind continues to expose deeper layers of the star, eventually revealing at the surface the ashes of helium burning. At this point, the surface nitrogen and helium abundance decrease while the carbon and oxygen abundances increase strongly. At the end of the evolution, carbon is the most abundant element on the surface.

The expulsion of gas from the cluster is usually attributed to supernova explosions, which are expected to start after about 3 Myr. The merger remnant loses most of its mass before this time. Table 5.6 gives the composition of the material lost from the merger remnant as well as the amount of material lost, split into three categories: ejecta from the collisions, mass loss due to stellar wind during the merger sequence and mass loss from the collision product after the end of the merger sequence. Most of the material is ejected in the form of a stellar wind between collisions, followed by the material that is lost during the collisions. The material that is lost by the collision product after the end of the merger sequence is significantly more helium rich than the material that was lost before, which simply reflects the increased surface helium abundance of the collision product. The material

Table 5.6: *Ejected mass and composition for the three computed merger sequences compared to a population of single stars. The first row lists the total mass ΔM (in solar units) lost through each of the three listed channels, the remaining rows give the abundances (by mass) of H, He, C, N and O. For each sequence the first column lists the ejecta from the collision, the second column lists the integrated values for the stellar wind during the merger sequence and the third column lists the values for the evolution of the merger remnant after the merger sequence has ended.*

	Single	Collision	Wind	Remnant
		Sequence 1		
ΔM	647.5	228.6	695.8	95.4
H	0.4806	0.5648	0.4006	0.0899
He	0.4965	0.4000	0.5794	0.8308
C	0.0040	0.0012	0.0003	0.0306
N	0.0092	0.0166	0.0132	0.0294
O	0.0040	0.0013	0.0010	0.0060
		Sequence 2		
ΔM		191.8	549.9	83.5
H		0.5599	0.3489	0.1944
He		0.4093	0.6311	0.7637
C		0.0090	0.0003	0.0133
N		0.0117	0.0133	0.0128
O		0.0044	0.0009	0.0081
		Sequence 3		
ΔM		142.3	456.6	102.0
H		0.5521	0.3361	0.2025
He		0.4305	0.6439	0.7553
C		0.0004	0.0003	0.0184
N		0.0105	0.0134	0.0123
O		0.0013	0.0008	0.0050

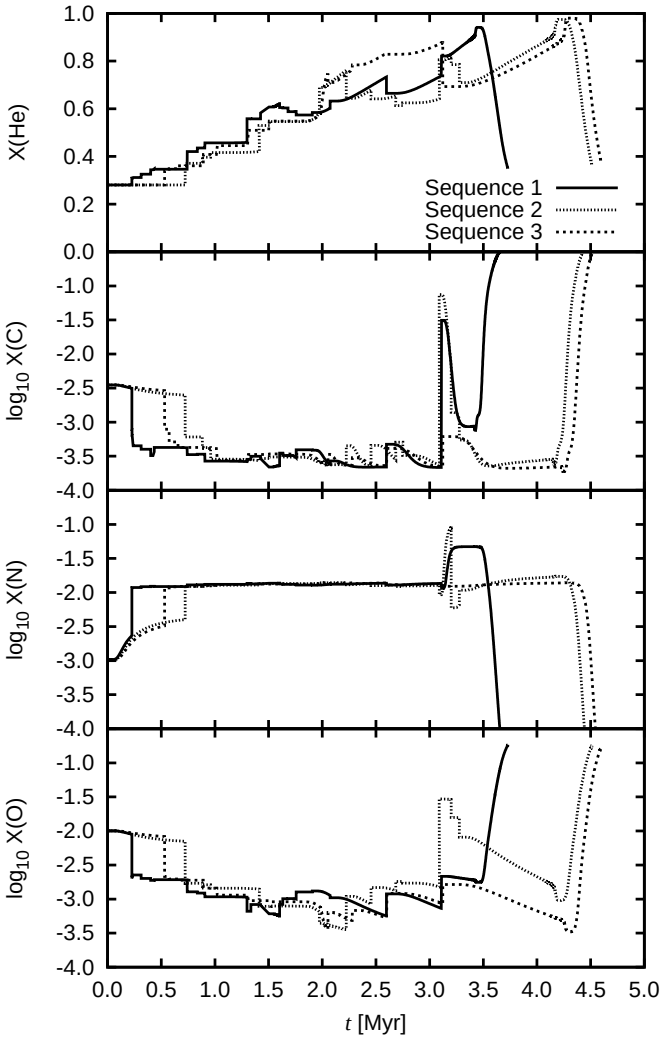

Figure 5.5: *Surface He, C, N and O abundances (by mass fraction) for as a function of time (in Myr) for the three $Z = 0.02$ sequences.*

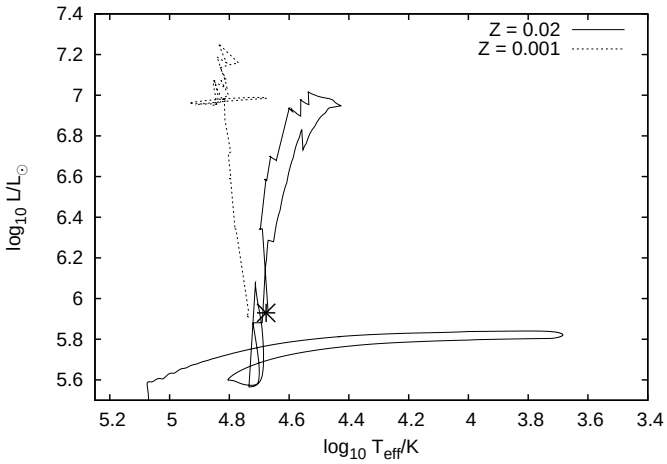

Figure 5.6: *Evolution track of the merger remnant of sequence 3 for* $Z = 0.02$ *(solid line) and* $Z = 0.001$ *(dashed line). Note that the* $Z = 0.001$ *track remains much brighter than the* $Z = 0.02$ *track.*

lost from the collisions is less helium rich than the material that is lost in the wind. This is partially due to the increase in the surface helium abundance between collisions (Figure 5.5) and partially due to the fact that the estimated mass loss from the collision is larger for more equal masses and becomes smaller when the mass ratio is more extreme, which is the case for later collisions when the collision product is both massive and helium rich.

If we compare the yields of the first sequence to the yields that would have been obtained if the stars involved in the merger had been allowed to evolve on their own (column 2 in Table 5.6) we first note that the single stars eject much less material than the merger sequence. This is because the merger sequence produces one $13.9\,M_\odot$ black hole, while the single stars above $30\,M_\odot$ all produce black holes of 8–24 $M_\odot$. The ejected material is also less helium rich than the material that is lost from the merger remnant: the single star models lose 321 $M_\odot$ of helium and 311 $M_\odot$ of hydrogen (He/H ≈ 1), while the merger product loses 574 $M_\odot$ of helium and 416 $M_\odot$ of hydrogen (He/H ≈ 1.4). This is directly related to the large size of the convective core: for the merger remnant, 90% of the material has undergone nuclear processing in the core, which is a much larger fraction than for the population of single stars.

5.3.4 Metallicity effects

Because mass-loss rates are lower at low metallicity we have recalculated sequence 3 for $Z = 0.001$. At this metallicity the mass-loss rates are about 13 times lower than for $Z = 0.02$, which means that the remnant can become more massive.

The mass of the remnant after the last collision in the sequence is $263\mathrm{M}_\odot$. We followed the evolution of the merger product through core helium burning until the core helium abundance has decreased to $Y_\mathrm{c} \approx 0.63$ (about one third of the core helium-burning lifetime), at which time the mass is $172\,\mathrm{M}_\odot$. Numerical problems prevented us from evolving this model further until carbon ignition. We extrapolated the mass loss as a linear function of the central helium abundance (rather than time) to the moment of helium exhaustion, which was found to give a good estimate of the final mass for $Z = 0.02$. Based on this extrapolation we expect the final mass to be $\sim 120\mathrm{M}_\odot$ by the time of carbon ignition. The expected fate of this merger remnant is a pair-creation supernova (Langer et al. 2007; Portegies Zwart & van den Heuvel 2007).

Because the opacity bump that gives rise to the core-halo structure is associated with iron, the core-halo structure does not appear at low metallicity and the collision product remains more compact. This is why in the bottom panel of Figure 5.3 the radius of the $Z = 0.001$ model (dash-dotted line) is smaller than the radius of the $Z = 0.02$ model until 2 Myr, when the latter becomes a WR star. The radius is always smaller than the radius assumed in the N-body calculations.

The lower mass-loss rate makes it easier to build up more massive remnants, but the smaller radius reduces the probability of a collision and may prevent the occurrence of a runaway merger. The thermal timescale is also shorter at low metallicity, meaning that the star will reach thermal equilibrium faster after the collision. An additional complication is that the lifetime of the stars is reduced at lower metallicity (because of their larger mass) so that there is less time to form the merger sequence. Fully self-consistent dynamical models (in which the stellar evolution, stellar collisions and stellar dynamics are all treated consistently) are necessary to determine which of these effects dominates in practice.

5.4 Discussion and conclusions

We have found that the end result of a runaway merger at solar metallicity is a $\sim 100\mathrm{M}_\odot$ WR star after the final collision that produces a $\sim 10\mathrm{M}_\odot$ black hole. Most of the mass is lost in the form of a stellar wind enriched in N and He. At lower metallicity the mass-loss rates are reduced and the remnant mass can be larger ($\sim 260\,\mathrm{M}_\odot$), possibly leading to a pair-creation

supernova. In none of the cases we studied an intermediate-mass black hole is formed.

The material that is lost from the collision remnant is helium rich and shows the signature of CNO processing (N enhancement, C depletion). Because the merger remnant loses most of its mass in the first 3 Myr, the timescale on which we expect the first supernovae to go off, the primordial gas may not yet have been expelled from the cluster. In this case the material that is lost from the merger remnant can be retained in the cluster and could be accreted onto other stars or used in further star formation. This offers the possibility of finding a chemical signature in clusters observed today where a merger sequence occurred in the past. In order to do this we require more detailed nucleosynthesis than the models described in this paper provide. The amount of ejected material is probably not enough to account for a second generation of helium-rich stars as is found in some globular clusters, since such a helium-rich population generally seems to comprise about 15–20% of the stars in the cluster (Pumo et al. 2008), which is larger than the fraction of mass mass lost from the merger remnant compared to the total cluster mass.

The main uncertainty in our models is the adopted mass-loss rate. We have used established mass-loss prescriptions from the literature. Our adopted Vink et al. (2001) rate is derived for stars that are further away from their Eddington luminosity than our collision products and is likely to be an underestimate of the true mass-loss rate for our stars.

When the surface hydrogen abundance $X_{\rm s} < 0.4$ we apply WR mass loss rates. This transition is somewhat arbitrary and ideally we would use a single mass loss recipe that predicts the mass-loss rate as a function of the local luminosity, temperature, effective gravity and composition. No such recipe is available in the literature at this time.

The mass-loss rate can become very high during the WR phase due to our extrapolation of the empirical rate to higher luminosity than for which it was derived. We have made sure that the power used to drive the wind is always less than that provided by the star's luminosity (Owocki et al. 2004). When the collision products first become WR stars, the mass-loss rate is still very high. In part this is due to the sudden transition to to WR mass loss rates when $X_{\rm s}$ drops below 0.4. We expect that if the transition is made more smoothly the mass-loss rate would increase earlier and avoid the high peak value found in our current models. This again stresses the need for a unified single mass loss prescription.

Our collision products have luminosities close to their Eddington luminosity and for a substantial amount of time exceed the Humphreys-Davidson limit. Stars close to this limit become luminous blue variables which can lose a large amount of mass in outbursts. A model that describes mass loss from stars that exceed their Eddington luminosity is the so-called porosity model (Owocki et al. 2004; Owocki & van Marle 2008). Our models come

close, but do not exceed their Eddington luminosity. We have made one trial run with the mass-loss rate artificially enhanced by a factor of 50 and found that even if collisions increase the mass of the star the star is very quickly stripped of its mass.

We have ignored rotation in this work. Rotational mixing is expected to be unimportant because our models are almost fully convective. Rapid rotation is also expected to enhance the mass-loss rate from stars, especially close to the Eddington limit. This enhanced mass loss is compounded by the need to lose angular momentum from the collision product before it can reach thermal equilibrium. In effect this increases the uncertainty in the already uncertain mass loss rate.

The radius of our detailed evolution models is different from the radius that was used to detect collisions in the N-body run. This demonstrates that it is important to perform fully self-consistent simulations of collision runaways. Calculations at lower Z are especially interesting since remnant masses can be higher due to a reduced stellar wind, but on the other hand collisions are less likely because the stars are more compact. Calculations like those by Belkus et al. (2007) in which the stellar evolution is treated with an analytic recipe, are an important step in this direction.

Acknowledgements

Evert thanks Jorick Vink and Allard Jan van Marle for useful discussion about mass-loss rates from luminous stars in general and Henny Lamers for the Wolf-Rayet mass-loss rates in particular. He also thanks Rob Izzard for more general discussion.

EG&EG are supported by NWO under grants 614.000.303 and 635.000.303. SdM is partially supported by NOVA. The research was conducted in the context of the MODEST collaboration.

6

Nederlandse samenvatting

Dit proefschrift gaat over sterren die gevormd zijn door het samensmelten van twee sterren als gevolg van een botsing. De structuur en ontwikkeling van sterren die op deze manier gevormd zijn kunnen afwijken van die van sterren die op een gewone manier gevormd zijn. In het vervolg zullen we kort ingaan op de vorming en evolutie van enkele sterren, om ons daarna te richten op sterbotsingen en de verdere ontwikkeling van de botsingsproducten. Vanaf sectie 6.2 komt de inhoud min of meer overeen met de engelstalige inleiding in hoofdstuk 1, waar ook de verwijzingen naar de literatuur te vinden zijn.

6.1 De vorming en evolutie van enkele sterren

Sterren worden gevormd uit gaswolken, zogenaamde interstellaire wolken die vooral (70–75% van de massa) uit waterstof bestaan. Door invloed van de zwaartekracht begint de gaswolk samen te trekken waardoor een protoster ontstaat. Het gas wordt samengedrukt en daardoor heter, totdat de temperatuur in het binnenste van de protoster hoog genoeg is om waterstof door kernfusie om te zetten in helium. Hierbij komt zeer veel energie vrij en de samentrekking komt (voorlopig) tot stilstand. De ster bevindt zicn nu in de zogenaamde *hoofdreeksfase* of waterstof-kern-verbrandingsfase. Ook de Zon bevindt zich in deze fase. De Zon is trouwens een heel "gemiddelde" ster, waardoor het vaak handig is om eigenschappen van sterren te vergelijken met die van de Zon: zo wordt de massa van een ster vaak gegeven als veelvoud van de massa van de Zon ($M_\odot = 2{\cdot}10^{30}$ kg)[1], de straal als veelvoud

[1] $2 \cdot 10^{30}$ wil zeggen: een 2 gevolgd door 30 nullen, of wel duizend maal een miljard maal een miljard maal een miljard.

van de straal van de Zon ($R_\odot = 0.7 \cdot 10^6$ km) en het uitgestraalde vermogen (de *lichtkracht*) als veelvoud van het vermogen van de Zon ($L_\odot = 4 \cdot 10^{26}$ W). De hoofdreeksfase duurt totdat de waterstofvoorraad in de kern van de ster is uitgeput. Wanneer dat gebeurt zal de ster andere energiebronnen aan moeten boren. Hoe dit precies in zijn werk gaat is afhankelijk van de massa van de ster, maar globaal gebeurt ongeveer het volgende.

Omdat in de kern van de ster geen energie meer wordt opgewekt begint deze door de eigen zwaartekracht opnieuw samen te trekken. De samentrekking van de oorspronkelijke gaswolk is als het ware onderbroken door de waterstofverbranding en gaat nu verder. Buiten de kern worden nu de temperatuur en de dichtheid hoog genoeg om waterstof om te zetten in helium: de ster bevindt zich nu in de *waterstof-schil-verbrandingsfase*. Tijdens deze fase verandert de structuur van de ster behoorlijk: de kern krimpt weliswaar, maar de buitenlagen zetten enorm uit. Van een redelijk compacte hoofdreekster verandert de ster in een rode reus. Sommige rode reuzen zijn groter dan de baan van de Aarde om de Zon. Na verloop van tijd zal de temperatuur in het binnenste van de ster hoog genoeg worden om helium te fuseren tot koolstof en zuurstof. De ster bevindt zich dan in de helium-kernverbrandingsfase. De overgang naar deze fase verloopt voor sterren lichter dan ongeveer 2.5 $M_\odot$ explosief (via de zogenaamde *heliumflits*) en voor zwaardere sterren geleidelijker. Als de ster zwaarder dan ongeveer 7 $M_\odot$ is zal na heliumverbranding koolstof worden omgezet in neon en magnesium. In sterren die lichter zijn dan ongeveer 9 $M_\odot$ is het daarna afgelopen: de ster verliest zijn mantel en de sterkern koelt langzaam af tot een witte dwerg ster. In zware sterren kunnen steeds zwaardere elementen worden verbrand tot uiteindelijk silicium wordt omgezet in ijzer, waarna de ster zijn leven eindigt in een supernovaexplosie. Hierbij vormt zich dan een neutronenster of een zwart gat.

Van alle verbrandingsfasen duurt de hoofdreeksfase veruit het langst, ongeveer 80% van de totale levensduur van de ster. Een gevolg hiervan is dat de meeste waargenomen sterren hoofdreekssterren zijn. We zullen ons hier ook vooral met hoofdreekssterren bezig houden, hoewel we ook even stil zullen staan bij sterren die zich in latere evolutiestadia bevinden.

Nu is er iets merkwaardigs aan de hand: zwaardere sterren hebben een grotere hoeveelheid waterstof tot hun beschikking, zodat we redelijkerwijs zouden kunnen denken dat ze langer kunnen leven dan lichte sterren. Toch is dit niet het geval en dat komt doordat zware sterren veel meer energie uitstralen (veel helderder zijn) dan lichte sterren: het is een beetje als een auto met een grotere tankinhoud die heel onzuinig rijdt, waardoor toch eerder getankt moet worden dan in een zuinige auto met een kleinere tankinhoud. De Zon heeft een levensduur van ongeveer 10 miljard (10^{10}) jaar. Een ster die twee keer zo zwaar is leeft ongeveer 1 miljard jaar (tien keer korter dus), een ster die maar half zo zwaar is als de zon kan ruim 100 miljard jaar (dus tien keer langer) leven.

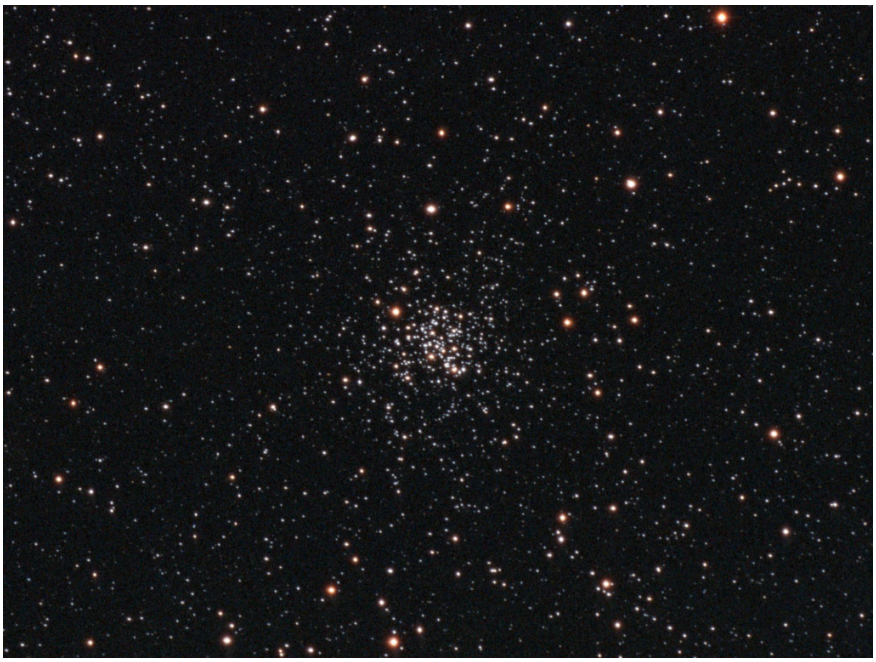

Figuur 6.1: *De open sterrenhoop M67*

Dit heeft een belangrijke consequentie: wanneer we een groep sterren hebben die gezamelijk gevormd zijn zullen de zwaarste (helderste) sterren in deze groep als eerste hun brandstof verstoken en onzichtbaar worden. Omdat we op grond van modelberekeningen weten hoe helder sterren van een bepaalde massa zijn en hoe lang zij kunnen leven kunnen we op grond van de helderste sterren in een groep bepalen hoe oud deze groep sterren is. Hierbij is wel van belang dat de groep waargenomen sterren ook daadwerkelijk (ongeveer) dezelfde leeftijd heeft. Zulke groepen sterren bestaan en worden *sterrenhopen* genoemd. Een voorbeeld is de sterrenhoop M67 in figuur 6.1.

6.2 De evolutie van sterren in sterrenhopen

Sterrenhopen zijn gebieden in de ruimte waar sterren veel dichter bij elkaar staan dan gemiddeld. Historisch worden ze onderverdeeld in open sterrenhopen en bolvormige sterrenhopen, hoewel dit onderscheid tegenwoordig niet meer op deze manier gemaakt wordt. Sterrenhopen worden wel eens "sterrenkundige laboratoria" genoemd omdat de sterren die hierin voorkomen allemaal op ongeveer dezelfde tijd gevormd zijn uit gas met dezelfde

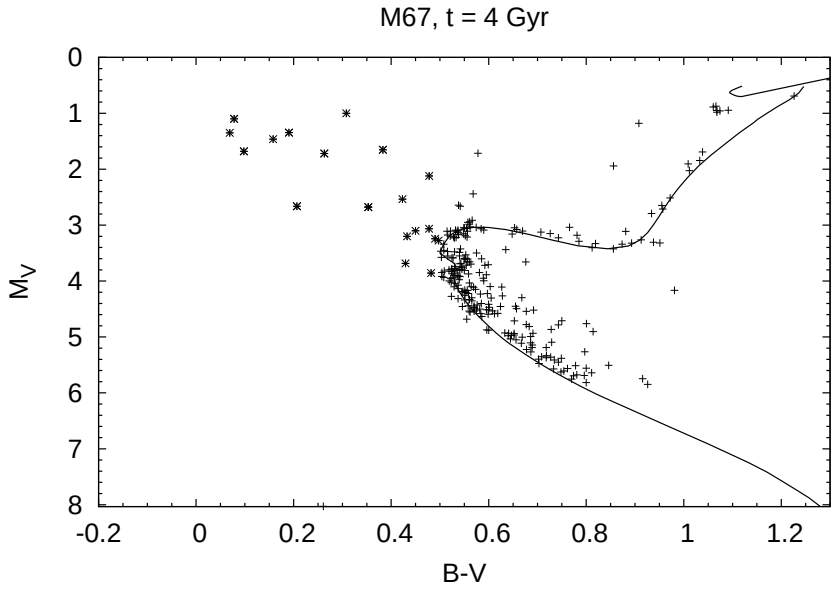

Figuur 6.2: *De doorgetrokken lijn in dit diagram laat het verwachte verband zien tussen de kleur ($B - V$, een maat voor de temperatuur) en de magnitude (M_V, een maat voor de helderheid) van sterren in de sterrenhoop M67, de aangegeven punten zijn waargenomen sterren. De met $*$ aangegeven sterren zijn blauwe achterblijvers. Zie ook figuur 3.6.*

samenstelling en aan dezelfde invloeden hebben blootgestaan, ongeveer zoals dat het geval zou zijn als we op Aarde een populatie sterren zouden kunnen maken onder gecontroleerde omstandigheden in een laboratorium. Dat het toch zo eenvoudig niet is blijkt uit de recente ontdekking van populaties met verschillende leeftijden in een aantal clusters, waar op dit moment nog geen goede verklaring voor gevonden is. Toch komen sterrenhopen van alle plaatsen in het heelal het dichtst in de buurt van het eerder genoemde "sterrenkundig laboratorium." Sterrenhopen zijn dus ideaal om ons begrip van sterevolutie en sterdynamica te testen.

Omdat de sterren in een sterrenhoop min of meer gelijktijdig gevormd zijn kunnen we de leeftijd van de sterrenhoop bepalen door te kijken naar de helderste sterren. Dit werkt in de praktijk goed en de meeste sterren in een sterrenhoop kunnen goed verklaard worden met standaard stermodellen. De meeste, maar niet allemaal.

In 1953 werd in de sterrenhoop M3 een populatie heldere blauwe sterren gevonden. Tegenwoordig weten we dat bijna alle sterrenhopen een dergelijke populatie blauwe sterren hebben, bijvoorbeeld ook de al genoemde sterren-

hoop M67. Ze zijn weergegeven in figuur 6.2. De ontdekking van deze sterren kwam als een verrassing: op grond van hun helderheid hadden deze sterren allang van de hoofdreeks af geëvolueerd moeten zijn. Het is alsof ze een beetje achtergebleven zijn in hun ontwikkeling. Deze sterren worden *blauwe achterblijvers* (Engels: *blue stragglers*) genoemd. De beste verklaring is echter dat de sterren niet zijn achtergebleven in hun ontwikkeling, maar dat ze oorspronkelijk lichter waren en pas later zwaarder geworden zijn. Ze hebben als het ware bijgetankt.

Er zijn in principe twee manieren waarop dit bijtanken kan gebeuren die waarschijnlijk allebei een rol spelen.

De meeste sterren die worden waargenomen maken deel uit van een dubbelstersysteem, een systeem waarin twee (of meer) sterren om elkaar heen draaien op dezelfde manier dat planeten om de zon draaien. In een nauwe dubbelster kan een van de twee sterren materiaal overdragen aan de begeleider. Dit is een relatief vaak voorkomend proces dat overal kan plaatsvinden.

De tweede mogelijkheid is een vorm van kosmisch kannibalisme: twee sterren komen zo dicht bij elkaar dat ze elkaar raken en samensmelten tot een nieuwe ster. Dit kan gebeuren in een dubbelster als een gevolg van dubbelsterevolutie, maar ook in gebieden waar sterren heel dicht bij elkaar zitten, met andere woorden, in sterrenhopen. In dit laatste geval is echt sprake van een sterbotsing. Overigens geldt ook in sterrenhopen dat de kans op een botsing veel groter is als de botsende sterren zich in dubbelstersystemen bevinden.

6.3 De evolutie van botsingsproducten

Als we veronderstellen dat veel blauwe achterblijvers inderdaad gevormd worden door botsingen tussen sterren is het van belang te begrijpen hoe het botsingsproduct van twee sterren zich verder ontwikkelt. We moeten dus de evolutie op lange termijn bestuderen. De manier waarop wij dit gedaan hebben is door het resultaat van een computerberekening van de botsing terug te voeren in een computerprogramma dat de evolutie van een ster kan uitrekenen, een zogeheten sterevolutieprogramma. Hiermee kan dan de evolutie op lange termijn bepaald worden.

Tijdens een botsing komt erg veel energie vrij. Het botsingsproduct zwelt hierdoor op en lijkt wel wat op een protoster. Toch is er een belangrijk verschil: in een protoster vinden stromingen plaats die de hele ster grondig mengen, dit is niet het geval voor de botsingsproducten waardoor de samenstelling van de sterren niet overal gelijk is. Er is ook een overeenkomst: het botsingsproduct zal net als een protoster onder zijn eigen zwaartekracht inkrimpen, totdat in het binnenste de temperatuur weer hoog genoeg wordt om waterstof om te zetten in helium. De evolutie verloopt vanaf dat mo-

ment min of meer gelijk aan die van een normale hoofdreeksster, maar met een paar verschillen. Doordat de chemische samenstelling in het inwendige afwijkt van die in een gewone ster is de helderheid eigenlijk groter dan we op grond van de massa hadden verwacht. Hierdoor is ook de levensduur van de ster korter dan we verwacht zouden hebben. Dit is van belang als we willen proberen de waargenomen blauwe achterblijvers te begrijpen.

6.4 Dit proefschrift

Voor dit proefschrift hebben we met twee doelen gekeken naar de evolutie van de overblijfselen van sterbotsingen. In de eerste plaats hebben we een bijdrage willen leveren aan het begrip van de al genoemde blauwe achterblijvers. Hiervoor hebben we gekeken naar botsingen tussen relatief lichte sterren, ongeveer zo zwaar als of iets lichter dan de Zon. In de tweede plaats hebben we gekeken naar botsingen tussen zware sterren, in het bijzonder naar wat er gebeurt als er herhaaldelijk sterren op elkaar botsen. Berekeningen aan sterrenhopen laten zien dat dit soort botsingsreeksen onder geschikte omstandigheden kan optreden.

In hoofdstuk 2 beschrijven we het sterevolutieprogramma dat we gebruikt hebben om de evolutie van de botsingsproducten door te rekenen en de methode die we gebruikt hebben om onze beginmodellen te maken. We passen dit programma vervolgens toe op een aantal sterbotsingen die waren opgetreden in een simulatie van de sterrenhoop M67 en vergelijken de resultaten van ons programma met eenvoudiger benaderingen: een recept om de ontwikkeling van gewone enkele sterren te bepalen en een benadering waarbij het botsingsproduct bij de botsing geheel gemengd wordt. Het blijkt dat de eerste methode een veel langere levensduur voorspelt dan onze gedetailleerde berekeningen, terwijl de tweede methode sterren voorspelt die veel blauwer (heter) zijn. Beide benaderingen geven dus aanleiding tot systematische afwijkingen die we met onze gedetailleerde berekeningen vermijden. We gebruiken ons sterevolutieprogramma vervolgens in hoofdstuk 3 om de evolutie van een groot aantal botsingsproducten uit te rekenen waarbij we steeds één grootheid variëren: hetzij de massaverhouding van de botsende sterren, hetzij de totale massa van de twee sterren, hetzij het tijdstip van de botsing. Hiermee kunnen we begrijpen hoe de eigenschappen (en dus de ontwikkeling) van het botsingsproduct afhangen van deze grootheden. Het blijkt dat we een eenvoudige afschatting kunnen maken waarmee we redelijk nauwkeurig de evolutie kunnen voorspellen als we de eigenschappen van de botsende sterren kennen. Dit kan gebruikt worden om berekeningen van de evolutie van botsingsproducten in simulaties van sterclusters te verbeteren. We vergelijken onze modellen ook met de waargenomen populatie blauwe achterblijvers in de sterrenhopen M67 en NGC 188 en het blijkt dat we deze redelijk zouden kunnen verklaren met behulp van botsingsproducten.

In hoofdstuk 4 en 5 passen we dezelfde procedure toe op botsingen tussen zware sterren. Het doel is hier niet het bestuderen van blauwe achterblijvers, maar het bestuderen van botsingsreeksen waarvan modelberekeningen van de sterdynamica laten zien dat ze in jonge dichte sterrenhopen kunnen voorkomen. Een belangrijke vraag hierbij is hoe het eindproduct van zo'n botsingsreeks eruit ziet: zou dit een zwart gat met een massa van 100 – 1000$M_\odot$ kunnen zijn? Dit soort zwarte gaten kan niet door gewone sterevolutie gevormd worden aangezien gewone sterren zelf niet zo zwaar zijn. Om deze vraag te beantwoorden bestuderen we in hoofdstuk 4 eerst de evolutie van botsingsproducten uit een enkele botsing (het zou de eerste botsing uit een reeks kunnen zijn) op dezelfde manier als we dat in hoofdstuk 3 voor sterren met een lage massa hebben gedaan. Het blijkt dat op de hoofdreeks de structuur en ontwikkeling van de botsingsproducten analoog zijn aan die voor de lichte botsingsproducten. Botsingen met sterren die net van de hoofdreeks af geëvolueerd zijn leveren ook een interessant resultaat op: een nieuwe ster met een abnormaal kleine heliumkern. Het belang hiervan is dat deze sterren zich duidelijk afwijkend van sterren met een normale heliumkern ontwikkelen. Ze blijven bijvoorbeeld lange tijd zichtbaar als blauwe superreuzen, een klasse van waargenomen sterren die met conventionele stermodellen nog niet bevredigend verklaard kan worden. Op basis van de inzichten in hoofdstuk 4 bestuderen we in hoofdstuk 5 de evolutie van een aantal botsingsreeksen die in de literatuur gepubliceerd zijn. Onze berekeningen laten zien dat in geen van deze gevallen een middelzwaar zwart gat gevormd wordt, in plaats daarvan wordt een minder zwaar zwart gat van ongeveer 10$M_\odot$ gevormd. De reden hiervoor is dat het botsingsproduct tijdens zijn evolutie al erg veel massa weg blaast in een zogenaamde sterrewind. Een botsingsreeks zou echter in een omgeving met een andere chemische samenstelling wel aanleiding kunnen geven tot een extreem heldere supernova die mogelijk overeenkomt met de in 2006 in het sterrenstelsel NGC 1260 waargenomen supernova 2006gy.

Dankwoord/Acknowledgements

Dankwoord

Het schrijven van een proefschrift is een merkwaardige bezigheid: enerzijds is het iets dat men geacht wordt alleen te doen, anderzijds is het iets dat niemand alleen kan volbrengen. Hierbij wil ik dus iedereen die naar mijn mening op enigerlei wijze heeft bijgedragen aan het succesvol afronden van dit boekwerk hartelijk bedanken. Het is een lange opsomming, dus ik zal waarschijnlijk niet iedereen met name kunnen bedanken en ik hoop dat wie zich in het vervolg niet bij naam genoemd ziet zich daar niet door gekwetst voelt.

Laat ik beginnen met mijn directe begeleider Onno Pols te bedanken voor de prettige en leerzame samenwerking gedurende de afgelopen jaren. Dank aan Simon Portegies Zwart en Frank Verbunt voor wijze raad vanaf de zijlijn.

Ik wil graag iedereen op het Sterrekundig Instituut Utrecht bedanken voor de leuke sfeer op het instituut. In de eerste plaats mijn kamergenoot Eveline zonder wie het aanmerkelijk stiller was geweest in mijn hoekje van het instituut, maar zeker ook de andere leden van de sterevolutiegroep: Selma met wie het altijd fijn praten is, of het nu over wetenschap gaat of iets anders tijdens een korte (of lange) pauze, Rob voor zijn cynische gevoel voor humor en discussies over wat er goed maar vooral slecht is aan alles en Nederland in het bijzonder, Matteo, Ines, Maria en Norbert voor gesprekken over wetenschap en het wetenschappelijk 'proces'. Een extra bedankje voor Bob voor het lezen van mijn Nederlandse samenvatting. Axel, heel erg bedankt voor de discussies over astrofysica waardoor ik mezelf scherp kon houden. Het spijt me als dit ten kostte gegaan is van jou geestelijk welzijn. Verder natuurlijk mijn hartelijke dank aan iedereen die verder verantwoordelijk is voor de goede sfeer op het instituut: Remco, Peter, Frans, Sabina, Garmt, Sandra, Ana, Laurens, Esteban, Klaartje. Niet in de laatste plaats dank aan degenen die het instituut achter de schermen draaiende houden: Marion, Ed en Sake.

Naast collega's uit Utrecht wil ik ook graag een paar mensen daarbuiten bedanken. In de eerste plaats Peter Eggleton, zonder wiens sterevolutieprogramma dit werk niet eens van de grond gekomen was. Daarnaast Evghenii Gaburov, mijn collega op het samenwerkingsproject tussen Utrecht en Amsterdam over sterbotsingen. Verder mijn dank aan iedereen die ik op conferenties en workshops ontmoet heb en daar leuke en leerzame ervaringen van gemaakt hebben: Piet Hut, Steve McMillan, James Lombardi en de rest van de MODEST gemeenschap, Jorick Vink, Ofer Yaron en andere gebruikers van 'de Eggleton-code': Haili Hu, Richard Stancliffe, Ross Church, John Eldridge en Stephen Justham.

Verder wil ik natuurlijk al mijn vrienden buiten Utrecht bedanken voor de leuke tijd voor, tijdens en hopelijk na mijn promotie: Pascalle, Mathilde, Koos, Gerben, Dave, Laura, Hendrik, Jet, Lydwin, Martijn, Gerben, Joop, Bernard, Yan, Paul, Vincent, Evy, Michiel, P.P. en de schakers van DOS Amsterdam: jullie hebben allemaal op enig moment op enige wijze bijgedragen aan de succesvolle voltooiing van dit werk. Mijn bijzondere dank aan Tine voor haar geduld en begrip. Het laatste half jaar van een promotie traject is niet de makkelijkste tijd om iemand te leren kennen.

Tot slot wil ik ook mijn familie wil ik graag bedanken: mijn Oma, tantes Eeke en Karin en oom Ron, mijn nichtjes Marieke en Femke en hun man en vriend Joost en Erik. Niet in de laatste plaats wil ik mijn moeder heel erg hartelijk bedanken voor alle belangstelling, steun en hulp gedurende de jaren.

Hartelijk dank allemaal! Ik had dit niet zonder jullie gekund.

Acknowledgements

Writing a PhD-thesis is a curious affair: on the one hand it's something one is expected to do alone, on the other hand it's not something that one can do alone. Here I would like to thank everyone who has contributed in some way to the successful completion of this booklet. It's a long list of names and probably I cannot thank everyone. Hopefully no one will be offended by not seeing their name appear below.

First of all let me thank my supervisor Onno Pols for the fun and educational collaboration over the past few years. Many thanks to Simon Portegies Zwart and Frank Verbunt for giving good advice on the side.

I want to thank everyone on the *Sterrekundig Instituut Utrecht* for the fun atmosphere at the institute. First of all my officemate Eveline without whom my corner of the institute would have been too quiet, but also the other members of the stellar evolution group: Selma, talking to whom was always great fun during short (or long) breaks, regardless of whether the topic was science or something different, Rob for his cynical sense of humour and talks about things that are good and bad in general and about the

Netherlands in particular, Matteo, Ines, Maria and Norbert for discussion about science and the scientific process. Extra thanks to Bob for reading my Dutch summary. Axel, many thanks for the discussions we had on astrophysics that helped me stay sharp. I'm sorry if this damaged your mental health. I also want to thank everyone else who contributed to the good atmosphere in the institute: Remco, Peter, Frans, Sabina, Garmt, Sandra, Ana, Laurens, Esteban, Klaartje. Last but not least, my thanks to those who keep the institute running in the background: Marion, Ed and Sake.

Apart from colleagues in Utrecht I would like to thank a few people from other departments. First of all Peter Eggleton, without whose stellar evolution code this work could not have been started. I also want to thank Evghenii Gaburov, my colleague in the stellar collision collaboration between Utrecht and Amsterdam. Many thanks also to everyone I met at conferences and workshops and helped turn these into fun and informative events: Piet Hut, Steve McMillan, James Lombardi and the rest of the MODEST community, Jorick Vink, Ofer Yaron and the other users of 'the Eggleton-code': Haili Hu, Richard Stancliffe, Ross Church, John Eldridge and Stephen Justham.

Of course I also want to thank my friends outside of Utrecht for all the fun we've had before, during and hopefully after my PhD: Pascalle, Mathilde, Koos, Gerben, Dave, Laura, Hendrik, Jet, Lydwin, Martijn, Gerben, Joop, Bernard, Yan, Paul, Vincent, Evy, Michiel, P.P. and the chess players at DOS Amsterdam: you all somehow contributed to the completion of this work at some point. I am especially grateful to Tine for her patience and understanding. The last half year of a PhD is not the best time to get to know someone.

Finally I want to thank my family: my grandmother, aunts Eeke and Karin, uncle Ron, my cousins Marieke and Femke and their husband and boyfriend Joost and Erik. Last but not least I want to thank my mother for her interest, support and help throughout the years.

Thank you all! I could not have done this without you.

Publication list

Refereed journals

1. R. G. Izzard & E. Glebbeek 2006, New Astronomy, 12, 161, Window to the Stars

2. R. J. Stancliffe, E. Glebbeek, R. G. Izzard & O.R. Pols 2007, A&A, 464L, 57, Carbon-enhanced metal-poor stars and thermohaline mixing

3. A. A. Bonacic Marinovic, E. Glebbeek & O. R. Pols 2008, A&A, 480, 797, Orbital eccentricity of binary systems with a former AGB star

4. E. Glebbeek, O. R. Pols & J. R. Hurley 2008 A&A submitted, Blue stragglers in N-body models of M67 (chapter 2)

5. E. Glebbeek & O. R. Pols 2008 A&A submitted, A grid of low-mass collisions (chapter 3)

6. E. Glebbeek, E. Gaburov, S. E. de Mink, O. R. Pols & S. F. Portegies Zwart 2008 A&A to be submitted, The evolution of runaway stellar collision products (chapter 5)

In preparation

1. E. Gaburov, E. Glebbeek, S. F. Portegies Zwart & O. R. Pols 2008 MNRAS, Structure and evolution of high mass stellar mergers (chapter 4)

2. R. J. Stancliffe & E. Glebbeek 2008, Thermohaline mixing and gravitational settling in carbon-enhanced metal-poor stars

3. R. G. Izzard, E. Glebbeek, R. J. Stancliffe & O. R. Pols 2008, Population synthesis of carbon-enhanced metal-poor stars

Proceedings/unrefereed

1. E. Glebbeek & O. R. Pols 2007, in *Unsolved problems in stellar physics: A conference in honour of Douglas Gough*, Stancliffe, Dewi, Houdek, Martin & Tout eds., `astro-ph/0710.1734`

2. S. E. de Mink, O. R. Pols & E. Glebbeek 2007, in *Unsolved problems in stellar physics: A conference in honour of Douglas Gough*, Stancliffe, Dewi, Houdek, Martin & Tout eds., `astro-ph/0709.2285`

3. E. Glebbeek & O. R. Pols 2007, in *Proceedings IAU symposium 246: Dynamical evolution of Dense Stellar Systems*, Vesperini, Giersz & Sills eds., `astro-ph/0710.1730`

Popular

1. E. Glebbeek & M. Cantiello 2008, *Zakkende zoutvingers*, Explore, 35-1

2. L. J. van den Horn, E. Glebbeek & P. Friedel 2002, *Een natuurlijke cosmische massaschaal*, Nederlands tijdschrift voor Natuurkunde, 68

Curriculum vitae

PERSONALIA

Name:	Evert Glebbeek
Date of birth:	6 December 1979
Nationality:	Dutch
Gender:	Male

EDUCATION

- PhD in Astrophysics, Utrecht University.
  On the evolution of stellar merger remnants. Expected June 2008
- Master of science (equivalent) in Theoretical Physics, University of Amsterdam. On double diffusive instabilities in proto-neutron stars. May 2004
- Cambridge ESOL Certificate of Proficiency in English, grade A. 2003
- Propaedeusis Exam in Physics (cum laude), University of Amsterdam 1999.
- Gymnasium diploma, Montessori Lyceum Amsterdam, 1998

WORKEXPERIENCE (APART FROM PHD WORK)

2004-2007 Teaching assitant for courses in stellar evolution, nucleosynthesis and cosmology at Utrecht University.

2006 Local organising committee National Dutch Astronomy Conference

2001-2003 Teaching assistant for computer courses at the University of Amsterdam
Student member of the education board for Physics and Astronomy at the University of Amsterdam in the years 2001/2002 and 2002/2003

2000-2002 University introduction for highschool students, 2000-2002

ATTENDED CONFERENCES AND WORKSHOPS

2004 MODEST 5a, Edinburgh, UK

2005 National Dutch Astronomy Conference (NAC), Blankenberghe, Belgium
Nucleosynthesis in Binary Stars, Leiden
MODEST 6, Evanston, USA
MODEST 6a, Lund, Sweden
MODEST 6d, Amsterdam, The Netherlands

2006 National Dutch Astronomy Conference (NAC), Ameland, The Netherlands
26th IAU General Assembly, Prague, Czech Republic, 2006

2007 National Dutch Astronomy Conference (NAC), Veldhoven, The Netherlands
MODEST 7f, Amsterdam, The Netherlands
Unsolved Problems in Stellar Physics, Cambridge, UK
MODEST 7a, Split, Croatia
IAU Symposium 246 (Dynamical Evolution of Dense Stellar Systems), Capri, Italy

2008 IAU Symposium 252 (The Art of Modelling Stars in the 21st Century), Sanya, China
National Dutch Astronomy Conference (NAC), Dalfsen, The Netherlands

CONFERENCE TALKS AND POSTERS

- Talk "When Stars Collide", Unsolved Problems in Stellar Physics, 2007

- Talk "Building Blue Stragglers from Stellar Collisions", Dutch Astronomy Conference 2007
- Talk "Evolving Stellar Merger Remnants", MODEST 6a, 2005

- Poster "Building Blue Stragglers from Stellar Collisions", IAU Symposium 246
- Poster "A Stellar Evolution Code for Merger Remnants", 26th IAU General Assembly 2006
- Poster "Evolution of Stellar Collision Products", Dutch Astronomy Conference 2006
- Poster "The Evolution of Stellar Mergers", Dutch Astronomy Conference 2005

POPULAR TALKS

- "De neus van Einstein en gedachten over het 'niets' " Public Observatory 'Vesta' 2004, joined with P. Weltevrede
- "Compacte objecten: witte dwergen en neutronen sterren" Public Observatory 'Vesta' 2001, joined with P. Friedel

Bibliography

Aarseth, S. J. 1999, PASP, 111, 1333

Afşar, M. & Bond, H. E. 2007, AJ, 133, 387

Ahumada, J. & Lapasset, E. 1995, AAPS, 109, 375

Ahumada, J. A. & Lapasset, E. 2007, A&A, 463, 789

Alexander, D. R. & Ferguson, J. W. 1994, ApJ, 437, 879

Anders, E. & Grevesse, N. 1989, Geochim. Cosmochim. Acta, 53, 197

Bailyn, C. D. 1995, ARA&A, 33, 133

Bailyn, C. D. & Pinsonneault, M. H. 1995, ApJ, 439, 705

Baumgardt, H., Makino, J., Hut, P., McMillan, S., & Portegies Zwart, S. 2003, ApJL, 589, L25

Belczynski, K., Kalogera, V., & Bulik, T. 2002, ApJ, 572, 407

Belkus, H., Van Bever, J., & Vanbeveren, D. 2007, ApJ, 659, 1576

Benz, W. & Hills, J. G. 1987, ApJ, 323, 614

Bettwieser, E. & Sugimoto, D. 1984, MNRAS, 208, 493

Böhm-Vitense, E. 1958, ZsAp, 46, 108

Bonatto, C., Bica, E., & Santos, Jr., J. F. C. 2005, A&A, 433, 917

Bonnell, I. A., Bate, M. R., & Zinnecker, H. 1998, MNRAS, 298, 93

Bromm, V., Coppi, P. S., & Larson, R. B. 1999, ApJL, 527, L5

Carraro, G., Chiosi, C., Bressan, A., & Bertelli, G. 1994, AAPS, 103, 375

Caughlan, G. R. & Fowler, W. A. 1988, Atomic Data and Nuclear Data Tables, 40, 283

Caughlan, G. R., Fowler, W. A., Harris, M. J., & Zimmerman, B. A. 1985, Atomic Data and Nuclear Data Tables, 32, 197

Clayton, D. D. 1983, Principles of stellar evolution and nucleosynthesis (Chicago: University of Chicago Press, 1983)

Dale, J. E. & Davies, M. B. 2006, MNRAS, 366, 1424

Davies, M. B., Amaro-Seoane, P., Bassa, C., et al. 2006, New Astronomy, 12, 201

Davies, M. B., Piotto, G., & de Angeli, F. 2004, MNRAS, 349, 129

de Jager, C., Nieuwenhuijzen, H., & van der Hucht, K. A. 1988, AAPS, 72, 259

De Marco, O., Shara, M. M., Zurek, D., et al. 2005, ApJ, 632, 894

Dull, J. D., Cohn, H. N., Lugger, P. M., et al. 2003, ApJ, 585, 598

Eggleton, P. 2006, Evolutionary Processes in Binary and Multiple Stars (Evolutionary Processes in Binary and Multiple Stars, by Peter Eggleton, pp. . ISBN 0521855578. Cambridge, UK: Cambridge University Press, 2006.)

Eggleton, P. P. 1971, MNRAS, 151, 351

Eggleton, P. P. 1972, MNRAS, 156, 361

Eldridge, J. J. & Tout, C. A. 2004, MNRAS, 348, 201

Eldridge, J. J. & Vink, J. S. 2006, A&A, 452, 295

Elmegreen, B. G. 1999, ApJ, 515, 323

Endal, A. S. & Sofia, S. 1976, ApJ, 210, 184

Evans, C. J., Lennon, D. J., Smartt, S. J., & Trundle, C. 2006, A&A, 456, 623

Ferguson, J. W., Alexander, D. R., Allard, F., et al. 2005, ApJ, 623, 585

Figer, D. F. 2005, Nature, 434, 192

Figer, D. F., Kim, S. S., Morris, M., et al. 1999, ApJ, 525, 750

Figer, D. F., Najarro, F., Morris, M., et al. 1998, ApJ, 506, 384

Freitag, M. & Benz, W. 2005, MNRAS, 358, 1133

Freitag, M., Dale, J. E., Church, R. P., & Davies, M. B. 2007, ArXiv e-prints, 710

Freitag, M., Gürkan, M. A., & Rasio, F. A. 2006, MNRAS, 368, 141

Gaburov, E., Glebbeek, E., Portegies Zwart, S., & Pols, O. 2008a, in preparation

Gaburov, E., Gualandris, A., & Portegies Zwart, S. 2008b, MNRAS, 384, 376

Gaburov, E., Lombardi, J. C., & Portegies Zwart, S. 2008c, MNRAS, 383, L5

Gebhardt, K., Rich, R. M., & Ho, L. C. 2002, ApJL, 578, L41

Gerssen, J., van der Marel, R. P., Gebhardt, K., et al. 2002, AJ, 124, 3270

Girardi, L., Bertelli, G., Bressan, A., et al. 2002, A&A, 391, 195

Glebbeek, E. & Pols, O. R. 2008, in preparation

Glebbeek, E., Pols, O. R., & Hurley, J. R. 2008, submitted

Gratton, R. G., Sneden, C., Carretta, E., & Bragaglia, A. 2000, A&A, 354, 169

Gürkan, M. A., Fregeau, J. M., & Rasio, F. A. 2006, ApJL, 640, L39

Heger, A., Langer, N., & Woosley, S. E. 2000, ApJ, 528, 368

Heggie, D. & Hut, P. 2003, The Gravitational Million-Body Problem: A Multidisciplinary Approach to Star Cluster Dynamics (The Gravitational Million-Body Problem: A Multidisciplinary Approach to Star Cluster Dynamics, by Douglas Heggie and Piet Hut. Cambridge University Press, 2003, 372 pp.)

Heggie, D. C., Giersz, M., Spurzem, R., & Takahashi, K. 1998, Highlights of Astronomy, 11, 591

Hillier, D. J., Davidson, K., Ishibashi, K., & Gull, T. 2001, ApJ, 553, 837

Hills, J. G. & Day, C. A. 1976, Astrophysical Letters, 17, 87

Humphreys, R. M. & Davidson, K. 1979, ApJ, 232, 409

Hurley, J. R., Pols, O. R., Aarseth, S. J., & Tout, C. A. 2005, MNRAS, 363, 293

Hurley, J. R., Pols, O. R., & Tout, C. A. 2000, MNRAS, 315, 543

Hurley, J. R., Tout, C. A., Aarseth, S. J., & Pols, O. R. 2001, MNRAS, 323, 630

Hurley, J. R., Tout, C. A., & Pols, O. R. 2002, MNRAS, 329, 897

Hut, P., McMillan, S., Goodman, J., et al. 1992, PASP, 104, 981

Hut, P., Shara, M. M., Aarseth, S. J., et al. 2003, New Astronomy, 8, 337

Hut, P. & Verbunt, F. 1983, Nature, 301, 587

Iglesias, C. A. & Rogers, F. J. 1996, ApJ, 464, 943

Ishii, M., Ueno, M., & Kato, M. 1999, PASJ, 51, 417

Ivanova, N. & Podsiadlowski, P. 2002, in Astronomical Society of the Pacific Conference Series, Vol. 279, Exotic Stars as Challenges to Evolution, ed. C. A. Tout & W. van Hamme, 245–+

Izzard, R. G., Jeffery, C. S., & Lattanzio, J. 2007, A&A, 470, 661

Johnson, H. L. & Sandage, A. R. 1955, ApJ, 121, 616

King, I. R. 1966, AJ, 71, 64

Kippenhahn, R., Ruschenplatt, G., & Thomas, H.-C. 1980, A&A, 91, 175

Kippenhahn, R. & Weigert, A. 1990, Stellar Structure and Evolution (Stellar Structure and Evolution, XVI, 468 pp. 192 figs.. Springer-Verlag Berlin Heidelberg New York. Also Astronomy and Astrophysics Library)

Kormendy, J. & Richstone, D. 1995, ARA&A, 33, 581

Kudritzki, R. P. 2002, ApJ, 577, 389

Kurucz, R. L. 1992, in IAU Symposium, Vol. 149, The Stellar Populations of Galaxies, ed. B. Barbuy & A. Renzini, 225–+

Lambert, D. L. & Rao, N. K. 1994, Journal of Astrophysics and Astronomy, 15, 47

Landau, L. D. & Lifshitz, E. M. 1980, Statistical physics. Pt.1, Pt.2 (Course of theoretical physics, Pergamon International Library of Science, Technology, Engineering and Social Studies, Oxford: Pergamon Press, 1980—c1980, 3rd rev.and enlarg. ed.)

Langer, N., Norman, C. A., de Koter, A., et al. 2007, A&A, 475, L19

Larsen, S. S. & Richtler, T. 1999, A&A, 345, 59

Leigh, N., Sills, A., & Knigge, C. 2007, ApJ, 661, 210

Lejeune, T., Cuisinier, F., & Buser, R. 1997, AAPS, 125, 229

Leonard, P. J. T. 1989, AJ, 98, 217

Leonard, P. J. T. & Livio, M. 1995, ApJL, 447, L121+

Lombardi, J. C., Thrall, A. P., Deneva, J. S., Fleming, S. W., & Grabowski, P. E. 2003, MNRAS, 345, 762

Lombardi, Jr., J. C., Proulx, Z. F., Dooley, K. L., et al. 2006, ApJ, 640, 441

Lombardi, Jr., J. C., Rasio, F. A., & Shapiro, S. L. 1995, ApJL, 445, L117

Lombardi, Jr., J. C., Rasio, F. A., & Shapiro, S. L. 1996, ApJ, 468, 797

Lombardi, Jr., J. C., Warren, J. S., Rasio, F. A., Sills, A., & Warren, A. R. 2002, ApJ, 568, 939

Maeder, A. & Meynet, G. 2000a, A&A, 361, 159

Maeder, A. & Meynet, G. 2000b, ARA&A, 38, 143

Makino, J. 2001, in Astronomical Society of the Pacific Conference Series, Vol. 228, Dynamics of Star Clusters and the Milky Way, ed. S. Deiters, B. Fuchs, A. Just, R. Spurzem, & R. Wielen, 87–+

Makino, J., Fukushige, T., Koga, M., & Namura, K. 2003, PASJ, 55, 1163

Mathieu, R. D., Latham, D. W., & Griffin, R. F. 1990, AJ, 100, 1859

Mathis, J. S. 1967, ApJ, 147, 1050

Mathys, G. 1991, A&A, 245, 467

Monaghan, J. J. 2005, Reports on Progress in Physics, 68, 1703

Montgomery, K. A., Marschall, L. A., & Janes, K. A. 1993, AJ, 106, 181

Nugis, T. & Lamers, H. J. G. L. M. 2000, A&A, 360, 227

Ouellette, J. A. & Pritchet, C. J. 1998, AJ, 115, 2539

Owocki, S. P., Gayley, K. G., & Shaviv, N. J. 2004, ApJ, 616, 525

Owocki, S. P. & van Marle, A. J. 2008, ArXiv e-prints, 801

Padmanabhan, T. 2001, Theoretical Astrophysics, Volume 2: Stars and Stellar Systems (Theoretical Astrophysics, by T. Padmanabhan, pp. 594. ISBN 0521562414. Cambridge, UK: Cambridge University Press, April 2001.)

Peterson, R. C., Carney, B. W., & Latham, D. W. 1984, ApJ, 279, 237

Petrovic, J., Pols, O., & Langer, N. 2006, A&A, 450, 219

Pinsonneault, M. H., Kawaler, S. D., Sofia, S., & Demarque, P. 1989, ApJ, 338, 424

Piotto, G., De Angeli, F., King, I. R., et al. 2004, ApJL, 604, L109

Platais, I., Kozhurina-Platais, V., Mathieu, R. D., Girard, T. M., & van Altena, W. F. 2003, AJ, 126, 2922

Pols, O. R., Schroder, K.-P., Hurley, J. R., Tout, C. A., & Eggleton, P. P. 1998, MNRAS, 298, 525

Pols, O. R., Tout, C. A., Eggleton, P. P., & Han, Z. 1995, MNRAS, 274, 964

Pooley, D. & Rappaport, S. 2006, ApJL, 644, L45

Portegies Zwart, S. F., Baumgardt, H., Hut, P., Makino, J., & McMillan, S. L. W. 2004, Nature, 428, 724

Portegies Zwart, S. F., Makino, J., McMillan, S. L. W., & Hut, P. 1999, A&A, 348, 117

Portegies Zwart, S. F. & McMillan, S. L. W. 2002, ApJ, 576, 899

Portegies Zwart, S. F., McMillan, S. L. W., Hut, P., & Makino, J. 2001, MNRAS, 321, 199

Portegies Zwart, S. F. & van den Heuvel, E. P. J. 2007, Nature, 450, 388

Press, W. H., Teukolsky, S. A., Vetterling, W. T., & Flannery, B. P. 1992, Numerical recipes in C. The art of scientific computing (Cambridge: University Press, —c1992, 2nd ed.)

Pumo, M. L., D'Antona, F., & Ventura, P. 2008, ApJL, 672, L25

Rogers, F. J. & Iglesias, C. A. 1992, ApJS, 79, 507

Rozyczka, M., Yorke, H. W., Bodenheimer, P., Mueller, E., & Hashimoto, M. 1989, A&A, 208, 69

Sandage, A. R. 1953, AJ, 58, 61

Sanders, W. L. 1977, AAPS, 27, 89

Sandquist, E. L. 2004, MNRAS, 347, 101

Sandquist, E. L. 2005, ApJL, 635, L73

Sandquist, E. L., Bolte, M., & Hernquist, L. 1997, ApJ, 477, 335

Schröder, K.-P., Pols, O. R., & Eggleton, P. P. 1997, MNRAS, 285, 696

Seaton, M. J., Yan, Y., Mihalas, D., & Pradhan, A. K. 1994, MNRAS, 266, 805

Serenelli, A. & Weiss, A. 2005, A&A, 442, 1041

Sills, A., Adams, T., & Davies, M. B. 2005, MNRAS, 358, 716

Sills, A., Adams, T., Davies, M. B., & Bate, M. R. 2002, MNRAS, 332, 49

Sills, A., Bailyn, C. D., & Demarque, P. 1995, ApJL, 455, L163+

Sills, A., Deiters, S., Eggleton, P., et al. 2003, New Astronomy, 8, 605

Sills, A., Faber, J. A., Lombardi, Jr., J. C., Rasio, F. A., & Warren, A. R. 2001, ApJ, 548, 323

Sills, A., Lombardi, Jr., J. C., Bailyn, C. D., et al. 1997, ApJ, 487, 290

Springel, V. 2005, MNRAS, 364, 1105

Stancliffe, R. J., Glebbeek, E., Izzard, R. G., & Pols, O. R. 2007, A&A, 464, L57

Stryker, L. L. 1993, PASP, 105, 1081

Suzuki, T. K., Nakasato, N., Baumgardt, H., et al. 2007, ApJ, 668, 435

Talon, S. 2007, ArXiv e-prints, 708

Tout, C. A., Aarseth, S. J., Pols, O. R., & Eggleton, P. P. 1997, MNRAS, 291, 732

Trac, H., Sills, A., & Pen, U.-L. 2007, MNRAS, 377, 997

Turner, J. A., Chapman, S. J., Bhattal, A. S., et al. 1995, MNRAS, 277, 705

Tylenda, R. & Soker, N. 2006, A&A, 451, 223

Ulrich, R. K. 1972, ApJ, 172, 165

van den Berg, M., Verbunt, F., & Mathieu, R. D. 1999, A&A, 347, 866

van der Marel, R. P., Gerssen, J., Guhathakurta, P., Peterson, R. C., & Gebhardt, K. 2002, AJ, 124, 3255

Vierdayanti, K., Mineshige, S., Ebisawa, K., & Kawaguchi, T. 2006, PASJ, 58, 915

Vink, J. S. & de Koter, A. 2005, A&A, 442, 587

Vink, J. S., de Koter, A., & Lamers, H. J. G. L. M. 2000, A&A, 362, 295

Vink, J. S., de Koter, A., & Lamers, H. J. G. L. M. 2001, A&A, 369, 574

von Hippel, T. & Sarajedini, A. 1998, AJ, 116, 1789

Webbink, R. F. 1984, ApJ, 277, 355

Weidner, C. & Kroupa, P. 2004, MNRAS, 348, 187

Weiss, A., Hillebrandt, W., Thomas, H.-C., & Ritter, H. 2004, Cox and Giuli's Principles of Stellar Structure (Cox and Giuli's Principles of Stellar Structure, by A. Weiss, W. Hillebrandt, H-C. Thomas, H. Ritter. Cambridge, UK: Princeton Publishing Associates Ltd, 2004.)

Yoon, S.-C. & Langer, N. 2005, A&A, 443, 643

Yoon, S.-C., Langer, N., & Scheithauer, S. 2004, A&A, 425, 217

Yungelson, L. R., van den Heuvel, E. P. J., Vink, J. S., Portegies Zwart, S. F., & de Koter, A. 2008, A&A, 477, 223

Zahn, J.-P. 1992, A&A, 265, 115